UNIVERSITY OF BERGAMO
School of Doctoral Studies

Doctoral Degree in Engineering and Applied Sciences

XXX Cycle
SSD: ING-IND/09

TITLE
Solar Cooling Technologies and Off-Grid Building Design in Hot Climatic Conditions

Advisor
Chiar.mo Prof. Antonio Perdichizzi

Doctoral Thesis
Giovanni BRUMANA
Student ID 54680

Academic year 2016/17

Solar Cooling Technologies and Off-Grid Building Design in Hot Climatic Conditions

'One thing I feel sure of...
...the human race must finally utilize direct sun power
or revert to barbarism'

F. Shuman (1914)

Acknowledgements

First and foremost, I would like to thank my advisor Professor Antonio Perdichizzi for his invaluable support and guidance. I feel privileged to have the opportunity to work closely with him.
I would also like to thank Professor Giuseppe Franchini, for his advice and patience.
I would especially like to thank the Research Group of Energy Systems and Turbomachinery of the University of Bergamo for their brilliant comments and suggestions.
A special thanks to my family. Words cannot express how grateful I am to my parents and my brother for their constant encouragement, support and unwavering belief in me.

I am gratefully acknowledging the collaboration of the Emirates Institution for Advanced Science and Technology (EIAST) and the Mohammed Bin Rashid Space Center (MBRSC).
Thanks are also due to the Saudi Institution King Abdullah City for Atomic and Renewable Energy.

Finally, I would like to thank my friends, my colleagues and all the people I met during the last years.

Table of Contents

Abstract

Global warming is the main problem of the century. The scientific community is addressing many efforts to face the environmental problems and solar cooling systems are one of the best candidates.
The thesis proposes a solution developed through the improvement of the three main aspects of the chain: building energy efficiency, cooling production and distribution. The selected location, the Middle East region, represents the challenge locations for developing new technologies for air conditioning.
This work proposes the improvement of sustainable buildings and promote an innovative design to reduce energy consumption.
The development of district cooling systems allows the optimization of the cooling production and reduces the waste associated with single users, enabling the installation of higher efficiency technologies.
Solar cooling systems, the main focus of this research, are the best available solution to significantly reduce power consumption. Moreover, even under the economic aspect can certainly replace the traditional systems that have so far been adopted.
Particular attention is devoted to the heat rejection systems, the only component that can improve the cooling plants performance in hot climates.
The sun, cause of the cooling load, must effectively turn into the solution of the problem.

Nomenclature

Introduction

	Name	Unit
ETC	Evacuate tube collector	
LiBr	Lithium Bromide	
1sABS	Single effect absorption chiller	
COP	Coefficient of Performance	
PTC	Parabolic trough collector	
2sABS	Double effect absorption chiller	
PV	Photovoltaic modules	

1 Hot Climatic Condition

	Name	Unit
UAE	Unit Arab Emirates	
KSA	Kingdom of Saudi Arabia	
DryTemp	Dry bulb temperature	deg. C
RH	Relative Humidity	%
GHI	Global Horizontal Irradiation	W/m^2
DNI	Direct Normal Irradiation	W/m^2

2 Off-Grid Building

	Name	Unit
PV	Photovoltaic modules	
U_{wall}	Wall U-value	$W/m^2/K$
U_{roof}	Roof U-value	$W/m^2/K$
$U_{-value,w}$	Window U-value	$W/m^2/K$
$G_{-value,w}$	Window solar factor	%
HX	Heat Exchanger	
COP	Coefficient of Performance	
EPS	Expanse Polystyrene	
HVAC	Heating, ventilation and air conditioning	
UAE	Unit Arab Emirates	
T roof in	Roof temperature, internal side	deg. C
T roof out	Roof temperature, external side	deg. C
T amb	Ambient temperature (dry bulb)	deg. C
P load max	Peak of cooling load	kW
Q load annual	Annual cooling load	kWh
TMR	Mean radiant temperature	deg. C
TOP	Operative temperature	deg. C
PMV	predicted mean vote	-3 to 3
PPD	percentage of person dissatisfied	%

3 District Cooling

	Name	Unit
N1	1.00 m/s and 1” insulation configuration	
N2	1.00 m/s and 2” insulation configuration	
N3	1.00 m/s and 4” insulation configuration	
N4	2.00 m/s and 1” insulation configuration	
N5	2.00 m/s and 2” insulation configuration	
N6	2.00 m/s and 4” insulation configuration	
N7	2.65 m/s and 1” insulation configuration	
N8	2.65 m/s and 2” insulation configuration	
N9	2.65 m/s and 4” insulation configuration	
N6S	2.00 m/s and 4” insulation configuration in Riyadh	
A disper	Surface of pipe	m^2/m
R ind	Undisturbed soil radius	m
Q	Thermal heat loss	W/m
Q int	Thermal heat loss	W/m^2

4 Solar Cooling Models

	Name	Unit
SF	Solar Fraction	%
Qsol	Cooling production from renewable energy	kWh
Qload	Cooling load	kWh
Qabs	Absorption chiller cooling production	kWh
Qaux	Auxiliary chiller cooling production	kWh
Epv	PV field electric production	kWh
Echiller	Compression chiller electric consumption	kWh
Esxp	Exported electric energy	kWh
Eimp	Imported electric energy	kWh
CC	Compression chiller	
COP	Coefficient of Performance	
PV	Photovoltaic modules	
GHX	Ground heat exchanger	
1sABS	Single effect absorption chiller	
2sABS	Double effect absorption chiller	
3sABS	Triple effect absorption chiller	
ADS	Adsorption chiller	
DEC	Desiccant evaporative cooling	
VEN	DEC ventilation configuration	
VSL	DEC ventilation sensible-latent control	
REC	DEC recirculation configuration	
HX	Heat exchanger	
ΔT	Temperature difference	deg. C
ΔX	Absolute humidity difference	g/kg
Qsens	Sensible load	kWh
Qlat	Latent load	kWh
m	DEC air mass flow rate	kg/h
Cp	Air specific heat	kJ/kgK
r	Latent heat of water vaporization	kJ/kg
Tsat	Wet bulb temperature of DEC air flowrate	deg. C
Tsetpoint	DEC Set point temperature	deg. C
FPC	Flate plate collectors	
a_0	Collector Optical efficiency	-
a_1	Collector first order loss coefficient	W/ m2 K
a_2	Collector second order loss coefficient	W2/ m2 K
T _bar	Mean temperature between inlet and outlet flowrates (°C)	deg. C
η	Efficiency	
GTI	Global tilted irradiation	W/m^2
ETC	Evacuate tube collectors	
PTC	Parabolic trough collectors	
BTI	Beam tilted irradiation	W/m^2
C	Concentration ration	
DNI	Direct Normal Irradiance	W/m^2
θ	Incidence angle	deg.
AIR	Dry cooler	
MFR	Mass flow rate	kg/s

CT	Cooling tower	
GW	groundwater	
GHX	Ground heat exchanger	

5 Optimizations

	Name	Unit
SF	Solar Fraction	%
FPC	Flate plate collectors	
ETC	Evacuate tube collectors	
PTC	Parabolic trough collectors	
CC	Compression chiller	
1sABS	Single effect absorption chiller	
2sABS	Double effect absorption chiller	
3sABS	Triple effect absorption chiller	
DEC	Desiccant evaporative cooling	
VEN	DEC ventilation configuration	
VSL	DEC ventilation sensible-latent control	
REC	DEC recirculation configuration	
AIR	Dry cooler	
CT	Cooling tower	
GW	groundwater	
GHX	Ground heat exchanger	
f_{min}	Cooling plant cost function	$
A_{ETC}	Aperture area of the solar field	m^2
$Cost_{ETC}$	Unit cost of collectors	$/m^2$
Cap_{Abs}	Capacity of the absorption chiller	kW
$Cost_{Abs}$	Unit cost of the absorption chiller	$/kW
Vol_{tank}	Tank volume	m^3
$Cost_{tank}$	Unit cost of the tank	$/m^3$
$Penalty_{(SF)}$	Penalty for configuration with SF<0.7	$
Vol_{hot}	Hot tank volume	m^3
Vol_{cold}	Cold tank volume	m^3
A_{PV}	Area of photovoltaic field	m^2
$Cost_{PV}$	Unit cost of PV field	$/m^2$
$Cap_{Battery}$	Battery capacity	kWh
$Cost_{Battery}$	Unit cost of the battery	$/kWh
$Cost_{fixed}$	Fixed cost of the compression chiller configuration	$

6 Solar Cooling Simulation and Results

	Name	Unit
SF	Solar Fraction	%
FPC	Flate plate collectors	
ETC	Evacuate tube collectors	
PTC	Parabolic trough collectors	
CC	Compression chiller	

1sABS	Single effect absorption chiller	
2sABS	Double effect absorption chiller	
3sABS	Triple effect absorption chiller	
DEC	Desiccant evaporative cooling	
VEN	DEC ventilation configuration	
VSL	DEC ventilation sensible-latent control	
REC	DEC recirculation configuration	
AIR	Dry cooler	
CT	Cooling tower	
GW	groundwater	
GHX	Ground heat exchanger	
Nmacchine	Number of Compression chiller switched on	N
PV prod	Photovoltaic field power output	kW
Erad	Available radiant energy	kWh
Ecoll	Energy collected by the solar field	kWh
Load	Cooling load	kWh
Eabs	Absorption chiller cooling energy production	kWh
Eaux	Auxiliary chiller cooling energy production	kWh
Qrad	Available solar radiation	kW
Qcoll	Solar radiation collected by the solar field	kW
Qabs	Absorption chiller cooling power	kW
Qaux	Auxiliary chiller cooling power	kW
TempTankTop	Temperature of the top of the tank	deg. C
TempTankBot	Temperature of the bottom of the tank	deg. C
TOE	Tonnes of equivalent oil	

7 Economic Analysis

	Name	Unit
SF	Solar Fraction	%
FPC	Flate plate collectors	
ETC	Evacuate tube collectors	
PTC	Parabolic trough collectors	
CC	Compression chiller	
1sABS	Single effect absorption chiller	
2sABS	Double effect absorption chiller	
3sABS	Triple effect absorption chiller	
DEC	Desiccant evaporative cooling	
VEN	DEC ventilation configuration	
VSL	DEC ventilation sensible-latent control	
REC	DEC recirculation configuration	
AIR	Dry cooler	
CT	Cooling tower	
GW	groundwater	
GHX	Ground heat exchanger	

Introduction

In recent years, the installation of cooling systems for all kinds of buildings has strongly increased. Unfortunately, this additional energy request accelerated the global warming and the greenhouse effect.
Nowadays, the scientific community is addressing many efforts to face this increasing energy request; the focus is on the development of cooling technologies driven by renewable energy sources. Among them, solar cooling systems are the most promising way to reduce the fossil fuel consumption and the related environmental impact.
To develop coherently renewable resources is not enough to propose and build energy-efficiency cooling plants, it is necessary to improve all the components that contribute to defining the cooling load.
This thesis aims to develop a solar cooling idea that integrates the development of low-energy buildings connected with a district cooling network to minimize dissipation and optimize energy efficiency.
Solar cooling systems have been developed in temperate climates to use solar collectors even during the summer season by increasing the energy and economic viability of a renewable plant.
A different approach is discuss the performance of solar cooling systems in very hot climates, where high levels of cooling demand and solar radiation take place, and cooling systems undergo critical operating conditions.
The selected locations for simulations are two cities of the Arab peninsula: Riyadh and Dubai. The choice is the result of material availability on the area's conditions and collaborations with major research centers.

The Middle East represents the best potential market for solar cooling systems. However, the spread of this application is limited by some critical issues.

The first one is of a physical nature, high temperatures limit the chiller operation when the refrigeration demand is greater.

The second one is of an ethical nature, it is not possible to use evaporative towers as water is too precious for and arid regions.

The third reason is economic and management, solar cooling technologies are expensive and difficult to handle for individual private users.

To proceed properly, it is necessary starting from the cooling load of the buildings considered as the envelope, the cooling distribution and the users.

In many developed countries, buildings and their use are responsible for approximately one-third of the total primary energy consumption and carbon emissions. Governments and scientific communities are aiming for new paradigms for energy-efficient buildings: the goal is to reduce the environmental impact of the construction sector as reported By Nejat et al. [1]. Many authors investigated the design principles for high-efficient buildings in cold climates [2, 3]. More recently, the interest in the development of passive buildings has grown also for hot regions [4, 5].

The development of sustainable solutions goes through the construction of more and more efficient buildings. At this regard, new concepts have gained wide international attention, such as Passive Houses, Nearly Zero Energy Buildings, Net Zero Energy Buildings and Energy+ Buildings [6].

The first step in order to comply with all high-efficiency standards is to reduce the energy consumption in buildings. Passive design strategies contribute to improve the interior comfort conditions, reducing the requirement of energy supply from active systems as proposed by Rodriguez-Ubinas et al. in [7].

The second part of the work is devoted to the development of the district cooling network, the most efficient way to connect cooling production and users. The development of energy distribution networks for air conditioning is closely linked to district heating in North European countries

The next step is to introduce the solar contribution in district heating systems with a rising solar fraction. To achieve this goal, it is essential to

design powerful predictive models of load management and storage tanks: Daniel Trier [8] has investigated district heating systems with a solar fraction of more than 70%.

Therefore, research is focused on improving the efficiency of the production plant [9] and the network [10]. Subsequently, the integration of the solar contribution is also extended to the cooling systems as a direct result of the development of solar cooling technologies for individual buildings [11].

Only a few articles deal with the integration of a solar contribution in district cooling systems [12, 13, 14]. Carolina Marugàn-Cruz et al. propose a specific case study: the integration of a solar tower with a district cooling system to enhance the energy surplus in the warm season [15].

A further improvement has been derived from the integration of energy storage both in district heating [16, 17] as well as in district cooling: Powell and al. in [18] present a new methodology to optimize the operation of the cooling unit coupled with tanks. Wenjie Gang et al. [19] too, have investigated the integration of the district cooling system in a trigeneration plant serving a residential compound with a consequent increase in the economic, environmental and energy savings.

Besides the development of buildings and district network, an improvement of the sustainability can be achieved by using high-efficiency cooling technologies coupled with renewable energy sources.

Several types of solar cooling systems have been investigated in the open literature [20, 21].

The solar cooling systems are large-scale solar power plants with heat recovery for cooling production via absorption or adsorption chillers. For smaller sizes, typically the solar field is directly connected to the thermally driven chiller [22, 23, 24]. The most common configuration is based on ETCs coupled with a single-stage LiBr absorption chiller [25]: evacuated tube collectors with selective surface exhibit efficiency higher than 65% for a fluid temperature in the range 85-100 deg. C, typical for the generator of 1sABS. A higher overall efficiency is expected from solar cooling systems based on two-stage and three-stage absorption chillers, whose COP is usually around 1.3 and 1.7. Such units require a supply temperature higher than 160 deg. C [26]. For these temperature levels, the

best solar field option is a medium concentration collector like a PTC. Although parabolic troughs can exploit only the beam radiation, the reduction of the heat loss area permits to keep high efficiency for relatively high fluid temperatures (up to 200 deg. C). Mazloumi et al. [27] investigated the operation of PTCs in a small-scale solar cooling system: they documented a collector efficiency higher than 68% when coupled to a 1sABS. El Fadar et al. [28] presented a numerical study related to a continuous adsorption refrigeration system powered by parabolic trough solar collectors, with operating temperatures varying in the range 20-160 deg C.

In the open literature, the potential benefits deriving from the integration of PTCs and 2sABS are substantially unexplored.

Among the available technologies, the option based on compression chiller driven by a PV field assisted by a battery pack is highlighted. A remarkable comparison between this solution and thermal solar cooling systems was done by Lazzarin [29] The results show that the performance is today comparable but the PV has a greater adaptability. Recently, huge investments in the electric storage technology have led to the spread of batteries for building applications and to the development of off-the-grid or stand-alone houses [30, 31].

The last aspect that will be investigated in this research is the economic feasibility. The energy validity of a system can be frustrated by a cost that puts it out of the market.

1 Hot Climatic Conditions

The demand cooling energy is becoming more and more in temperate regions as well as in hot areas.
In this work, two special locations for their hot climate were selected: Dubai (UAE) and Riyadh (KSA). Both locations are on the 24th parallel but with remarkable climatic differences.
The fast development in the Middle East of recent decades has increased the demand of cooling energy exponentially. This cooling request is related to the construction of new buildings that could be equipped with solar cooling systems.
Today, for Arabian Peninsula's countries, the electricity request for residential buildings is nearly 40% of the global demand, and approximately 65% of the power consumption in buildings is due to air conditioning [1].
Middle East countries seem to be the ideal candidates for the development of cooling systems based on renewable sources. This project collides with the reality that sees this technology scarcely applied.
Subtropical climates lead to critical conditions solar cooling systems [2, 3, 4] and especially the hot and humid ones [5]. So, contrary to common thought, solar cooling systems suffer from hot climates.
A critical issue is often due to the difficulty of obtaining data in particular areas of the world [6] and the choice of these locations is dictated by the availability of data.

The city of Dubai represents the combination of humidity, due to the presence of the sea, and high temperatures. The capital of Saudi Arabia has a dry desert climate. It is located on a plateau of the shield of the Arabian Peninsula.

Figures 1.1 and 1.2 show the ambient air temperature and relative humidity for the location of Dubai and Riyadh. The temperature difference is minimal while relative humidity is considerably higher in Dubai due to the presence of the sea.

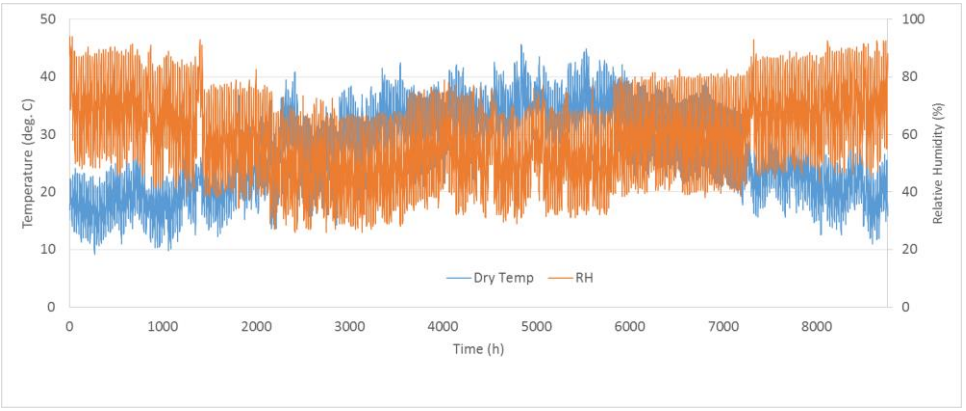

Fig. 1.1 - Ambient temperature and relative humidity (Dubai)

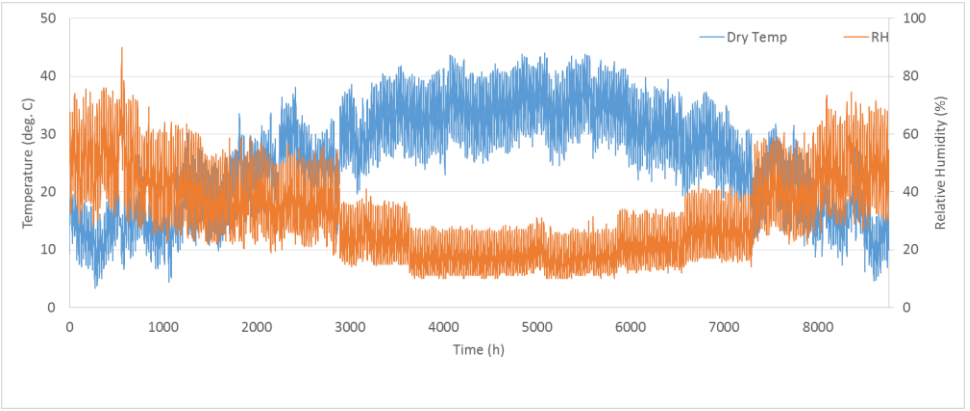

Fig. 1.2 - Ambient temperature and relative humidity (Riyadh)

Figures 1.3 and 1.4 show the radiation available in the form of Global Horizontal Irradiation (GHI) and Direct Normal Irradiation (DNI). Table 1.1 shows the annual radiation available. The presence of the sea also adversely affects the available direct radiation, which is definitely lower for coastal locations.
Figures 1.5 and 1.6 show the available radiation on a monthly basis.
Bar charts show the difference of direct radiation especially in the summer, when it would be more useful for solar cooling systems.

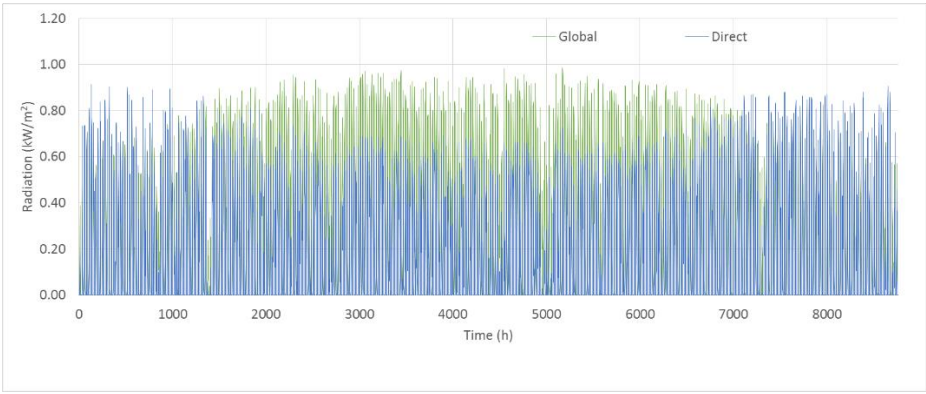

Fig. 1.3 - Direct Normal Irradiation and Global Horizontal Irradiation (Dubai)

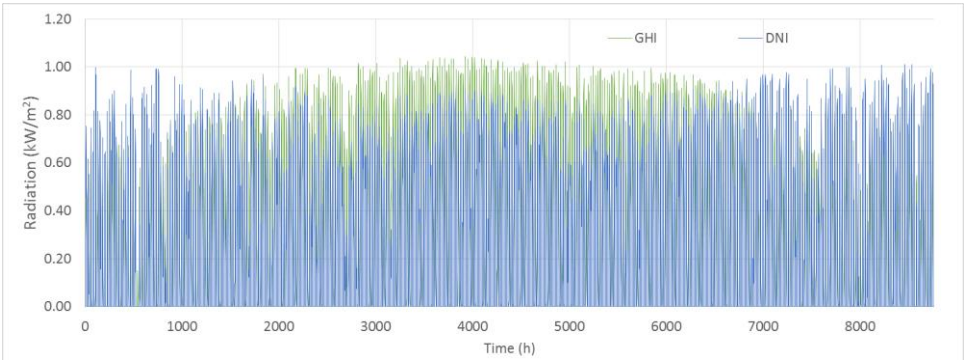

Fig. 1.4 - Direct Normal Irradiation and Global Horizontal Irradiation (Riyadh)

Table 1.1 - Solar irradiation in the two selected locations

Dubai (UAE)			Riyadh (KSA)		
	unit	value		unit	value
GHI	kWh	1957.36	GHI	kWh	2217.18
DNI	kWh	1605.04	DNI	kWh	2296.01

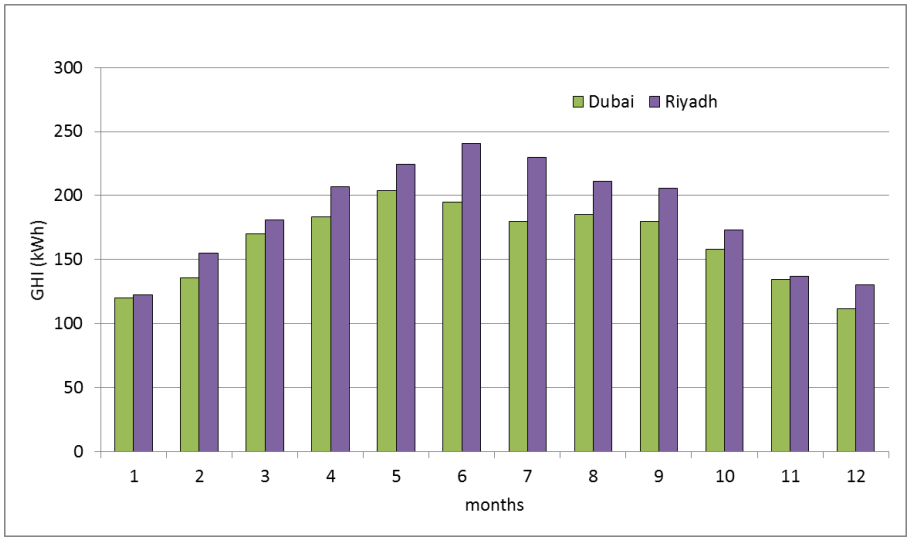

Fig. 1.5 - Global horizontal irradiation in the two selected locations

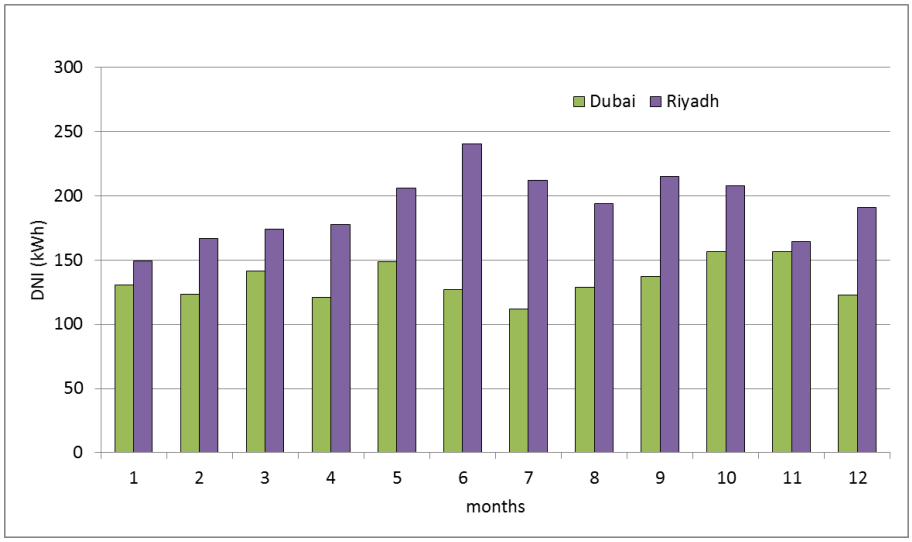

Fig. 1.6 - Direct normal irradiation in the two selected locations

2 Off-Grid Building

The severity of environmental problems is forcing the construction sector in hot climate regions to introduce new paradigms in the design and erection of energy-efficient buildings. The growing interest in the development of passive buildings for hot climates [1] is inextricably linked to the climatic conditions of the site as well enlightened by Schnieders et al. [2].

This process involves new energy systems and a new shell design [3], The development of sustainable solutions goes through the construction of more and more efficient buildings, such as Nearly Zero Energy Buildings [4] and Zero Energy Buildings [5].

Besides the development of well-insulated thermal envelopes according to the Passive House standards, an important step for improving the building sustainability is the use of high-efficiency cooling technologies coupled with renewable energy sources. Several types of solar cooling systems are available [6].

Starting from previous researches on solar cooling systems for buildings in hot climates, the present paper deals with the modeling and the design of the first Energy+ Building in Dubai, virtually off-the-grid. The developed computer models aimed to predict the energy performance and the thermal comfort, and was used to dictate the design choices for the building construction.

2.1 Off-Grid Building Design

Geometry and orientation of the two floor office building (Fig. 2.1) aim to reduce as much as possible the primary energy consumption taking into account the irradiation on the walls during the day and across the seasons.
The surface to volume ratio is minimized. A small patio shrinks the radiation on the glazed elements and keeps the office areas in shadow as demonstrate in [7] when efficient shading devices reduce energy consumption. This solution allows for avoiding window shields even in daylight hours.
The diffused light naturally illuminates the 550 m^2 floor surface and – at the same time – the solar gains are minimized.
A timber trimmed structure is designed to support the photovoltaic field, to promote the ventilation on PV modules and to shade the flat roof. The outline elements of the windows are protruding to limit direct radiation.
A lightweight load bearing structure made by wood supports timber walls and roof. The walls are designed to reduce as much as possible the building cooling load. The balance between mass and insulation improves the energy performance: the insulation thickness is designed to minimize thermal transmittance and the phase shift is controlled by adding mass layers. Walls are painted with a special reflective paint to curtail the absorption of solar radiation on the outer layer. Similarly, the roof is treated with a reflective film and infrared reflector films are inserted inside the walls. Windows are specific for warm climates with very low U and G values to limit the solar gains.
The building envelope is designed according to the Passive House standard and the energy plants are selected to reach the level of Energy+ building.
Power supply is ensured by the rooftop PV field. A battery pack is available to store electricity during light hours and to supply electricity after sunset. The solution has been investigated in the literature [8] when a remarkable comparison between this option and absorption chiller driven by solar collectors was done. The results show that the performance is today comparable but the PV has a greater adaptability. In this contest, the study of Viera et al. [9] evaluates the performance of a residential building equipped with photovoltaic modules and batteries.

The building is virtually off-grid (power import is possible for emergency) and the electric overproduction is delivered to the grid.
The growth of the self-production energy and battery capacity leads to the development of the buildings called off-the-grid or stand-alone [10] [11]. These buildings do not require connection to the grids, can supply the own energy needs and jointly maintain high standards of comfort. The management of the self-produced energy is another topical point, as illustrated by Chekired et al. in [12], especially when the overproduction is exported to the network [13] [14]. The importance of the consumption of electrical equipment in buildings is well illustrated by Widen in [15].
A high-efficient air-water reversible heat pump - specifically designed for hot-humid climates meets the cooling and dehumidification demand, and the production of domestic hot water. The cooling system is based on a combination of 3 different technologies: floor cooling, mechanical ventilation and fan-coils.
The radiant floor cooling maintains a high level of comfort, the air handling unit with high-efficient heat recovery controls temperature and humidity of the inlet air, and the fan-coils fulfil the cooling peak loads.
In the energy-efficient buildings a primary interest is the comfort perception: predictive techniques for quantifying and qualifying the indoor comfort are included in several building models [16] [17]. Frequently the goal of a high level of comfort perception is achieved through radiant floor cooling systems [18].
The integration of high-efficient technologies both in the thermal envelope and energy systems is the key of the project performance.

Fig. 2.1 - The Plus Energy building presented in November 2016

2.2 Building Model Simulation and Results

The models developed for building simulation and solar cooling system performance are based on Trnsys® v.17. (Fig. 2.2). Weather data with hourly resolution have been provided by the Mohammed Bin Rashid Space Center.

The detailed architectural building model is based on Trnsys Multizone Building Type and developed by the 3D cad software Google Sketch Up®, with the plug-in Trnsys3D for geometry and shading. The building model includes 10 homogeneous thermal zones and all main building parameters are listed in Table 2.1. Technical data of the materials were selected in design phase and have been implemented in the model, thus allowing a realistic prediction of the building envelope behavior.

The care of the details is necessary to develop a simulation for assessing the building energy performance [19] [20], especially when they are coupled with experimental measures [21]. The difficulty of performing reliable predictions of the thermal behavior and the energy consumption of buildings is well illustrated in [22] by Song et al.

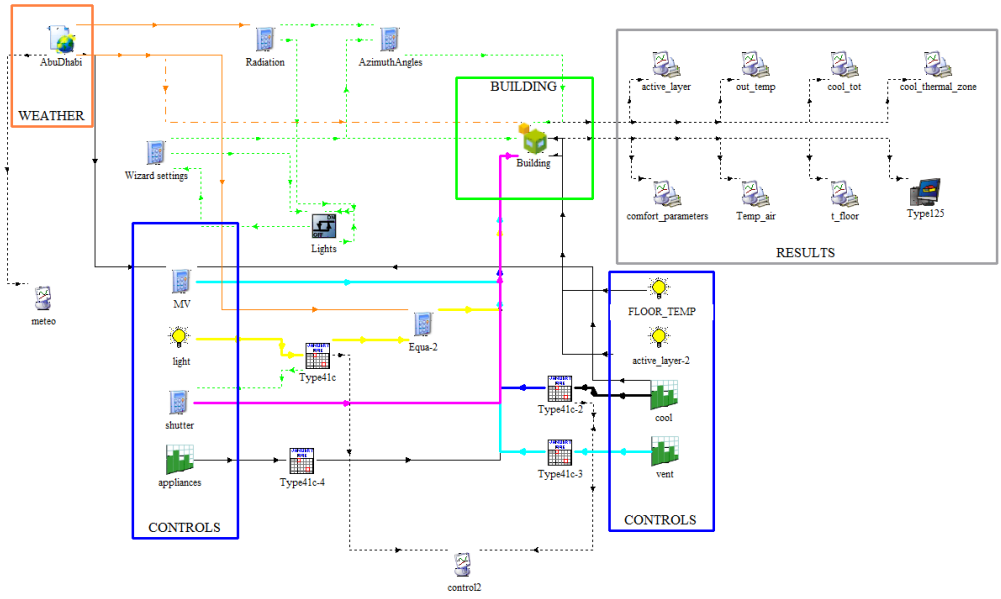

Fig. 2.2 - Trnsys deck with the building parameters

Internal loads due to lights and appliances have been carefully evaluated, according to the study of Hoxha and Jusselme [23], they show the relevance of using efficient lights and appliances adapted to new low-impact buildings. The occupancy is considered as an average attendance including random occurrence of overload events. Indeed the analysis of occupancy reveals its relevant impact on the energy performance as well documented by Blight and Coley [24].

The simulation results (Tab. 2.2) show the strong impact of latent loads due to high relative humidity levels. The dehumidification demand influences both the peak load and the annual demand respectively by 60% and 30%.

The total cooling load is shown in Fig 2.3, the short load cumulative curve is due to the high performance of building envelope and to the cooling management.

Table 2.1 - Comfort settings, internal gains and envelope characteristics

Comfort & Gains			Wall layers & Windows		
	unit	value		unit	value
Set point temperature	°C	24	U_{wall}	W/m^2/K	0.063
Set point relative humidity	%	50	Wall thickness	m	0.603
Mean ventilation ratio	Vol/hr	0.60	Wall solar absorptance	%/100	0.3
HX efficiency	%	80	U_{roof}	W/m^2/K	0.061
Infiltration	Vol/hr	0.06	Roof thickness	m	0.566
Lighting (peak)	W/m^2	5	Roof solar absorptance	%/100	0.2
Internal gains (peak)	kW	6	$U_{\text{-value,w}}$	W/m^2/K	0.7
Occupancy	Nr.	20	$G_{\text{-value,w}}$	%/100	0.294

Table 2.2 - Building cooling load

Peak Load			Annual Load		
	unit	value		unit	value
Air Load - sensible	kW	6.83	Air Load - sensible	kWh	7954.67
Air Load - latent	kW	20.49	Air Load - latent	kWh	11920.78
Floor Load	kW	8.42	Floor Load	kWh	13844.50
Total Load	kW	27.03	Total Load	kWh	33719.95

Table 2.3 - Building Comfort Parameters

	Unit	Max	Min	Average
Mean Radiant Temperature	deg. C	24.23	22.34	23.66
Operative Temperature	deg. C	24.11	22.25	23.75
Predicted Mean Vote	[-3 ; 3]	0.26	-0.27	0.16
Percentage of Person Dissatisfied	% [5 ; 100]	6.51	5.00	5.69

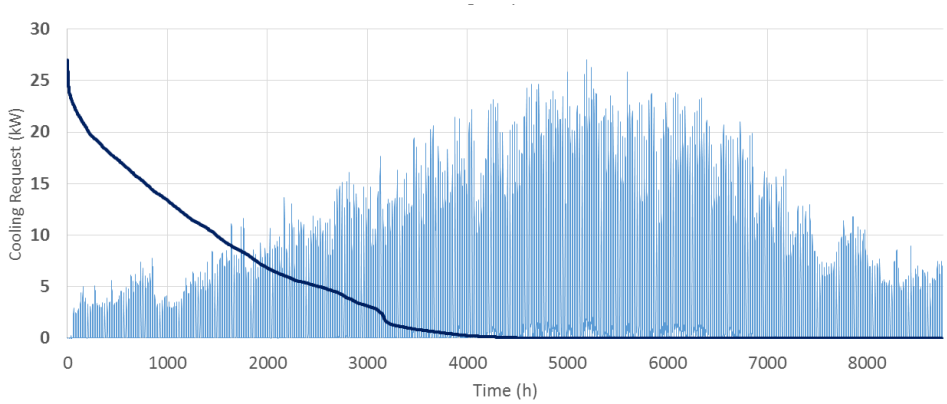

Fig. 2.3 - Building cooling load and load duration curve

The light color of the walls, coupled with the reflective film, limits the absorption of solar radiation. Fig. 2.4 reports the temperature trends of the part of flat roof not shaded by PV modules for 2 summer days. In spite of a strong temperature variation in the external side (with peak higher than 42°C), the temperature level on the internal side is stable at 25°C.

Fanger's comfort parameters were also considered to improve the design quality. Table 2.3 shows the calculated comfort parameters: the excellent level is achieved thanks to the integration of different air conditioning systems. The predicted mean vote is very near to the desired value and the maximum deviation (0.27) are very small compared to the comfort region (-0.5 to 0.5) extension. Furthermore, the value of the percentage of person dissatisfied is close to the minimum value.

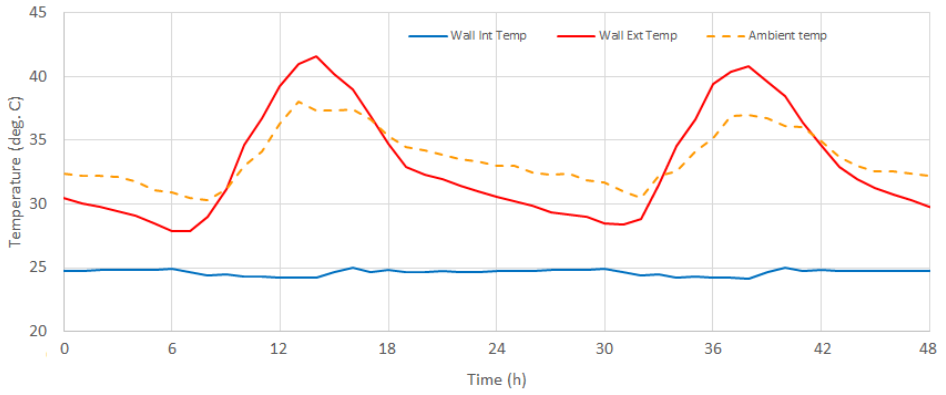

Fig. 2.4 - Roof temperature patterns

2.3 Energy Source and Cooling Plant Simulations and Results

The energy source model is based on multi-crystalline PV panels coupled to a battery pack. Power generated drives the reversible heat pump and all technical systems, and the overproduction is exported into the grid when batteries are at full capacity.

The cooling plant model includes the air-cooled heat pump performance map provided by the manufacturer (Fig. 2.5). The chiller is designed to operate up to 50 deg. C and the cooling capacity was selected to fulfil the peak demand of the building. The specification of the energy models are reported in Table 2.4.

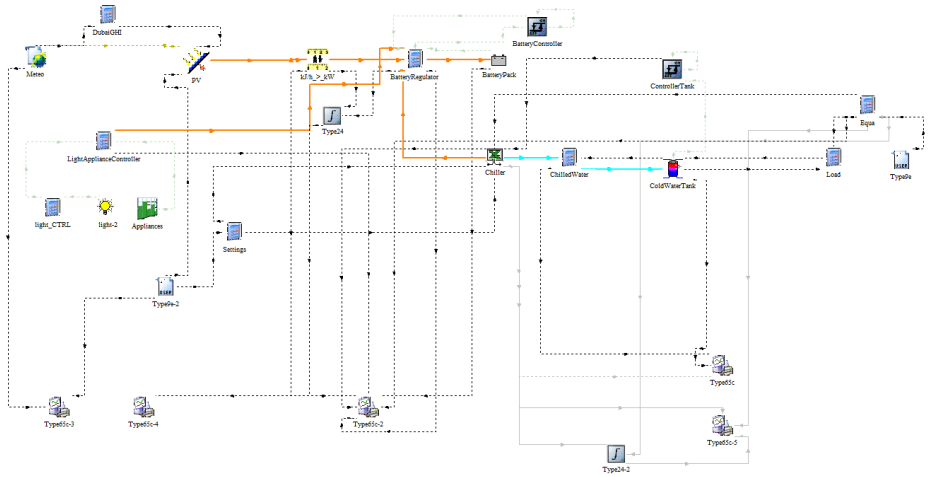

Fig. 2.5 - Operative Trnsys deck of the power and cooling systems

Table 2.4 - PV field and cooling plant characteristics

PV field and Battery specifications			**Cooling Plant Data**		
	unit	value		unit	value
Area	m^2	268	Chiller capacity*	kW	21.70
Nominal efficiency	-	0.149	COP*	-	2.94
Efficiency modif temp	1/deg.C	-0.0041	Power input*	kW	7.39
P_{max} Voltage	V	30.5	**Cold Tank Specifications**		
Open circuit voltage	V	37.6	Cold tank volume	m^3	1
Battery capacity	kWh	25	Tank insulation (EPS)	m	0.2

* Ambient temperature 30 deg. C; chilled water 7-12 deg. C, load fraction 100%, off-design from 30% to 140%.

The results of a transient simulation carried out for a one-year period are shown in Table 2.5. It can be seen that power consumption for air conditioning is about half of the total electricity consumption. The electricity production to meet the off-the-grid requirement results to be more than two time the Net-Zero Energy standard (export = import over one-year period). This has a heavy impact on the design of the photovoltaic field. Because the energy import must be zero at any time, PV system must be large enough to ensure the energy autonomy of the building. The simulation results document that the battery charge level (Fig. 2.6) is always above 60% of the full capacity (25 kWh), even in the peak periods.

Table 2.5 - Electric production and consumption

Electric Consumption			**Electric Production and Grid Balance**		
	unit	value		unit	value
Chiller consumption	kWh	11400	PV production	kWh	56460
Light and appliances	kWh	11915	Grid import	kWh	0.00
Total electric load	kWh	23315	Grid export	kWh	33124

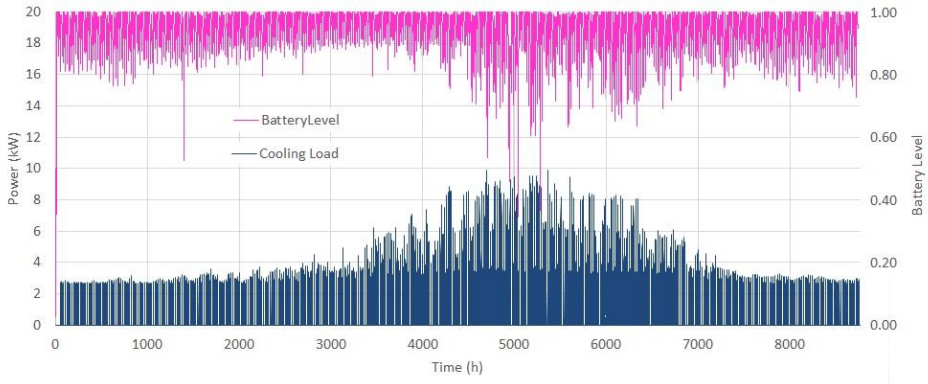

Fig. 2.6 - Cooling load and battery level

Figure 2.7 shows the trend of the heat pump cooling production and power consumption for two typical summer days. The resulting COP (according to the chiller performance map) results to be strongly affected by the high ambient temperatures. The cooling load rises a few hours before the PV production and the energy is taken from the batteries. Chiller consumption is higher in the morning when internal temperature must shift from nighttime to daytime set point.

The patterns of power production and consumption are shown in Figure 2.8. The energy demand is met according to the following priority order: by PV (when available or sufficient), by batteries and, in the last case, by import from the grid. Power consumption for appliances and light depends on the occupancy and the activities in the thermal zones. The PV field drives the heat pump as priority and the surplus recharges the battery pack. The electricity overproduction, when the battery level is full, is delivered to the grid according to a net-metering scheme.

Figure 2.9 shows the annual energy fluxes: PV production, total power consumption (heat pump, light and appliances) and the export to the network on a monthly basis. In winter months, when the cooling request is low and the heat pump efficiency is high thanks to the low ambient temperature, the electric energy delivered to the grid is around 70% of the global PV production. During the warm season this ratio decreases to 50%. The results show a perfect autonomy of the building even under severe load conditions: the PV field exports electricity to the grid for several hours, whilst importation does not occur all year round, making the house an Energy+ building able to operate also in Off-the-Grid conditions.

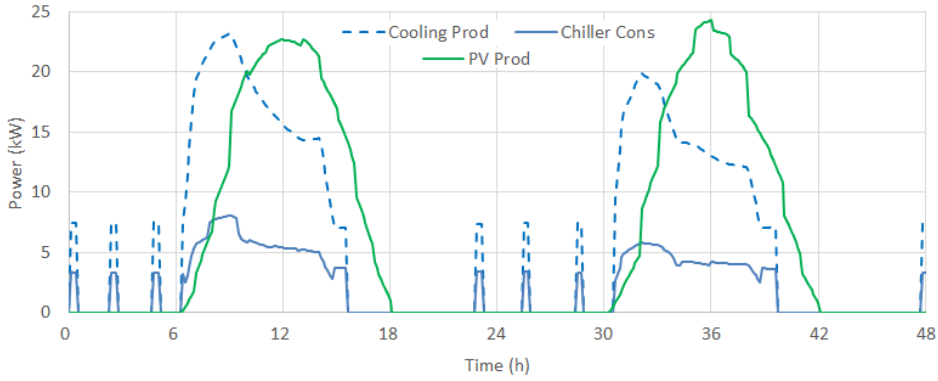

Fig. 2.7 - PV and heat pump energy fluxes

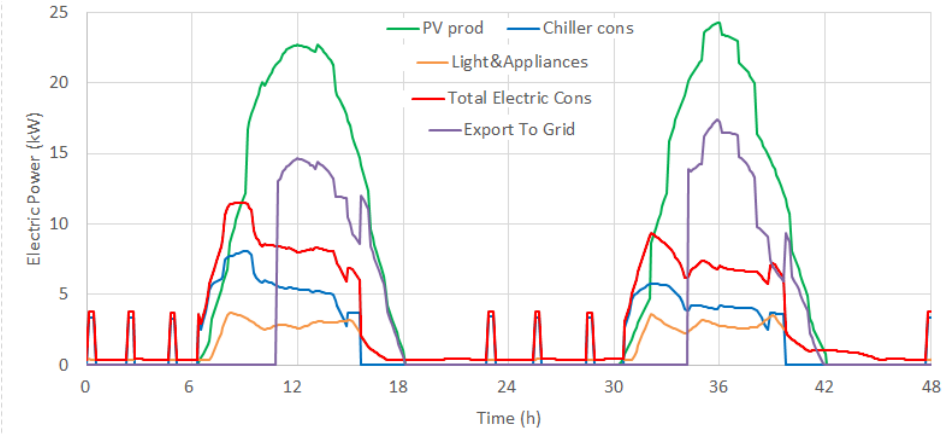

Fig. 2.8 - Grid exchange and consumption details

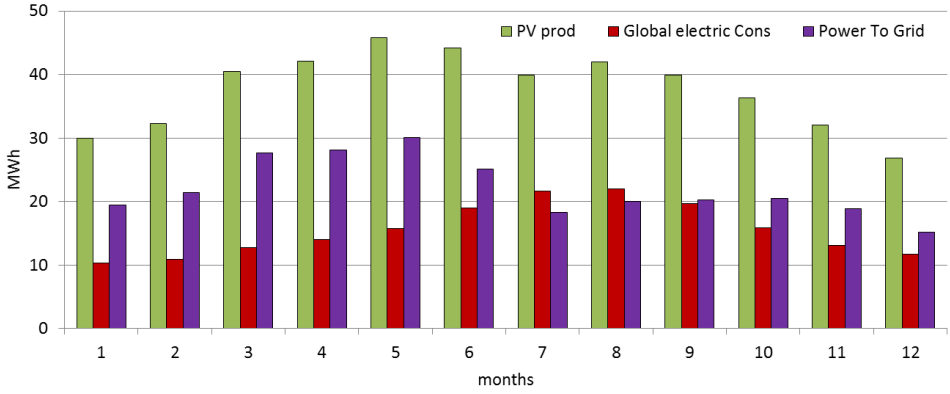

Fig. 2.9 - Monthly energy production, consumption and export

2.4 Building Model Validation

The Plus-Energy building has been fully instrumented. A monitoring system has been installed for a remote real time access to all collected data (with a frequency of 1 sample per second). This equipment makes possible to monitor with high level of detail the building energy performance under real operating conditions. The monitoring system includes thermocouples in the wall layers, thermo-hygrometers in the rooms, power meters on the PV field, the battery package and all electric boards, temperature and flow rate sensors in all circuits of the HVAC system. Table 2.6 summarizes the main monitoring data.

Table 2.6 - Monitoring system equipment

Weather	**PV Field & Grid**
Ambient temperature	PV production
Ambient Humidity	Grid Import/Export
Wind Velocity - Direction	Battery level
Radiation Parameters	Energy balance
Building Envelope (N-S-E)	**Cooling Plant**
Wall temperatures (int/ext)	Cooling production
Roof temperatures (int/ext)	Chiller electric consumption
Floor temperatures	AHU in/out temperatures
Comfort	Floor cooling in/out temp.
Air temperature	Storage temperature
Humidity	Water Flowrate
CO2	**Thermal Loads**
Air velocity	Lighting consumption
Luminosity	Appliance consumption
	Office electronics

It has to be reminded that this building is a pioneering pilot-project. The goal is to prove that new sustainable construction standards are possible in the UAE and that this is a viable solution to reduce the carbon footprint in the region. The monitoring activity is fundamental to demonstrate that the predicted performance is confirmed under real operating conditions.

Figures 2.10 - 2.13 show the simulation results and the experimental data for two consecutive days in September. Figure 2.10 refers to the cooling demand. The curves related to the model prediction (dashed line) and the measurements (solid line) exhibit a very good superposition: the model appears able to estimate the peak values, the hourly trend and the daily

integral value. As mentioned before, in addition to the overall thermal loads the Trnsys model can predict the trend of detailed parameters, like wall and roof temperatures. Figure 2.11 shows the trend of internal and external temperatures for the well-insulated roof. The daily pattern for the outer side temperature (influenced by the incident solar radiation and the ambient temperature) is well predicted, in spite of a small time shift. The inner side temperature is perfectly estimated.

Moving to the energy systems, Figure 2.12 reports the 48-hour trend of the PV production and the power consumption due to light and appliances and for the chiller operation. The chart shows a small underestimation of the PV power output (-9.5% as integral value), whilst the power consumption for lighting and electrical equipment is very well predicted. A far as the chiller consumption is concerned, the monitored data show a slightly different patterns during the day and higher peak levels. The hourly variation of the power input is related to the trend of the real cooling demand documented in Fig. 2.10, while the higher peak levels and the higher daily integral values indicate a lower-than-expected chiller efficiency (-12.8%).
As mentioned in the previous paragraphs, when the batteries are full charged the electricity surplus is supplied to the grid. Figure 2.13 shows the power export compared to the PV production. The model exhibits a good capability to predict the amount of electricity delivered to the grid and the time interval of the power exchange. When the battery package is full (at 11.30 a.m.) the model predicts an instantaneous shift to the exportation mode, whilst monitoring data show a soft ramp starting 2 hours before achieving the full capacity condition: this is due to the physical behavior of the electric storage that is not perfectly implemented in the model. Nevertheless, the integral value of the exported electricity is well predicted: the error model vs. monitoring is only 2.0%

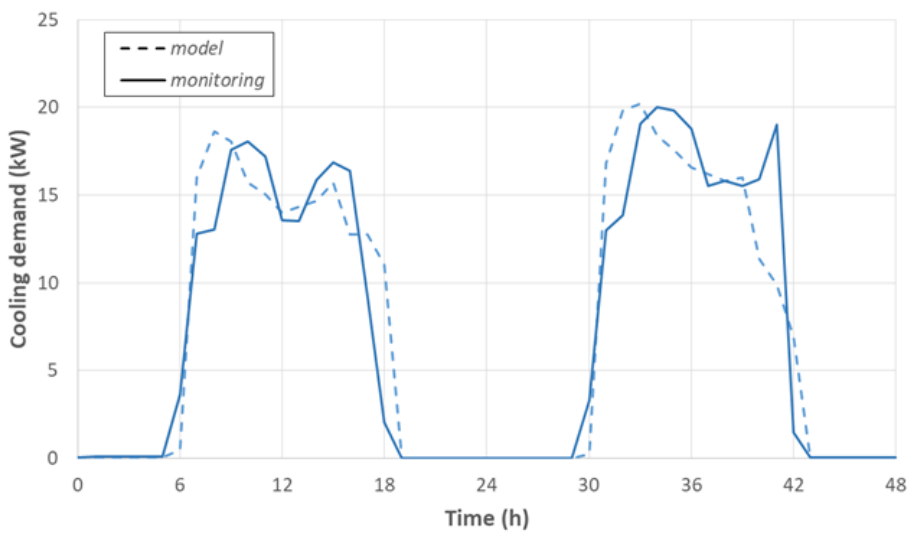

Fig. 2.10 - Cooling demand (model vs. monitoring).

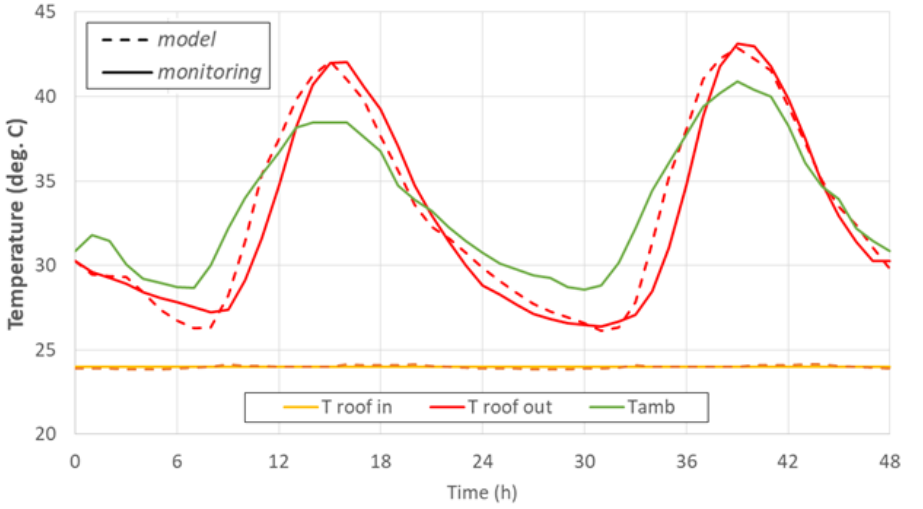

Fig. 2.11 - Roof temperature (model vs. monitoring).

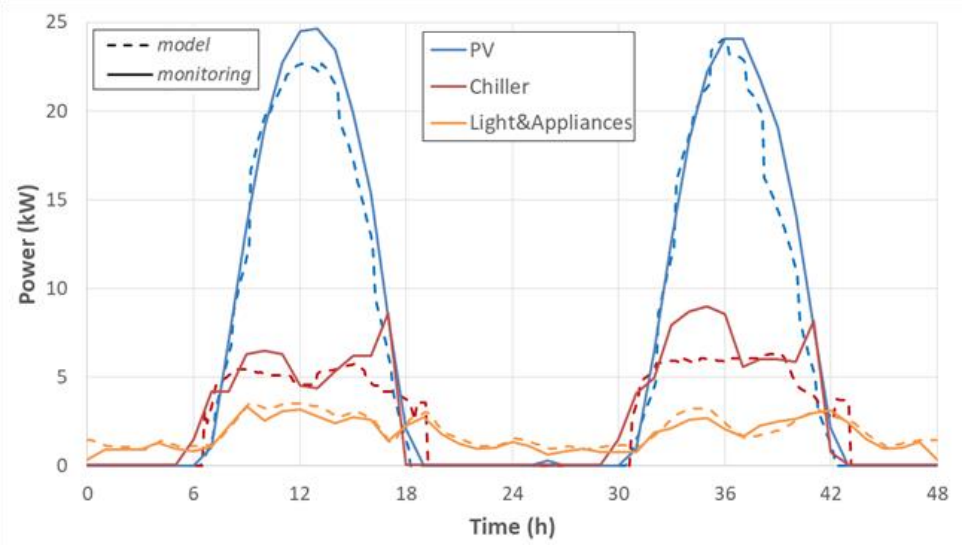

Fig. 2.12 - Power production and consumption (model vs. monitoring)

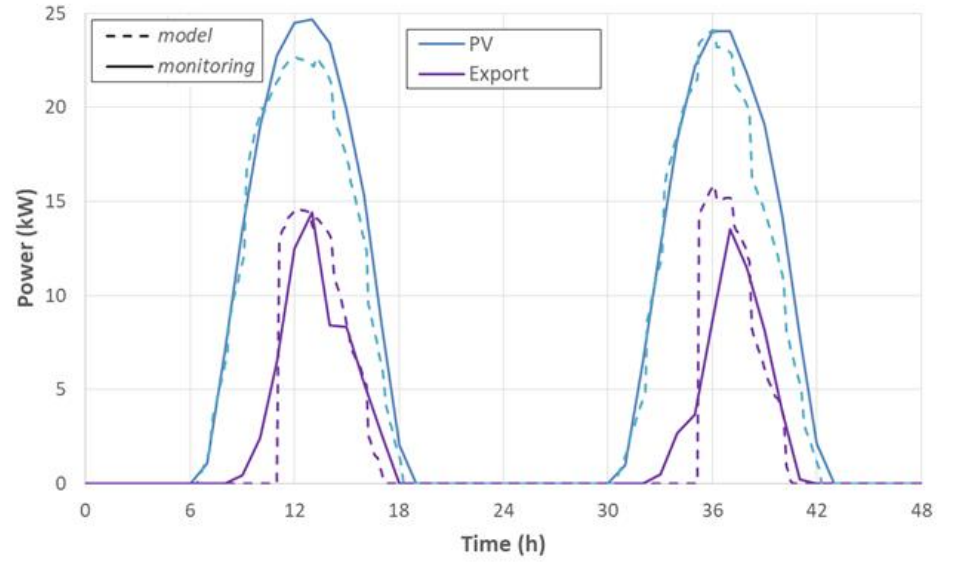

Fig. 2.13 - PV production and electricity export (model vs. monitoring)

2.5 Comparative and Economic Analysis

The demonstrative building is designed for offices, but since its design, the goal is to develop a solution for a residential version for the new low-impact compounds. For this reason, new building standards have been developed such as the Green Building Regulation and Specification [25] of the Government of Dubai and the Green Building Guidelines [26] by the Central Government of the United Arab Emirates.

To assess the behavior of the developed building its energy performance has been compared with other buildings that meet different regulations.

To perform this analysis, simulations of three different types of construction have been simulated: the real building (called Passive House) in a residential version, the building that respects the government's guidelines (GreenBuilding) and the version built according to the previous construction standards (Standard building).

Table 2.7 shows the input parameters of the simulation for the three building types. The first part of the table shows the set points and loads used in the simulations. The second part shows the parameters of opaque and transparent surfaces, these parameters comply with the above mentioned norms.

Table 2.8 shows simulation results for the selected buildings. The table is divided into two parts, the first part presents the results with the energy performance, the second one shows the comfort parameters obtained.

The annual cooling load of the Passive House is only 20% of the Standard building request.

Even the Green Building is an improvement with respect to the standard building and represents the target for new buildings.

Table 2.7 - Comparative analisys parameters

	unit	Passive House	GreenBuilding	Standard
Destination		residential	residential	residential
Location		Dubai	Dubai	Dubai
Cooling system		Air + Floor	Air cooling	Air cooling
Set-point and loads				
Set point temperature	deg. C	24	24	22
Humidity set point	%	55	55	55
Ventilation	Vol/h	0.3	0.3	0.6
Heat exchanger efficicency	%	80	0	0
Infiltration	Vol/h	0.06	0.4	0.5
Ligh	W/m2	5	5	20
Internal gains max	kW	3	3	3
Occupancy	Nr.	10	10	10
Walls and windows				
U wall	W/m2K	0.063	0.57	0.57
wall thickness	m	0.603	0.27	0.22
wall solar absorptance	%/100	0.3	0.3	0.4
U roof	W/m2K	0.061	0.3	0.44
roof thickness	m	0.566	0.27	0.29
roof solar absorptance	%/100	0.2	0.2	0.4
windows U-value	W/m2K	0.7	1.9	2.89
windows G-value	%/100	0.294	0.621	0.789

Table 2.8 - Comparative analysis results

	unit	Passive House	GreenBuilding	Standard
Destination		residential	residential	residential
Location		Dubai	Dubai	Dubai
Cooling system		Air + Floor	Air cooling	Air cooling
Energy performance				
P load max - air - sensible	kW	3.46	18.30	35 .00
P load max - air - latent	kW	7.62	20.56	16.84
Pload max - air	kW	10.35	37.02	49.57
Pload max - floor	kW	2.81	0.00	0.00
Pload max - Total	kW	13.09	37.02	49.57
Pload max - Total	%	-73.6%	-25.3%	100
Q load annual - air - sensible	kWh	2922	55129	115338
Q load annual - air - latent	kWh	18303	49861	53784
Q load annual - air	kWh	21225	104990	169122
Q load annual - floor	kWh	15972	0	0
Q load annual - Total	kWh	37197	104990	169122
Q load annual - Total	%	-78.0%	-37.9%	100
Comfort performance				
TMR - max	deg. C	24.23	25.31	26.27
TMR - min	deg. C	22.34	22.87	20.57
TMR - average	deg. C	23.66	24.07	23.80
TOP - max	deg. C	24.11	23.66	24.13
TOP - min	deg. C	22.25	22.43	20.34
TOP - average	deg. C	23.75	23.04	22.88
PMV - max	[-3:3]	0.26	0.11	0.23
PMV - min	[-3:3]	-0.27	-0.28	-0.76
PMV - average	[-3:3]	0.16	-0.05	-0.09
PPD - max	%	6.51	6.58	17.22
PPD - min	%	5.00	5.00	5.00
PPD - average	%	5.69	5.15	5.66

Part of the results are shown in the following charts, Figure 2.14 shows the duration cooling load curves for the three building versions. The peak load of the PassivHaus is a fraction of the standard building and the trend of the curve shows the efficiency of the envelope and the design adopted.
Figure 2.15 shows the monthly cooling load that highlights the cooling demand difference, especially in summer months when the passive house require a very low energy input.

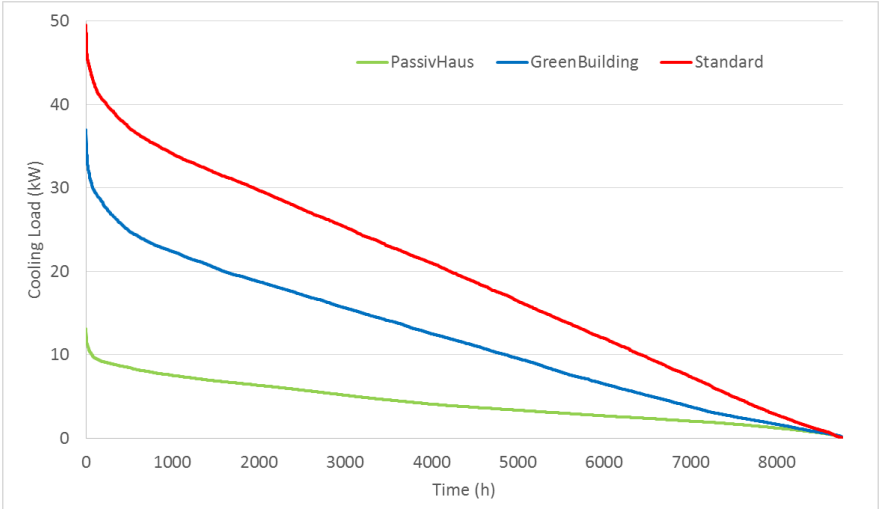

Fig. 2.14 - Load duration curve of different building envelope

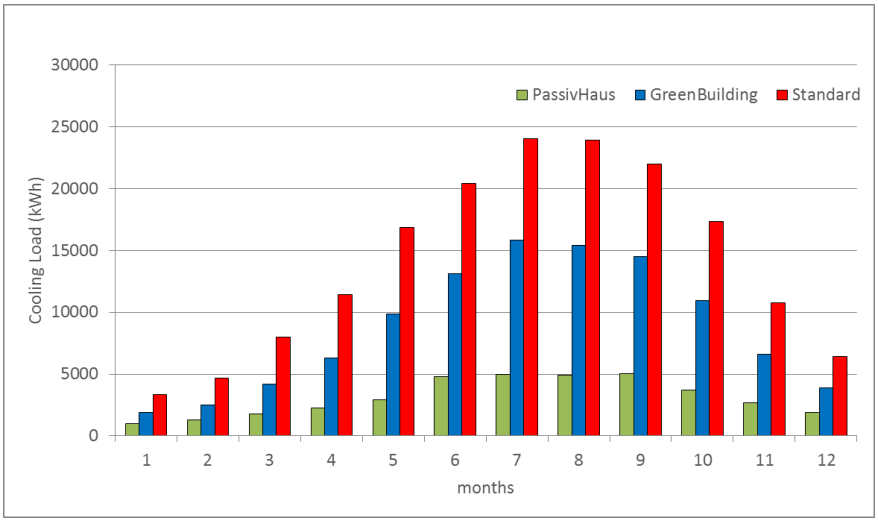

Fig. 2.15 - Monthly cooling load of different building envelope

2.5.1 Selected building

The use of the off-the-grid design for building of a district cooling development is penalized, the high performance achieved makes the distribution network cost untenable. The building model chosen is the one that meets the requirements of the Green Building Regulation based on the geometry used for the prototype.

This is the model that will be realized in the coming years and the one to which solar district cooling technology would best apply.

Table 2.9 shows the results of the simulations for the selected building in terms of peak power and annual cooling load for the two locations.

Cooling load and duration curve are shown in the figure 2.16.

The cooling load differences highlighted are the result of the diversity between the climates of the two selected locations. For the same building, changing the location, the cooling load doubles both in terms of peak power and annual cooling energy.

Table 2.9 - Green Building cooling loads

Dubai (UAE)			**Riyadh (KSA)**		
Peak Load	**unit**	**value**	**Peak Load**	**unit**	**value**
Sensible Cooling Load	kW	18.30	Sensible Cooling	kW	17.67
Latent Cooling Load	kW	20.56	Latent Cooling	kW	3.98
Total Cooling Load	kW	37.02	Total Cooling Load	kW	17.77
Annual Load	**unit**	**value**	**Annual Load**	**unit**	**Value**
Sensible Cooling Load	kWh	55129	Sensible Cooling	kWh	48162
Latent Cooling Load	kWh	49861	Latent Cooling	kWh	417
Total Cooling Load	kWh	104990	Total Cooling Load	kWh	48579

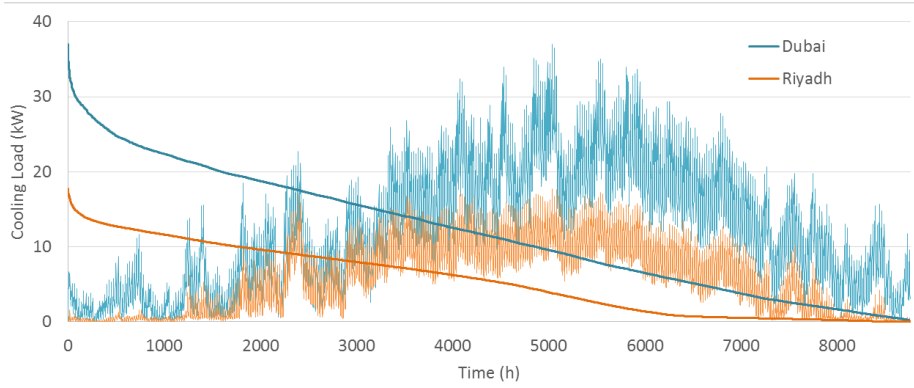

Fig. 2.16 - Cooling load of the Green Building in the two selected location

3 District Cooling

The district network has attracted great interest over the last decades thanks to the undeniable energy, environmental and economic benefits that it offers accompanied by high efficiency and reliability. Boran and al. [1] examine the district heating systems and conclude that they allow an environmental saving of CO_2 equal to 33%.

Many papers focus on improving the system at the network level. The operation is analyzed in [2] in which an efficient numerical model of the network is provided based on a quasi-static model for the hydraulic and transient model for the thermal part.

The growth of district cooling systems is due to the development and marketing of absorption chillers: Mohammad Ameri and Zahed Besharati [3] evaluate different integration scenarios including cogeneration, trigeneration and district heating and cooling.

Wenjie Gang et al. [4], have investigated the integration of the district cooling system in a trigeneration plant serving a residential compound with a consequent increase in the economic, environmental and energy savings.

Technological developments have continued with the integration of renewable sources as in [5] where Peng YenLiew et al. analyzed and presented several proposals to achieve a complete combination of energy systems in different types of building complexes.

3.1 Models and Optimization

The models presented in this chapter are the result of a parametric analysis to obtain the best district cooling configuration. The simulations aim to identify the combination that ensures the best balance between thermal loss and load losses.

In Figure 3.1 is represented the compound topology hypothesized with the typical size of the new Dubai districts.

The project is based on four sub-districts of 24 buildings for a total of 96 buildings and 12000 m of piping. Each sub-district is supplied by a dedicated pump group and comprises three blocks of 8 individual buildings.

The chiller station is positioned laterally to the compound to reduce the size of the network and simultaneously close to the solar field and the storage tanks.

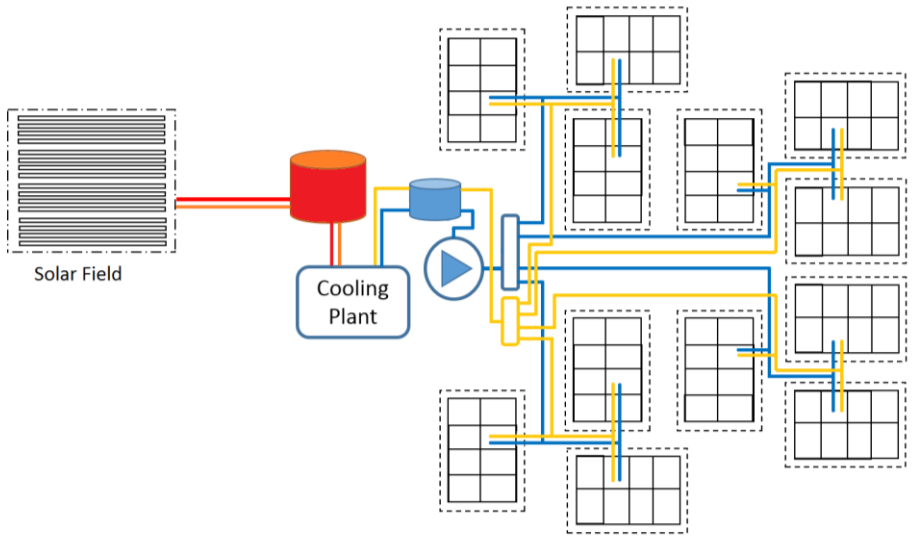

Fig. 3.1 - Topology of the selected district cooling network

The analyzed configurations cover the market available standards for pipe diameters and insulation thickness, even water speeds setting represent the standard for district applications.
Water speed and insulation thickness are taken into account in order to perform a parametric analysis that can compare both the thermal and the mechanical aspects. The best isolation study for district cooling networks was developed by Lund and Mohammadi in [6].
Table 3.1 lists the network configurations that are being analyzed. The insulation thickness selected ranges from 1" to 4" according to the market availability. The selected water speed values reflect different design philosophies from 1 m/s up to 2.65 m/s, beyond which the load losses become unsustainable. The parametric analysis was conducted for Dubai conditions and the network design parameters were extended to the conditions of Riyadh.

Table 3.1 - Cooling network models

	Insulation (inch)		
Max Speed (m/s)	1	2	4
1.00	N1	N2	N3
2.00	N4	N5	N6
2.65	N7	N8	N9

The computation of the thermal losses of the grid to the ground depends on the type of piping and the soil considered. For each combination of insulation thickness and maximum speed, thermal losses in W/m have been calculated and used in the successive simulations in Trnsys to achieve total annual losses in transient mode (Fig. 3.2). Table 3.2 presents the starting parameters for the thermal part of the calculated network characteristics.

Table 3.2 - Thermal characteristics of pipes (Dubai based)

		D (m)	Thick Insu (inch)	A disper (m2/m)	Rind (m)	Q (W/m)	Q int (W/m2K)
V = 1.00 m/s	**N1**	0.12	1	0.377	0.458	11.672	1.290
		0.17	1	0.534	0.747	13.423	1.047
		0.2	1	0.628	0.931	14.228	0.943
	N2	D (m)	Thick Insu (inch)	A disper (m2/m)	Rind (m)	Q (W/m)	Q int (W/m2K)
		0.12	2	0.377	0.331	8.422	0.931
		0.17	2	0.534	0.555	9.985	0.779
		0.2	2	0.628	0.705	10.768	0.714
	N3	D (m)	Thick Insu (inch)	A disper (m2/m)	Rind (m)	Q (W/m)	Q int (W/m2K)
		0.12	4	0.377	0.233	5.924	0.655
		0.17	4	0.534	0.393	7.070	0.552
		0.2	4	0.628	0.503	7.681	0.509
V = 2.00 m/s	**N4**	D (m)	Thick Insu (inch)	A disper (m2/m)	Rind (m)	Q (W/m)	Q int (W/m2K)
		0.08	1	0.251	0.254	9.701	1.608
		0.12	1	0.377	0.458	11.672	1.290
		0.14	1	0.440	0.570	12.447	1.179
	N5	D (m)	Thick Insu (inch)	A disper (m2/m)	Rind (m)	Q (W/m)	Q int (W/m2K)
		0.08	2	0.251	0.179	6.855	1.136
		0.12	2	0.377	0.331	8.422	0.931
		0.14	2	0.440	0.417	9.092	0.861
	N6	D (m)	Thick Insu (inch)	A disper (m2/m)	Rind (m)	Q (W/m)	Q int (W/m2K)
		0.08	4	0.251	0.127	4.852	0.804
		0.12	4	0.377	0.233	5.924	0.655
		0.14	4	0.440	0.293	6.404	0.607
V = 2.65 m/s	**N7**	D (m)	Thick Insu (inch)	A disper (m2/m)	Rind (m)	Q (W/m)	Q int (W/m2K)
		0.07	1	0.220	0.208	9.092	1.723
		0.1	1	0.314	0.352	10.768	1.428
		0.12	1	0.377	0.458	11.672	1.290
	N8	D (m)	Thick Insu (inch)	A disper (m2/m)	Rind (m)	Q (W/m)	Q int (W/m2K)
		0.07	2	0.220	0.147	6.404	1.213
		0.1	2	0.314	0.251	7.681	1.019
		0.12	2	0.377	0.331	8.422	0.931
	N9	D (m)	Thick Insu (inch)	A disper (m2/m)	Rind (m)	Q (W/m)	Q int (W/m2K)
		0.07	4	0.220	0.104	4.555	0.863
		0.1	4	0.314	0.177	5.409	0.717
		0.12	4	0.377	0.233	5.924	0.655

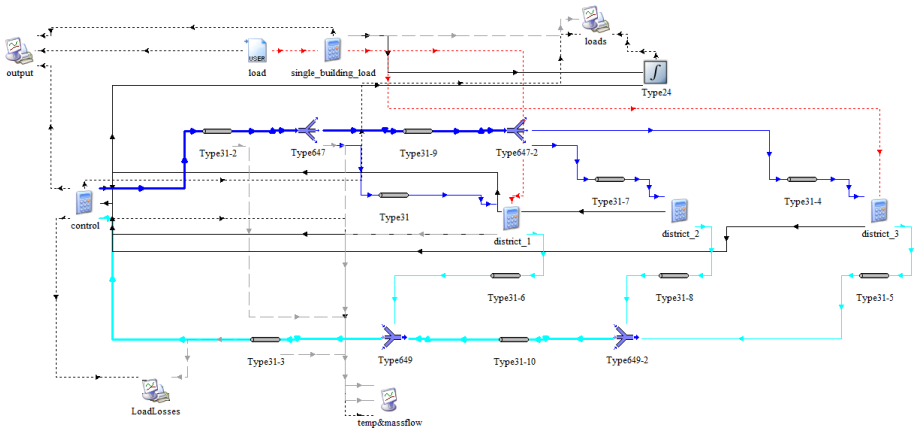

Fig. 3.2 - Trnsys deck of sub-district thermal loss computation

The major load loss analysis is performed with a quasi-static approach.
For each time-step, the network load losses due to the speed of water is calculated. In the computation, only distributed load losses are considered.
The analysis of the load losses and the power required by the pumping station are detailed analyzed in [7] and the authors concluded that the use of variable speed pumps increases the efficiency of the system. Pirouti, Marouf, et al in [8] proposed to increase the temperature difference between delivery and return. The analysis also suggests the use of higher speeds to reduce the pipes size even if it involve an increase in load losses.

3.2 Simulations and Results

District cooling simulation results are presented in the form of comparative graphs, avoiding listing all the numerical data.
Figures 3.3 and 3.4 show the values of thermal losses, peak and annual, with the different insulation thicknesses analyzed and the different hypothesized speeds.
Starting from these results, also in the form of a bar chart in Figure 3.5, the benefit of the increase in isolation is well underlined. Even the increase in the maximum water speed in the branch reduces thermal losses but, as opposed to isolation, leads to increased load losses and, therefore, higher pumping costs (Figures 3.6 and 3.7). On the other side, reducing the speed in the pipes entails less leakage but increases thermal losses and also the cost of the network. In fact, lower speed means larger diameters with increased digging costs and buried material. Increasing insulation also increases the cost but lesser than modifying the diameters as reported in the economic analysis.

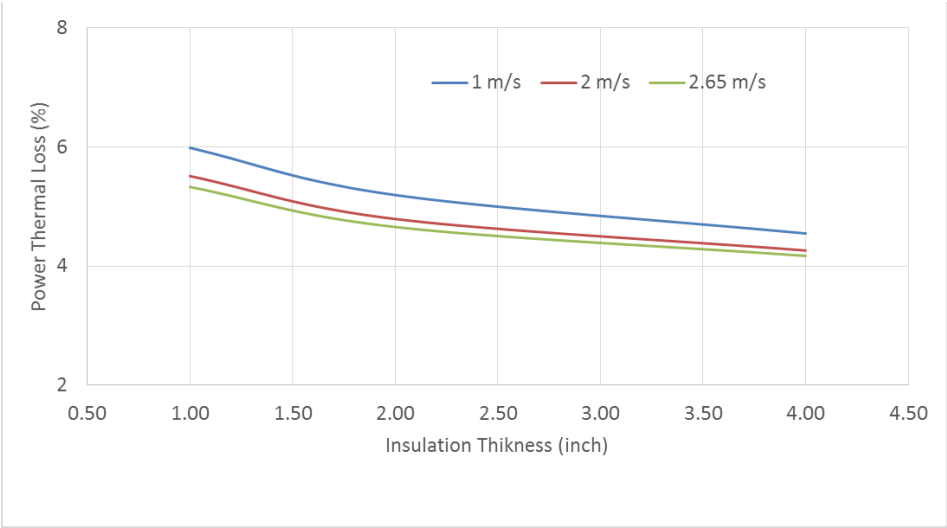

Fig. 3.3 - Power thermal loss for different maximum water speed

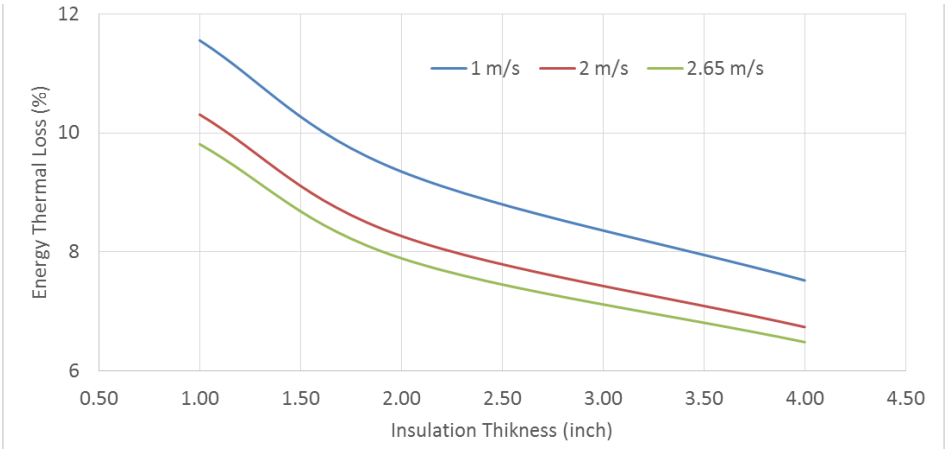

Fig. 3.4 - Annual thermal loss for different maximum water speed

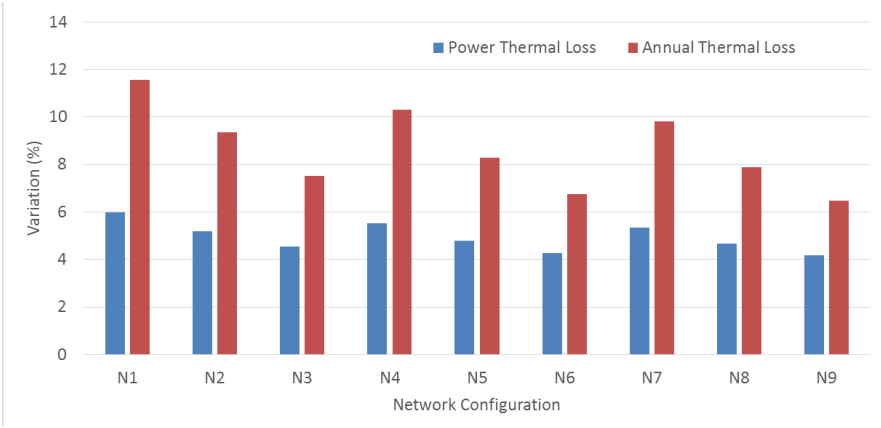

Fig. 3.5 - Thermal loss (power and energy) for different configurations

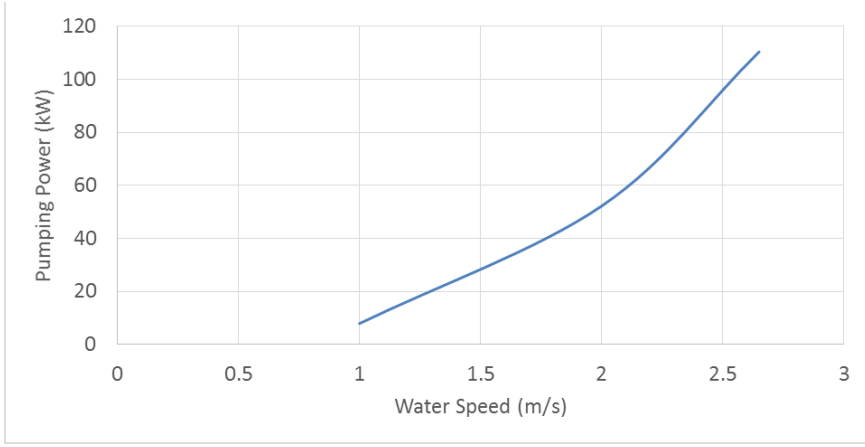

Fig. 3.6 - Peak pumping power for different water speed

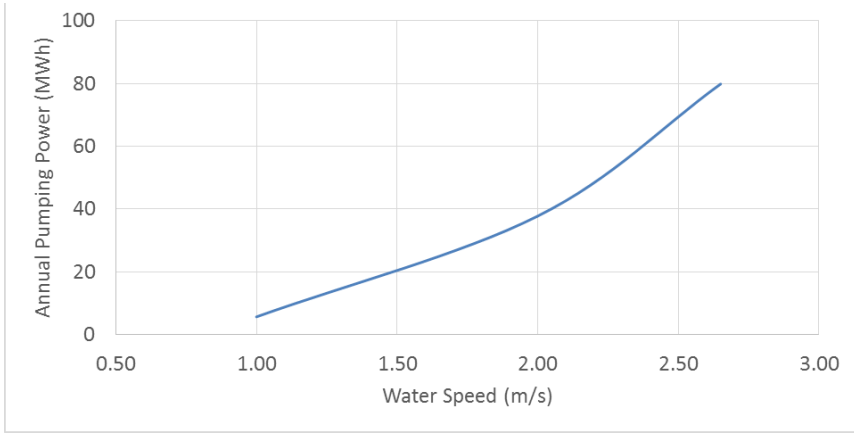

Fig. 3.7 - Annual pumping energy consumption for different water speed

Figures 3.8 and 3.9 show the peak and annual major load losses for all configurations, based on the diameters used. The N6S case represents the N6 configuration in the Riyadh conditions.

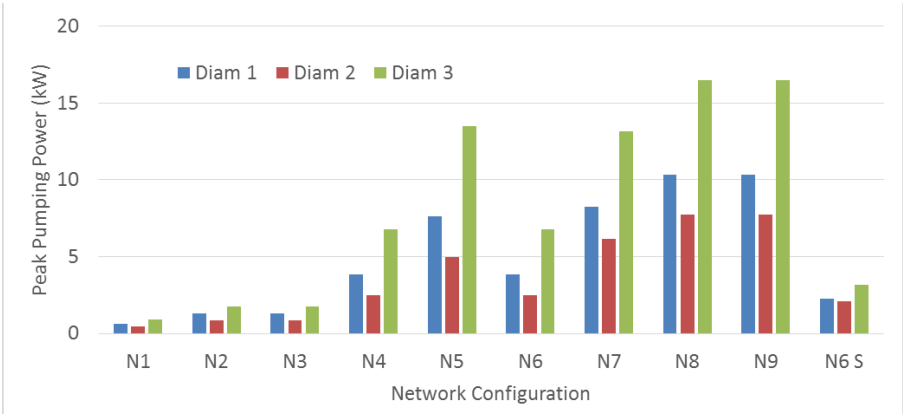

Fig. 3.8 - Sub-district (24 houses) pumping power for different branches

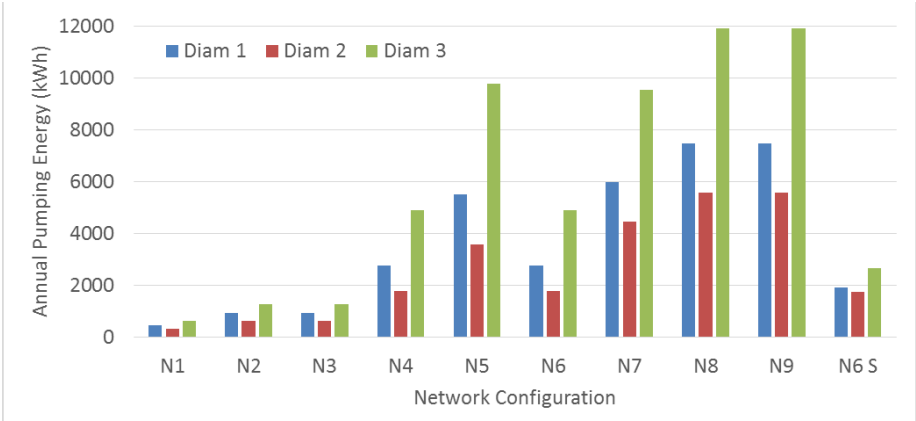

Fig. 3.9 - Sub-district (24 houses) annual pumping energy for different branches

3.3 District Network Economic Analysis

The costs of the district network was estimated starting from published data both technical report [9] as scientific papers [10, 11].

Figure 3.10 shows the results of parametric analysis carried in economic terms. The trend highlights the increase in the cost of the network respect the insulation rises, more than proportional to the diameter of the pipes. Setting high speeds is counterproductive because cost savings are balanced by increased load losses that grow exponentially with speed.

The cost for different configurations is not derived from a proportional count but reflects the real composition of the network in terms of diameters used and pipes lengths. In addition, for example, the cost of the heat transfer substation remains fixed in all configurations because it is not affected by the cost of branches.

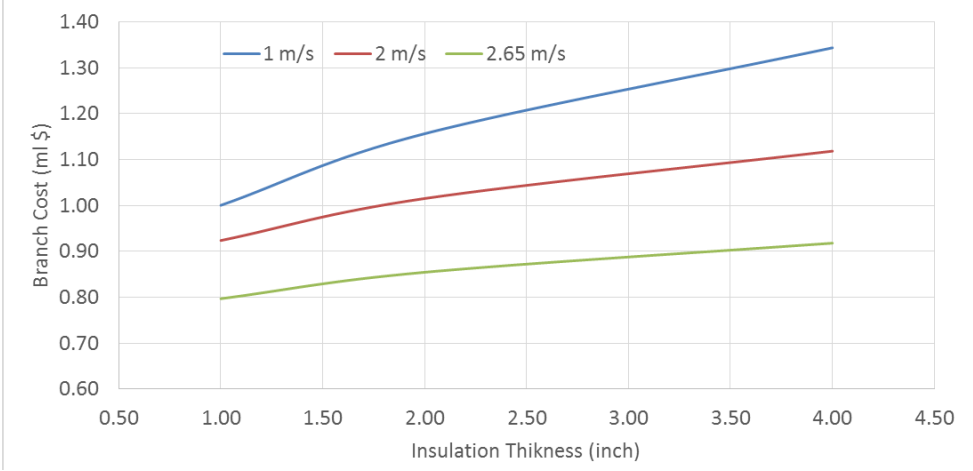

Fig. 3.10 - Parametric analysis of district network cost

3.4 Selected District Network

From economic analyzes in literature, it is well-established that optimum speed is about 1.5-2.5 m/s, the reported speed minimizes investment without causing expensive load losses [12].

Based on these values, the configuration with a maximum speed of 2.00 m/s and a 4" (0.10 m) of insulation was selected in the previous parameter analysis. The numerical value of load losses in Pa/m is similar to that obtained in [19] by Yan et al.

Table 3.3 shows the piping parameter adopted and the Table 3.4 listed the values of the district network performance used in simulations of solar cooling systems.

The Table 3.5 shows the network cost for the selected case divided into the main items.

Table 3.3 - Selected charecteristics of piping

V = 2.00 m/s	DUBAI					
	D (m)	Thick Insu (inch)	A disper (m2/m)	Rind (m)	Q (W/m)	Q int (W/m2K)
	0.08	4	0.251	0.127	4.852	0.804
	0.12	4	0.377	0.233	5.924	0.655
	0.14	4	0.440	0.293	6.404	0.607
	RIYADH					
	D (m)	Thick Insu (inch)	A disper (m2/m)	Rind (m)	Q (W/m)	Q int (W/m2K)
	0.06	4	0.188	0.083	4.242	0.938
	0.08	4	0.251	0.127	4.852	0.804
	0.1	4	0.314	0.177	5.409	0.717

Table 3.4 - Selected district cooling performance

Dubai (UAE)			**Riyadh (KSA)**		
Peak Load	**unit**	**value**	**Peak Load**	**unit**	**value**
Single building load	kW	36.79	Single building	kW	17.64
Input load	kW	3531.60	Input load	kW	1693.80
Output load	kW	3682.09	Output load	kW	1782.94
Thermal loss	kW	150.49	Thermal loss	kW	89.14
Thermal loss	%	4.26	Thermal loss	%	5.26
Pumping Power	kW	52.20	Pumping Power	kW	29.93
Annual Load	**unit**	**value**	**Annual Load**	**unit**	**Value**
Single building load	kWh	104987	Single building	kWh	48578
Input load	kWh	10078748	Input load	kWh	4663466
Output load	kWh	10757895	Output load	kWh	5103308
Thermal loss	kWh	679147	Thermal loss	kWh	439842
Thermal loss	%	6.74	Thermal loss	%	9.43
Pumping Energy	kWh	37773	Pumping Energy	kWh	25313

Table 3.5 - District cooling network cost

DISTRICT NETWORK			
		Dubai (UAE)	**Riyadh (KSA)**
Infrastructure	Ml USD	0.510	0.367
Branch	Ml USD	0.388	0.307
Heat Interface Unit & Heat Meter	Ml USD	0.221	0.221
TOTAL COST	**Ml USD**	**1.118**	**0.895**

4 Solar Cooling Models

Various types of solar cooling systems located in hot climates can be taken into consideration and many studies make a careful analysis [1].
Solar cooling technologies include open-cycle systems, like Desiccant Evaporative Cooling units, and closed-cycle systems, based on absorption or adsorption chillers. The systems based on absorption chillers represent the majority of installed units, due to the commercial availability of the chillers for a wide range of cooling capacity (from 15-35 kW up to hundreds of kW). In the open literature, a large number of papers investigates the performance of both solar cooling systems [2]. Many works discuss the influence of the temperature levels in the external circuits [3], and the fundamental role of the hot water storage tank between the solar field and the chiller. A further improvement has been derived from the integration of energy storage both in district heating [4, 5] as well as in district cooling: Powell and al. in [6] present a new methodology to optimize the operation of the cooling unit coupled with tanks.
Other authors focused the analysis on the control strategy, which can strongly affects the efficiency of the whole system: Shirazi et al. [7] analyzed the performance improvement due to the mass flow rate regulation thanks to a variable speed pump. In the best configuration, the overall performance increases by 11%.
Other studies have compared different technologies available for chiller absortion systems [8]. Components parameters must be set with great care as illustrated by Assilzadeh et al. in 2005 [9].

The cooling plants are sized to achieve a solar fraction of 0.70, peak loads was covered by backup systems based on compression chiller.
The solar fraction is calculated on the basis of equation 4.1 for the absorption/adsorption chiller systems. For the case of the PV-based system without storage, the equation is the eq. 4.2 that becomes the eq. 4.3 in the version equipped with battery and cold tank respecting the equivalence 4.4.

$$(4.1)\ SF = \frac{Q_{sol}}{Q_{load}} \cong \frac{Q_{abs}}{Q_{abs} + Q_{aux}}$$

$$(4.2)\ SF = \frac{Q_{sol}}{Q_{load}} \cong \frac{E_{PV}}{E_{chiller}}$$

$$(4.3)\ SF = \frac{Q_{sol}}{Q_{load}} \cong \frac{E_{PV} - E_{exp}}{E_{chiller}} = \frac{E_{chiller} - E_{imp}}{E_{chiller}}$$

$$(4.4)\ E_{PV} + E_{imp} = E_{chiller} + E_{exp}$$

4.1 Chiller Models

The following sections show and illustrate the models developed in Trnsys 17 to simulate solar cooling systems in detail.
All models presented with a solar field based on water collectors have a variable speed pump as suggested by the literature. There is also always a hot storage or battery.
The cold tank, present in some adopted configuration, has the function of prolonging the cooling capacity of the system and, at the same time, avoiding continuous chiller on/off.
Cold storage allows the use of the chillers in design conditions. The ratio between the hot tank and the cold tank volume is set equal to 2.

4.1.1 Compression Chiller (CC)

Cooling systems based on compression chiller represent most of the existing plants and continue to be installed as a backup in case of failure or to cover the peak load. In the investigated configurations, the compression chiller is indicated by the CC mark.

Trnsys models of the compression chillers used in the simulations come from the operating maps of a York model (kindly supplied by Johnson Control Italia). Tables 4.1 and 4.2 show the main parameters of the two chillers used.

The water-cooled version (Table 4.1) was implemented for simulations with a cooling system based on cooling tower, groundwater and ground heat exchanger. Tab 4.2 shows data for the air cooled version.

The compression chiller size is fixed to 1 MW and the cooling load is covered using units multiple chiller.

The Trnsys deck reproduces two configurations, with and without storage. In both cases, the energy is supplied by a photovoltaic field.

The first configuration does not include electrical or thermal storage, in this case the power grid is used as storage (Figure 4.1). Operative Trnsys deck of this configuration is very simplified as shown in Figure 4.2 where the chiller is coupled with Ground Heat Exchanger. This model represents a comparison for all subsequent models as it has an infinite capacity electrical storage at no cost.

Table 4.1 - Air cooled compression chiller technical data

Compression Chiller		
Nominal Capacity*	kW	1000
Rated COP*	-	3.36
Chiller water	kg/h	170000
Air flowrate	m^3/h	378000

*Chilled water 7-12 deg. C; air temp 35 deg. C.

Table 4.2 - Water cooled compression chiller technical data

Compression Chiller		
Nominal Capacity*	kW	1000
Rated COP*	-	5.65
Chiller water	kg/h	170000
Cooling water	kg/h	203000

*Chilled water 7-12 deg. C; cooling water 30-35 deg. C.

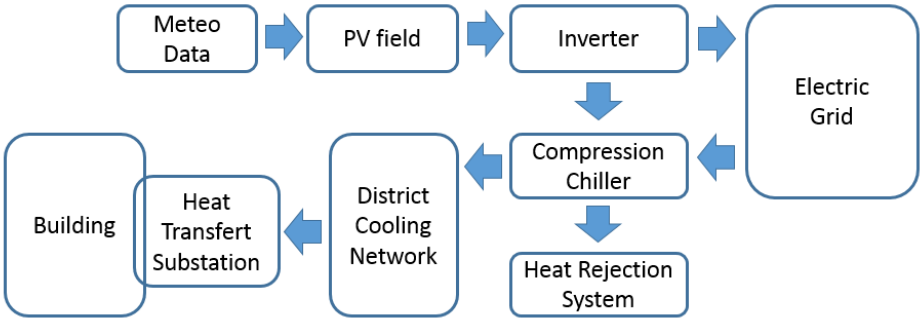

Fig. 4.1 - Block diagram of the solar cooling plant based on PV + compression chiller

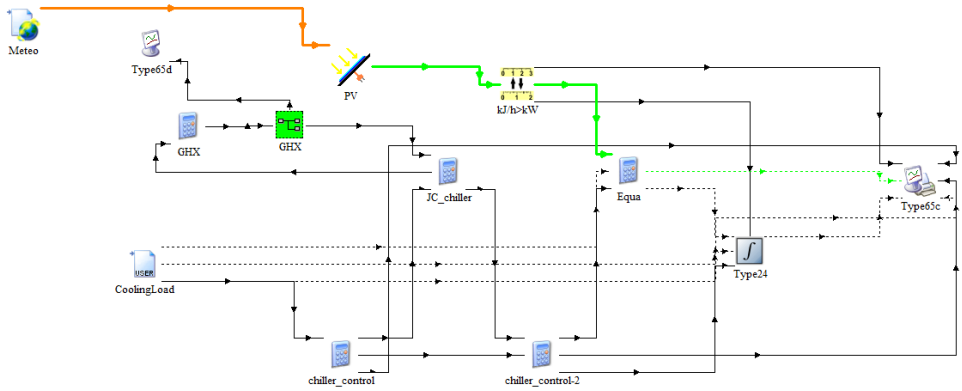

Fig. 4.2 - Operative Trnsys deck based on PV + CC + GHX

A second Trnsys model with a battery storage and a cold tank is developed to simulate the realistic version of a possible solar cooling application with a compression machine.

The energy produced by the photovoltaic field is converted and used primarily to cover the cooling load and then to recharging the battery. The electrical surplus is delivered to the network.

The cooling production is sent through a cold storage tank to the district cooling and delivered to the users (Fig. 4.3).

In the reported Trnsys Deck (Fig. 4.4), all the components mentioned and the evaporative tower heat recovery system can be recognized.

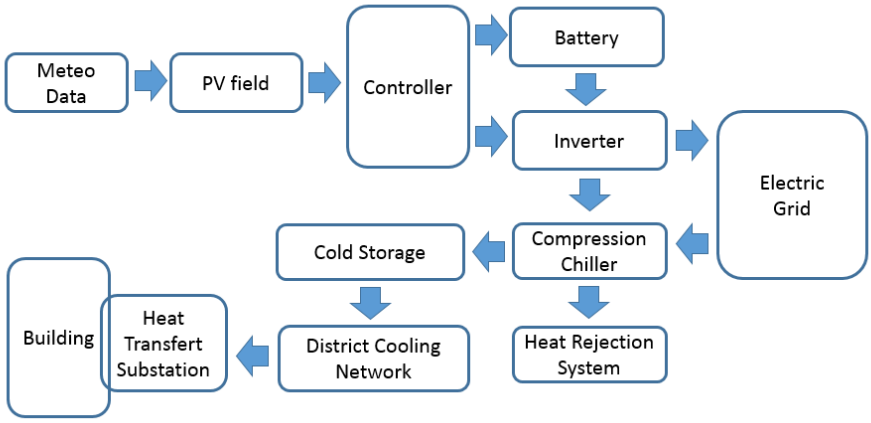

Fig. 4.3 - Block diagram of the solar cooling plant based on PV + compression chiller

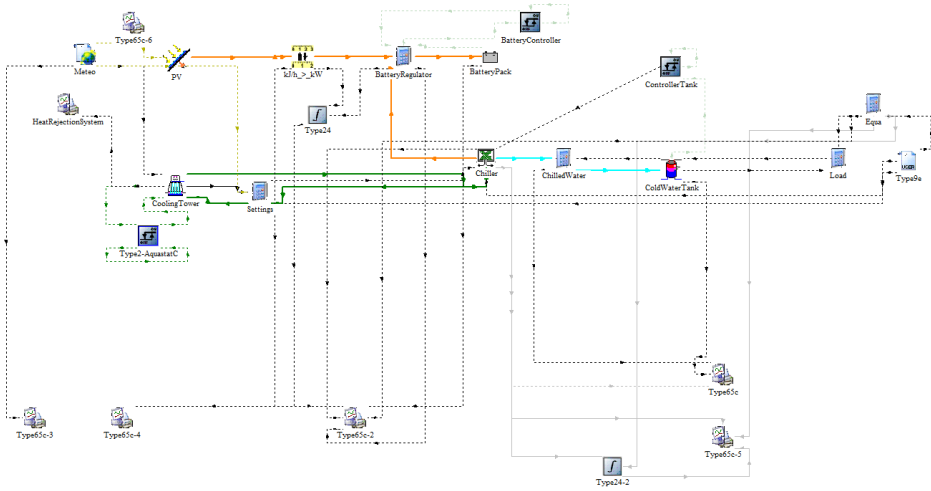

Fig. 4.4 - Trnsys operative deck of the PV+CC configuration

4.1.2 Single Effect Li-Br Absorption Chiller (ABS)

Absorption chiller driven by Solar Collectors is the most common solar cooling configuration [10]. The solar field provides heat to the hot storage tank, and a variable speed pump regulates the flow rate to keep the temperature level at the set point. The hot water tank drives the chiller, which is assumed to operate in On/Off mode (Figure 4.5). Figure 4.6 shows the operative Trnsys deck. A control system switches on the chiller when the temperature in the cold tank rises up to 10° C, whilst the chiller turns off at 5°C. An auxiliary chiller provides additional cooling when the absorption chiller is not able to keep the chilled water temperature under 11°C. Table 4.3 reports the design parameters related to the absorption chiller. An efficiency map of a commercial LiBr single-stage absorption chiller provides performance data for variable operating conditions (Fig. 4.7). The control system switches off the absorption chiller to avoid crystallization problems when hot water from the solar field and cooling circuit reach the lower (70°C) and upper (32°C) temperature limits respectively.

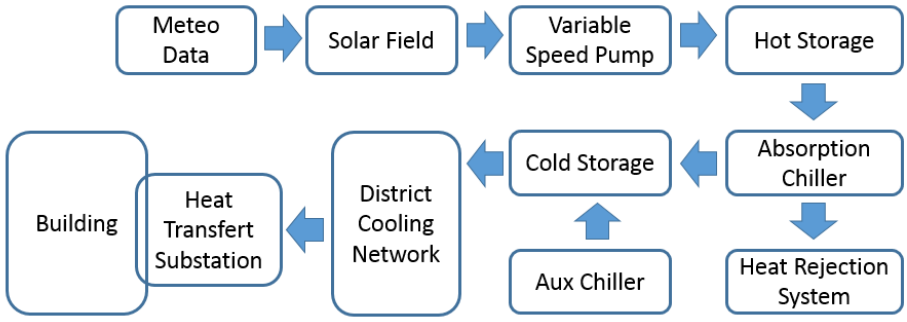

Fig. 4.5 - Block diagram of the solar cooling plant based on absorption chiller

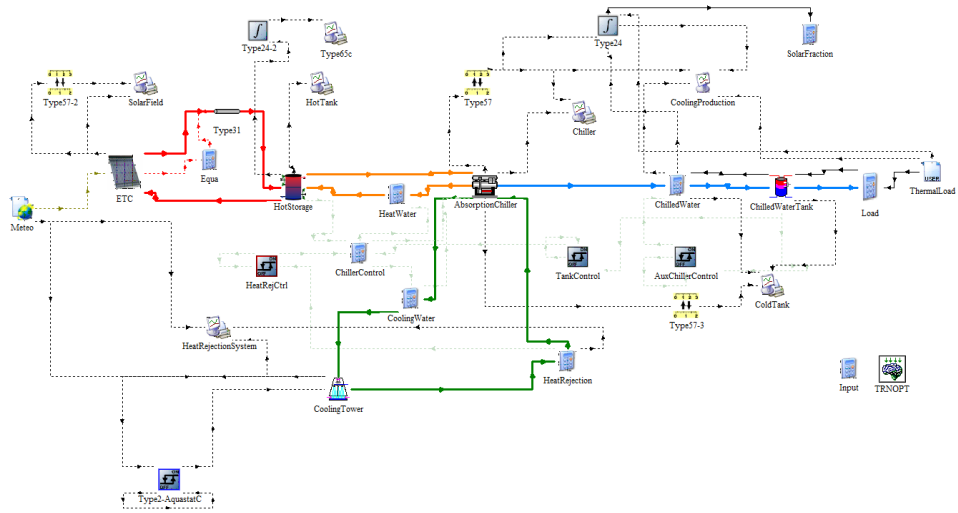

Fig. 4.6 - Trnsys deck of the solar cooling plant based on the absorption chiller

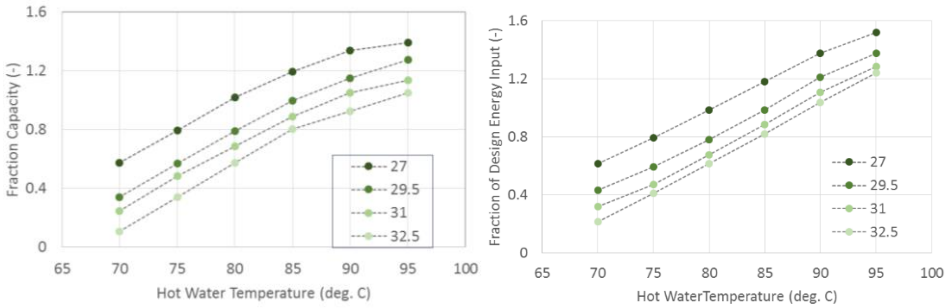

Fig. 4.7 - Performance maps of the absorption chiller

Table 4.3 - Absorption chiller technical data

Absorption Chiller		
Nominal Capacity*	kW	105
Rated COP*	-	0.6966
Chiller water	kg/h	16488
Cooling water	kg/h	55080
Hot water	kg/h	25920

*Chilled water 7-12.5 deg. C; cooling water 31-35 deg. C; hot water 88-83 deg. C.

4.1.3 Double Effect Li-Br Absorption Chiller (2sABS)

Double stage absorption chillers represent the new generation of chiller commercially available for solar cooling systems. Trnsys deck resemble the model developed for the Single Effect Absorption chiller in which control parameters have been modified. In this case the chiller is fed to hot water under pressure at a temperature of 165 deg. C so, even the whole solar circuit and the hot tank are under pressure with an increase in costs.
The control system, in this model, stop the chiller when the solar field and cooling circuit reach the lower (121°C) and upper (35°C) temperature limits respectively.
The model includes efficiency maps provided by manufacturer and reported in Fig. 4.8 and all model data are reported in Table 4.4.

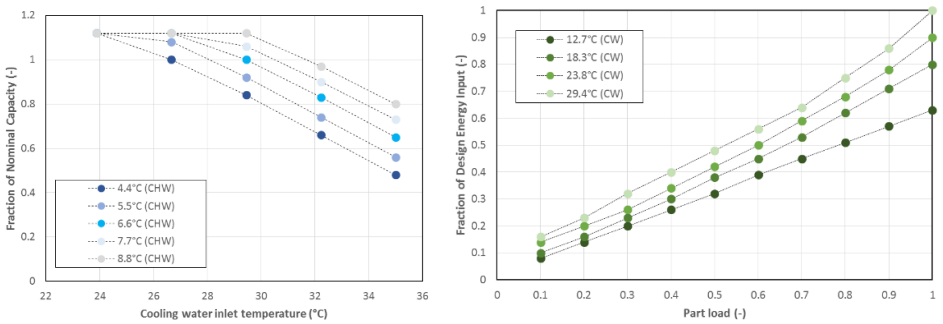

Fig. 4.8 - Performance maps of the double effect absorption chiler

Table 4.4 - Two stage absorption chiller technical data

2s Absorption Chiller		
Nominal Capacity*	kW	1163
Rated COP*	-	1.39
Chiller water	kg/h	200000
Cooling water	kg/h	245000
Hot water	kg/h	51200

*Chilled water 7-12 deg. C; cooling water 30-37 deg. C; hot water 180-165 deg. C.

4.1.4 Triple Effect Li-Br Absorption Chiller (3sABS)

The triple effect absorption fridge powered by hot water at a temperature of 220 deg. C is the model with the highest performance available. Triple-stage systems have been developed since the 90s, but the market version is only a few months old. There are few manufacturers with the triple-effect absorbing chiller in the catalog and, among them, water feeds are the minority. Table 4.5 reported the main parameters of the chiller and the operating maps are shown in Fig. 4.9.

Table 4.5 - Triple effect absorption chiller technical data

2s Absorption Chiller		
Nominal Capacity*	kW	1040
Rated COP*	-	1.62
Chiller water	kg/h	172000
Cooling water	kg/h	199000
Hot water	kg/h	26650

*Chilled water 7-12 deg. C; cooling water 28.5-35.5 deg. C; hot water 220-200 deg. C.

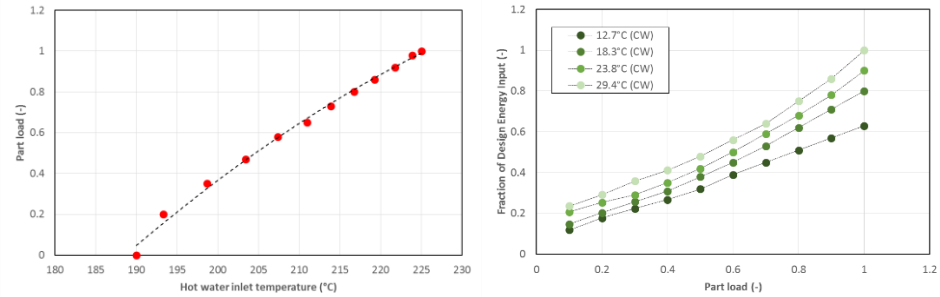

Fig. 4.9 - Performance maps of the triple effect absorption chiller

4.1.5 Adsorption Chiller (ADS)

The adsorption chillers are highly appreciated for the low temperature input required but the operating parameters must be set with great care [11]. The technical characteristics of the absorption chiller used in the simulations are listed in Table 4.6. The operating maps, supplied by the manufacturer, are shown in Figure 4.10.

Table 4.6 - Adsorption chiller technical data

Adsorption Chiller		
Nominal Capacity*	kW	1060
Rated COP*	-	0.603
Chiller water	kg/h	181000
Cooling water	kg/h	637000
Hot water	kg/h	270000

*Chilled water 9-14 deg. C; cooling water 31-34.8 deg. C; hot water 85-79.4 deg. C.

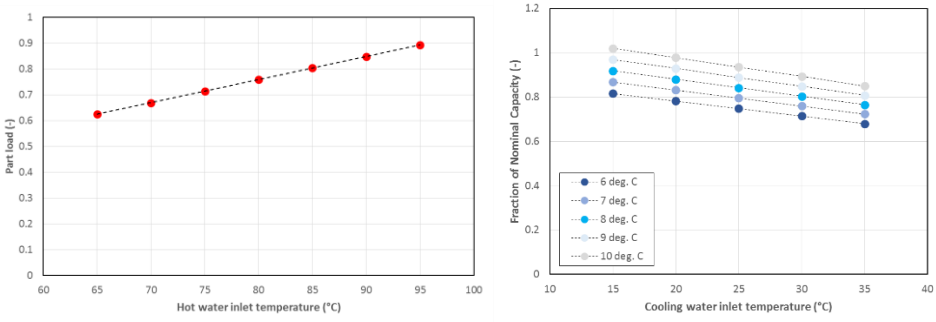

Fig. 4.10 - Performance maps of the adsorption chiller

4.1.6 Solar Desiccant Evaporative Cooling (DEC)

The influence of the ambient conditions is closely linked with Desiccant Evaporative Cooling systems, which produce the cooling effect by processing the ambient air, without a chiller contribution. Muzaffar et al. [12] developed a model to simulate DEC systems for five different climate zones worldwide.

Most works focus on the evaluation of the plant performance: Ma and Guan [13] investigated a DEC system installed in different Australian sites. Dayao et al. [14] discussed the behavior of renewable energy applications in buildings for different climate conditions in China.

Of this particular and promising air conditioning system three distinct models have been developed to recreate the operating conditions:

Ventilation (VEN), Ventilation Sensitive-Latent (VSL), Recirculation (REC).

4.1.6.1 Ventilation Configuration (VEN)

In a solar desiccant evaporative cooling system in ventilation configuration, the ambient air flow rate crosses all components from outside to the building. Firstly, the dehumidification occurs in the lower part of the desiccant wheel. Then, the temperature is lowered by crossing an air-to-air heat exchanger and by evaporative cooling. The exhaust air exiting the building is firstly saturated by humidification process; then, it is used to cool the entering fresh air and for the desiccant wheel regeneration. Solar contribution allows exhaust air to increase the temperature level up to 80°C before entering the rotor. An auxiliary chiller provides cooling effect when the DEC system is not able to keep temperature or humidity at the set points. This configuration is widely studied, for example Tobias Bader et al. [15] Analyze DEC in ventilation configuration, in different climates located in different regions around the world. The block diagram of DEC System is reported in Fig. 4.11 and the Trnsys deck of the considered DEC system is reported in Fig. 4.12.

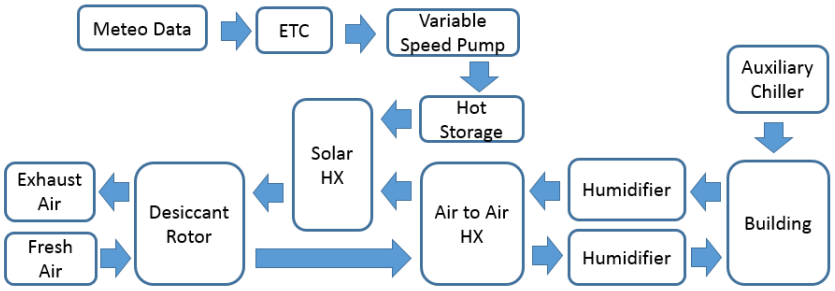

Fig. 4.11 - Ventilation configuration of solar DEC

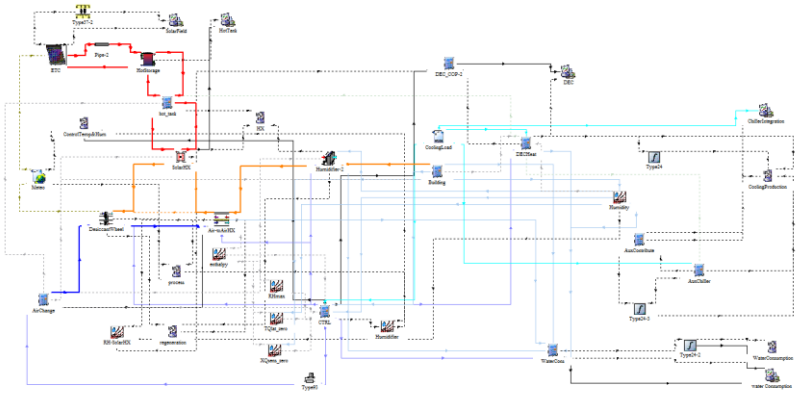

Fig. 4.12 - Trnsys deck of solar DEC model in ventilation configuration

The component responsible for the evaporative cooling effect is the humidifier (on the fresh air side) after the air-to-air HX. A user-defined Trnsys 'type' models this component. The algorithm reads the sensible and latent loads from the building model; then, it solves the equations (4.5) to calculate the correct air-flow rate and the entering conditions (temperature and humidity) to meet simultaneously the sensible and latent cooling demand. Figure 4.4 shows the temperature and humidity set point, and the evaporative cooling effect on the entering air flow. ΔT is the temperature difference between the outflow of the air-to-air heat exchanger and the set point and ΔX is the absolute humidity difference between the same point. The humidifier on the exhaust flow is set to reach the saturation point.

$$(4.5)\ \begin{Bmatrix} Q_{sens} = \dot{m} \cdot c_p \cdot \Delta T \\ Q_{lat} = \dot{m} \cdot r \cdot \Delta X \end{Bmatrix}$$

This operating mode allows, with temperate weather conditions, the absence of the auxiliary system. The control system ensures all thermal parameters of the fresh air.

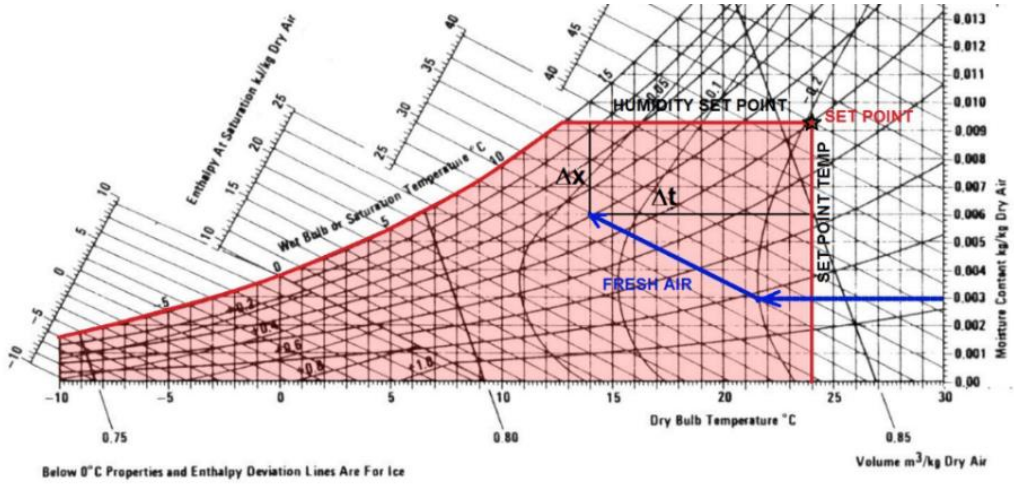

Fig. 4.13 - Humidifier operation of ventilation DEC system

4.1.6.2 Ventilation Sensible-Latent Configuration(VSL)

The management of the DEC-based air conditioning system is particularly complex, so a more intuitive and, in some cases, more efficient versions have been developed.

The presence of the auxiliary chiller allows another system control mode. In this configuration, the system keeps the airflow flow constant and air humidification in the humidifier reaches the maximum (98%).

The output air from the ait-to-air exchanger reaches the wet bulb temperature by humidifying and the control system considers two aspects. The controller evaluates whether the difference between the sensitive and the latent load is positive (4.6) and then compares if the output air temperature from the DEC is below the set-point temperature (4.7). In the positive case the compressor chiller will remove excess moisture. This configuration fully integrates auxiliary refrigerator in the plant (Fig. 4.14) and allows the system to operate for several hours a year by increasing cooling production.

$$(4.6)\ Q_{sens} + Q_{lat} > 0$$

$$(4.7)\ T_{sat} < T_{setpoint}$$

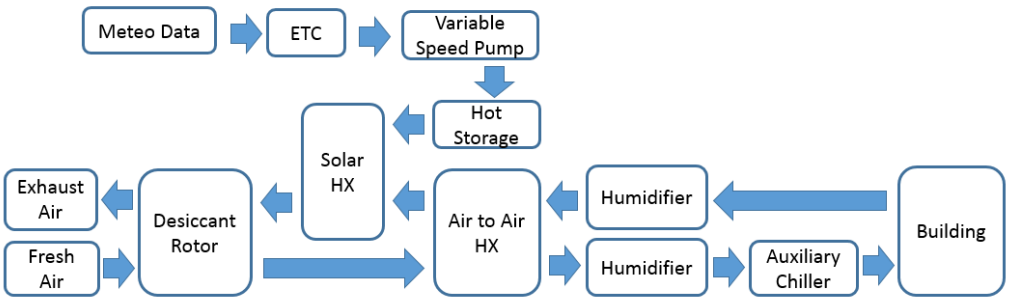

Fig. 4.14 - Enhanced ventilation configuration of solar DEC

4.1.6.3 Recirculation (REC)

Ventilation DEC are not the only ones developed over the years in different research groups. Many configurations are analyzed in [16] and optimized under the expected operating conditions [17]. Fong et al. In [18] propose some DEC recirculation configurations in the sub-tropical climate of Honk Kong.

The recirculation configuration is different from the previous one because the air flows crossing the components following a different path (fig. 4.15).

The air for air conditioning is taken from inside the building by eliminating the variability of climatic conditions on this side of the system. On the regenerative side the air is taken from the outside, reach the wet bulb temperature by evaporative cooling and sent into the air-to-air exchanger to cool the fresh air. the air flow is heated to regenerate the desiccant rotor and expelled into the environment. This type of management in dry climates provides considerable benefits.

The recirculation system is the one that allows the greatest performance because the mass flow rate of treated air is significantly higher than the other configurations. The use of external air for the regeneration circuit allows the recirculation system to obtain higher COP as evidenced by the literature.

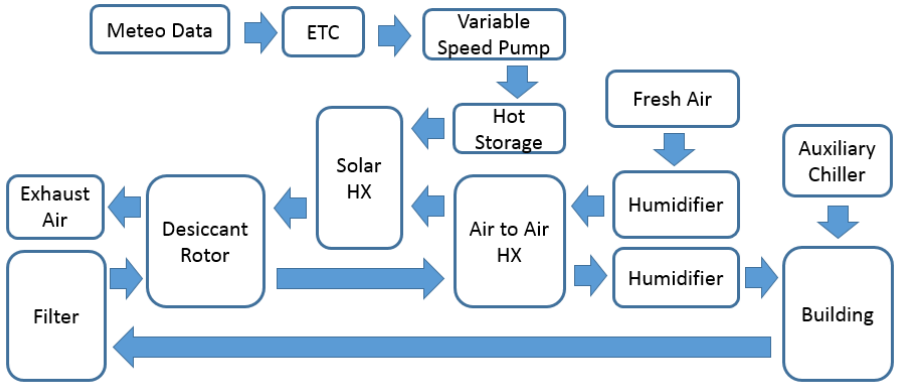

Fig. 4.15 - Recirculation configuration of solar DEC

4.2 Energy Sources

This section presents the parameters and technical characteristics of the systems used to collect solar energy and convert it to the energy vector necessary for the production of cooling energy.

4.2.1.1 Photovoltaic (PV)

Photovoltaic modules have known, in recent years, an important cost reduction, this step has made the PV configuration more competitive than other systems. The parameters adopted for the photovoltaic field are listed in Table 4.7.

Table 4.7 - Photovoltaic parameters

	unit	value
Area	m^2	-
Nominal efficiency	-	0.149
Efficiency modif temp	1/°C	-0.0041
P_{max} Voltage	V	30.5
Open circuit voltage	V	37.6
Tracking	-	fixed
Azimut	deg.	0
Slope	deg.	24

4.2.1.2 Flat Plate Collectors (FPC)

Flat plate collectors represent the solar radiation devices system designed for low temperatures. This type of collector is used in plants that requiring a thermal input below 100 deg. C. Flate plate collectors are simulated without a tracking system. Intercepted radiation is a fraction of global projected radiation.

The quadratic efficiency curve (4.8) is based on the parameters given in Table 4.8.

Table 4.8 - flate plate collectors parameters

	unit	value
Field area	m^2	60
FPC coeff a_0	-	0.793
FPC coeff a_1	$W/ m^2 K$	4.04
FPC coeff a_2	$W^2/ m^2 K$	0.0182
Array flow rate (max)	kg/h	48000
Tracking	-	fixed
Azimut	deg.	0
Slope	deg.	24

$$(4.8)\ \eta = a_0 - a_1 \frac{(T - T_{amb})}{GTI} - a_2 \frac{(T - T_{amb})^2}{GTI}$$

4.2.1.3 Evacuate Tube Collectors (ETC)

The Evacuate Tube Collectors are the most used type for solar cooling systems. They show a good efficiency in the range of temperatures required by solar cooling systems. The quadratic efficiency curve (4.9) is based on the parameters given in Table 4.9. Intercepted radiation is a fraction of global projected radiation.

$$(4.9)\ \eta = a_0 - a_1 \frac{(T - T_{amb})}{GTI} - a_2 \frac{(T - T_{amb})^2}{GTI}$$

Table 4.9 - Evacuated tube collector parameters

	unit	value
Field area	m^2	60
ETC coeff a_0	-	0.718
ETC coeff a_1	W/ m^2 K	0.984
ETC coeff a_2	W^2/ m^2 K	0.005
Array flow rate (max)	kg/h	48000
Tracking	-	fixed
Azimut	deg.	0
Slope	deg.	24

4.2.1.4 Parabolic Trough Collectors (PTC)

The Parabolic Trough Collectors are the best solution for high temperature applications and are difficult to integrate into small-scale systems.

The PTC field is Nord-South oriented and equipped with 1-axis tracking device. The field efficiency is computed according with the quadratic equation (4.10); the loss coefficients are kept from the data sheet of a commercial trough and are reported in Table 4.10.

$$(4.10)\ \eta = a_0 - a_1 \frac{(T - T_{amb})}{BTI \cdot C} - a_2 \frac{(T - T_{amb})^2}{BTI \cdot C}$$

Because of the 1-axis tracking system, the troughs do not collect the DNI, but the beam tilted irradiance, defined as follows (4.11):

$$(4.11)\ BTI = DNI\ \cdot \cos\theta$$

Table 4.10 - Parabolic trough collector parameter

	unit	value
Field area	m^2	60
PTC coeff a_0	-	0.7719
PTC coeff a_1	$W/m^2 K$	0.180
PTC coeff a_2	$W^2/m^2 K$	0.0258
Array flow rate (max)	kg/h	48000
Tracking	-	1 axes
Azimut	deg.	N-S
Slope	deg.	variable

4.3 Heat Rejection Systems

In the present work, four different heat rejection systems have been considered: dry air cooler, cooling tower, groundwater and geothermal. The study of different heat recovery systems has already been well-analyzed in numerous studies [19, 20].

Dry cooler is the most common heat rejection system for residential applications: in hot climates, air-cooled chillers exhibit low efficiency because of the high ambient air temperature [21, 22]

Cooling towers perform well with low wet bulb temperatures, but they require water make-up, and this could be critical in countries with water scarcity.

If available, shallow groundwater or seawater can be used as heat sink, with average temperature typically lower than air temperature: this has a beneficial impact on the water-cooled chiller efficiency.

The use of geothermal probes as a heat rejection system can be a good alternative to avoid water consumption and keeping the cooling circuit at temperatures that ensure excellent performance.

4.3.1 Air Cooler (AIR)

Air cooling systems represent the majority of residential installations, especially in regions with scarcity of water resources.

The use of dry coolers in solar cooling applications based on absorption-adsorption chiller is very complicated [23]. In fact, to avoid lithium bromide crystallization problems, the chillers are switched off when the cooling circuit temperature reaches 32 deg.

The technical specifications of the dry cooler model used are reported in Table 4.11.

Table 4.11 - Air cooler technical data

	unit	value
Nominal capacity	kW	70.00
Outlet set point	deg. C	27
Inlet set point	deg. C	32
MFR fluid	kg/h	12000
MFR air flow	kg/h	48000

4.3.2 Cooling Tower (CT)

Heat rejection circuits based on cooling tower are the current standard for industrial application. They are particularly efficient with low relative humidity and provide a water supply at ideal temperatures for the chillers operation. Table 4.12 shows the technical specifications of the model used in the simulations.

Table 4.12 - Cooling tower technical data

	unit	value
Nominal Capacity	MW	1.00
Sump volume	m^3	4.00
MFR air flow	m^3/h	100000
Natural air flow	m^3/h	20000
Water flow rate	kg/h	120000
Inlet water temp	deg. C	35
Outlet water temp	deg. C	28

Sea Water and Groundwater (GW)

Hot climate affected the performance of cooling system; the high temperature of air limit the capacity of chiller with heat rejection chiller based on dry cooler and high relative humidity reduce the efficiency of cooling tower.

A solution is use the seawater or the groundwater for the cooling circuit of the chiller. This is possible because the temperature of the subsoil is almost constant during the year.

The possibility of using groundwater for cooling application is related to two main parameters: presence and salinity as reported in fig 4.16 [24].

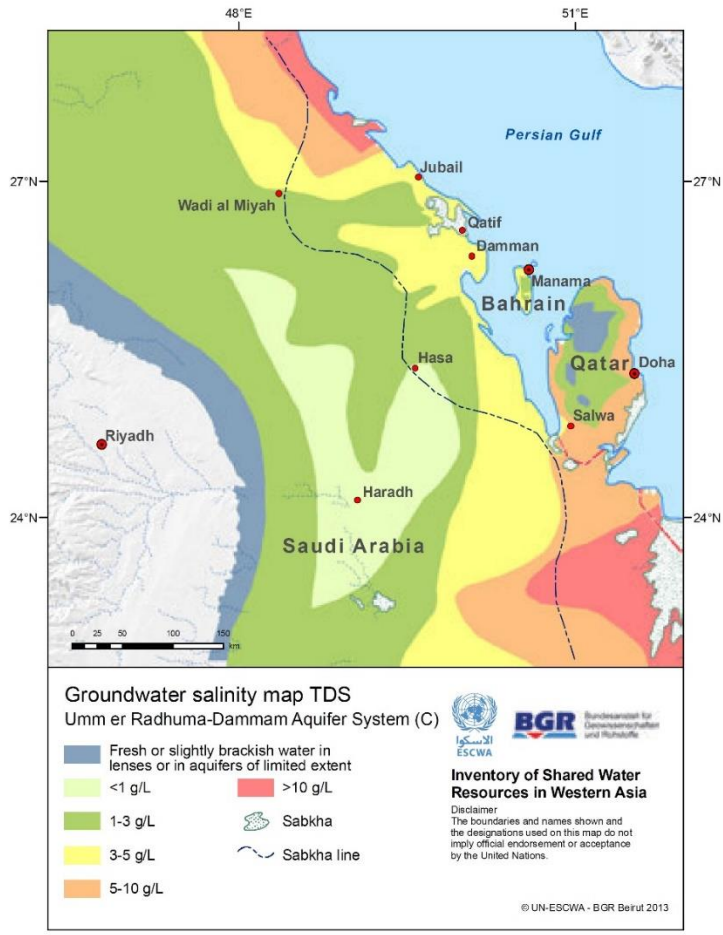

Fig. 4.16 - Groundwater salinity [24]

To solve the problem of the groundwater presence a difficult study of the geology and hydrogeology of the region concerned needs to be developed. Some study have shown the complexity of the hydrogeology of the Arabian Peninsula [25, 26]. In addition to the availability of water you must also consider its potentiality.

Fresh water plays a particularly important role in these arid regions [27, 28, 29] where water resources depend on scarce rainfall [30] and their variation during the years [31, 32] tending to a gradual deterioration [33, 34].

The importance of precipitation is linked to the aquifers recharging, for this reason the study of vertical permeability and water exploitation through wells is particularly complex [35].

The low water salinity is directly related to the possibility of collect drinking water, or easily transform into fresh water, from the subsoil [36] also in the central region of Saudi Arabia [37, 38] where the use of drainage wells is a widespread practice [39]. Especially in highly urbanized regions where the course of the fluid can exhibit important variations [40, 41].

The presence of salt is due to seawater intrusion [42] into the coastal aquifer. Also caused by tides [43] and pumping wells [44] that raise saline wedge (fig 4.17).

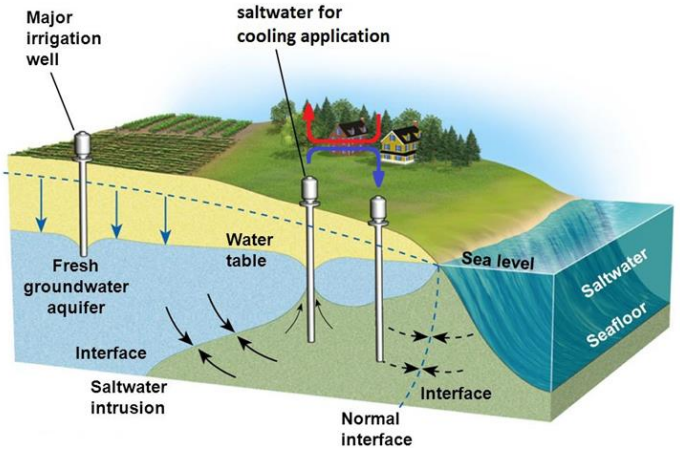

Fig. 4.17 - Saltwater intrusion and interface modification

The salinity is related of the salt feed by the evaporites rocks in some inland regions. This type of water is not suitable for human use but usually employed for livestock, agricultural and gardening [45].
The use of groundwater for energy purposes is advantageous where the thermal flow is high [46] or where an aquifer is available. Although in this case problems with the increase in water temperature are possible [47].
Thermal conductivity of soil is related to the water content [48] and underground flows that can significantly change soil temperature [49]. The presence of water in the subsoil also affects the energy-pile as it increases the thermal flow [50].
The water for cooling application is pumped by a supply well and reintroduced in the ground by a return well to avoid the consumption of the resource. The idea for cooling system is based on a water-to-water heat exchanger that cooling circuit of the chiller. The water pumped by the well feed the cold side of the heat exchanger.
Wells are created by drilling a hole with a diameter of 300 mm at a depth of 70 meters. The borehole is produced using the casing drilling method or the rotary drilling method. The well is made with a filter and surrounding space is refilled with gravel.
In coastal regions water is pumped directly from the sea, but the temperature of the surface water is particularly hot [51, 52] and the backdrops of the peninsula are shallow. To draw water at a correct temperature it is necessary to use long drainage pipes. Direct drawing of water for energy purposes is therefore discarded.

4.3.2.1 Geology and Hydrogeology Survey

The geological conditions of the Arabian Peninsula are well studied for the presence of important hydrocarbon resources, these data can also be used to understand hydrogeology and soil characteristics of the regions with completely different purposes [53, 54].
Geological stratifications [55, 56, 57] are very important in order to understand the type of water present in the subsoil. By combining the available data in the various sources, a map of the type of water is reported in Figure 4.18.
Some research show the presence of groundwater in the west regions [58] of Saudi Arabia [59, 60] and the study of underground flows [61].

The average depth of shallow aquifer varying between 3-16 m in the alluvional wadi deposit and between18-62 m in the sedimentary part [62]. The quality of the groundwater in the Red Sea Region [63] is modified by seawater intrusion into some of the inland localities that increase the salinity of the water. The quality of water and its flows [64] remain a particularly important aspect for modeling a supply well.

The soil of Gulf Regions is characterized by very high permeability and the aquifer of Damman and Umm-er-Radhuma system is exploited for agricultural development and industrial purpose. [65]. The stratigraphies of the coastal region show layers with different permeability [66]

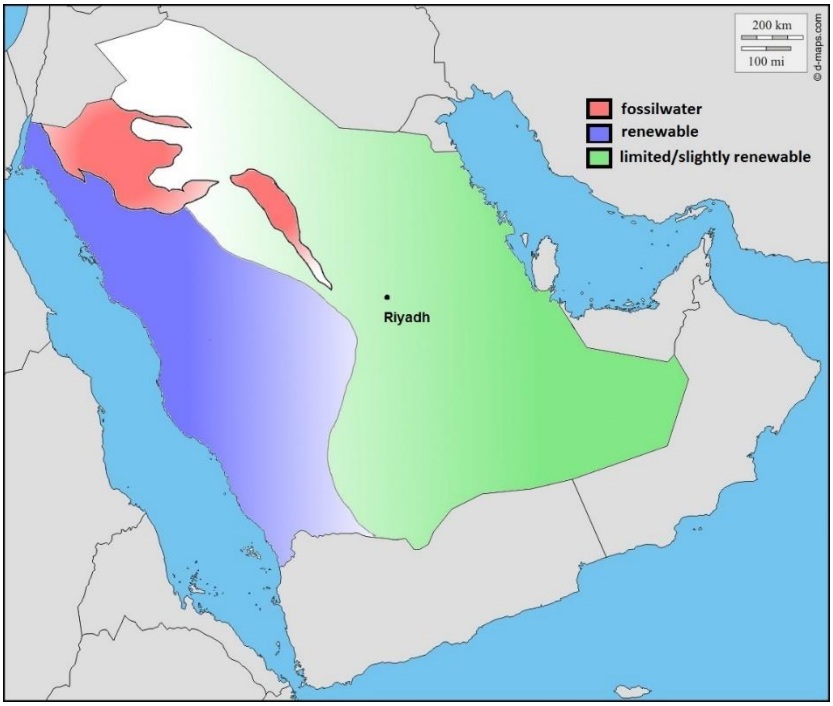

Fig. 4.18 - Renewability of groundwater in the Arabian Peninsula

The groundwater depth in the Emirates region was calculated by interpolating the data obtained from the wells in the literature (Fig. 4.19). The average depth of the groundwater in this region progressively increases from the coast to the depth of more than 120 m. In the study area, the depth of groundwater surface is 60 m. Unfortunately, as the depth increases, the groundwater surface level moves into soil layers with less permeability as shown in the stratigraphy of Dubai (Fig. 4.20), this stratigraphy is resumed by the various scientific surveys carried out for the study of the soil.

Another important parameter is the groundwater temperature and its variations. A relevant datum is shown in the map in Fig. 4.21 [67]. The water temperature drawn from the wells is around 25 deg., but just a few kilometers around the average temperature can rise up to about 30-32 deg.

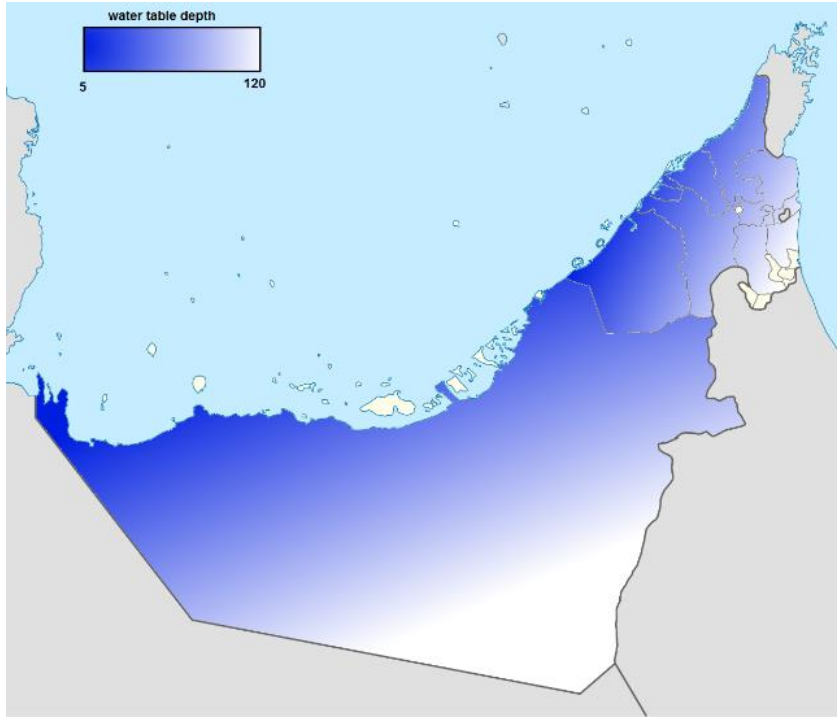

Fig. 4.19 - Groundwater table depth in the UAE region

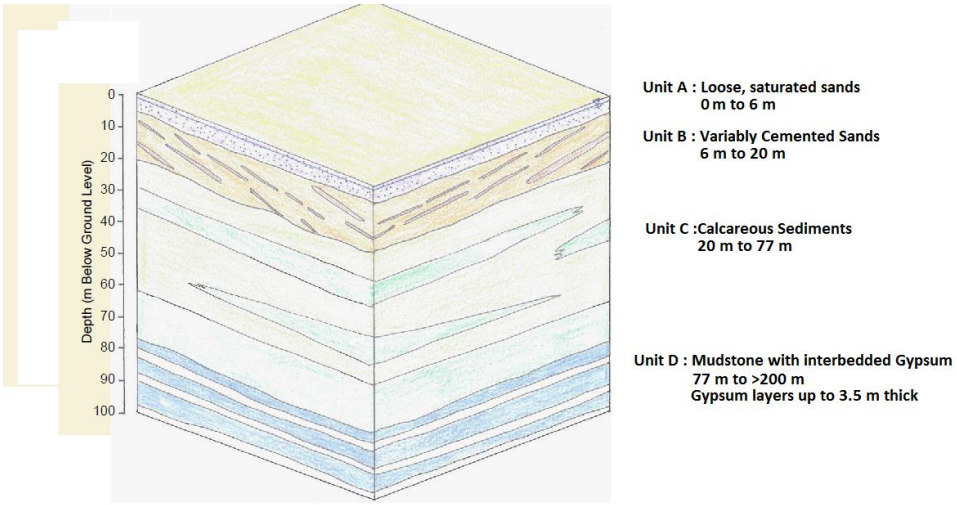

Fig. 4.20 - Dubai soil stratigraphy

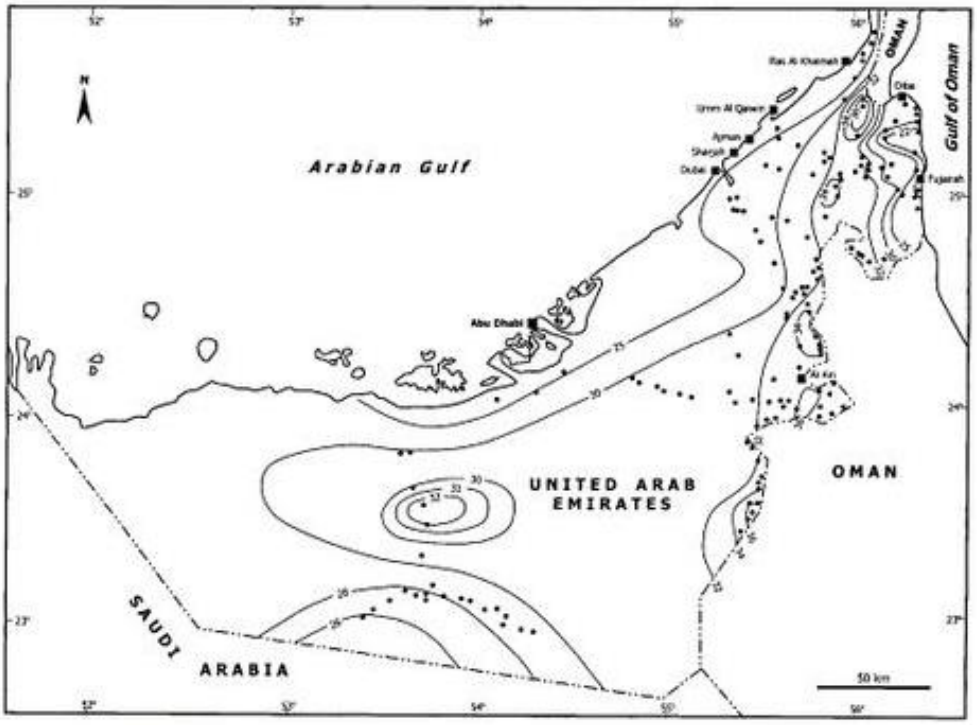

Fig. 4.21 - Groundwater temperatures (deg. C) in the UAE [67]

The groundwater resources in Riyadh Regions [68] are feed by Jubalia Limestone that is one of the secondary aquifer of Saudi Arabia. The depth range of the aquifer (Fig. 4.22) is estimated from 20 to 200 m and the permeability is good. The water is not suitable for human use but usually employed for livestock and agricultural.

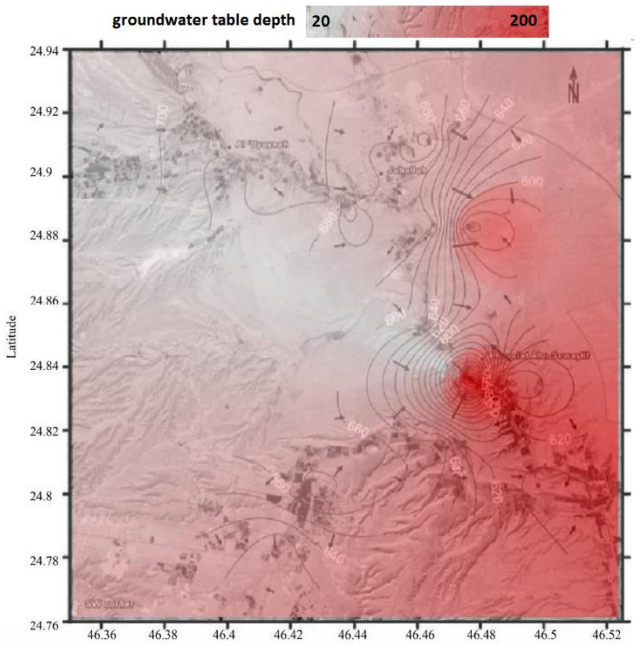

Fig. 4.22 - Groundawater table depth in the Riyadh region

The use of underground water for cooling purposes is an effective method to reject the waste heath from cooling systems and to increase chiller efficiencies. It is a fully renewable resource as the only environmental impact is a weak heating (5-10°C) of the re-injected water.

It has to noticed that underground water is generally characterized by a significant level of salinity, both in the internal and coastal areas, so there is no competition with the freshwater for human use.

This method worth to be investigated as groundwater is practically available in most of the urbanized areas of UAE.

4.3.2.2 Model

To evaluate the behavior of a supply well a mathematical model of the behavior of the groundwater field was developed through a Trnsys macro.
The Trnsys macro includes an Excel type that uses a Visual Basic Application macro to perform the calculation. The type uses some inputs provided by the simulation studio and combines them with ground and well parameters set directly into the Excel file. At the end of the computation the macro returns the outputs needed for the simulation. The inputs, parameters and outputs are listed in Table 4.13.

Table 4.13 - Groundwater model inputs and outputs

INPUT	**Symbol**	**Unit**
Time	t	h
Water temperature	T1	deg. C
Heat rejection flowrate	MFR	kg/s
PARAMETER	**Symbol**	**Unit**
Timestep	ts	h
Borehole number		N
Borehole diameter	Dw	m
Max water table level drop	Δmax	m
Layer thickness	L	m
Water level (t=0)	H	m
Hydraulic conductivity*	k	m/s
Water density	ρ	Kg/m^3
Specific yield	e	m^3/m^3
Well diameter	2R	m
OUTPUT	**Symbol**	**Unit**
Outlet water temp	T2	deg. C
Water flowrate	MFR (delivered)	kg/s
Weel radius	Rind	m

*Transmissivity for Aquiclude (m^2/s)

The purpose of the model is to reproduce the behavior of the groundwater field in an approximate way to evaluate the performance of the solar cooling system.
Two restrictions have influenced the choice: the model must interact directly with Trnsys and no dedicated software has been used (simulations require high computing times).
The model simulates the withdrawal of water from a well in groundwater and reproduce the groundwater table field.

By deriving the fundamental equations of the three-dimensional flow, the Dupuit formula of the groundwater field is obtained (4.12)

$$(4.12)\ h = \sqrt{{H_P}^2 + \frac{\dot{Q}}{\pi\, k}\, ln\frac{2r}{2R}}$$

From the (4.12) we obtain the flow equation for a stationary groundwater well (Dupuit formula). The model is based on the modified solution of the equation (4.13).

$$(4.13)\ \dot{Q} = \frac{\pi\, k\, (H^2 - {H_P}^2)}{ln\frac{2r}{2R}}$$

The soil volume considered for the simulation is ideally divided into concentric cylinders of varying radius according to the soil's hydraulic conductivity. The inner cylinder represents the well.
Each cylinder is considered as a circular crown tank. The volume of water contained in these tanks is related to the specific yeld (*e*) of the soil layer (4.14). The model considers the porosity of the soil layer to evaluate the water contained under ground level ground volume.

$$(4.14)\ V_{WR1} = \left({R_1}^2 - {R_0}^2\right) \cdot \pi \cdot e$$

To operate in transient mode, small cells are adopted and a time-related term is introduced. (4.15). The mark Q_r indicates the incoming charge flow into the well from the last circular region.

$$(4.15)\ \dot{Q}_r = \frac{\pi\, k\, (H^2 - {H_P}^2)}{ln\frac{2r}{2R}} \cdot \theta_t$$

This information is used to calculate the volume of moving water between two contiguous regions. As reported in the eq (4.16), the water level of each circular region in the timestep (t+1) is given by the level in the previous timestep (t) algebraically added to the inflow and outflow.

$$(4.16)\ H^R{}_{t+1} = H^R{}_t + \Delta H^{R+1}{}_t - \Delta H^{R-1}{}_t$$

The variation in the level of the circular regions is related to the charging flows with respect to the area of the circular region considered (4.17).

$$(4.17)\ \Delta_H{}^R = \frac{Q^{R+1} - Q^{R-1}}{A_R}$$

The variation of well level is related to the flow rate (MFR) and the charge flow. (4.18) where A_B represents the area of the diameter well D.

$$(4.18)\ \Delta_{Hp} = \frac{\dot{Q}_r - \widetilde{MFR}}{A_B}$$

The model includes a proactive control to avoid the depletion of the groundwater. The system controls the dynamic level and compares it with flows at each time step by limiting the MFR. The limit of the hydraulic head is selected by the user with parameter Δ_{max}.
The MFR flow rate is the minimum between the maximum flow rate that brings the dynamic level of the groundwater field to the minimum admissible (MFRmax) and the required flowrate MFR (4.19); with MFR_{max} evaluated in (4.20).

$$(4.19)\ \widetilde{MFR} = \min(MFR_{max}\,; MFR)$$

$$(4.20)\ MFR_{max} = \dot{Q}_r - \Delta_{max} \cdot A_B$$

The Fig. 4.23 show the water table level during a dynamic simulation, the single vertical cylinder are underlined and the level variation is represent in an off-scale chart.

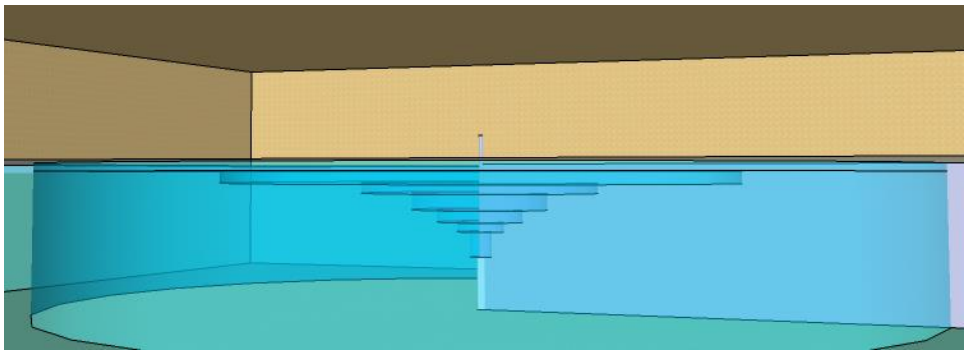

Fig. 4.23 - Groundwater table level during the simulation.

4.3.2.3 Model Validation

The validation of a numerical model of a well is particularly complex. To simplify the procedures and obtain a good degree of approximation, the following procedure has been adopted.

The model has been validated by performing a step drawdown test.

The parameters of a real case was setting in the model and, after the simulation, comparing the characteristic curves. In the reference case all the fundamental parameters and soil characteristics are known.

The Step Drawdown test follows the steps shown in Table 4.14 and the test results are shown in the graph in Figure 4.24. The real and simulated characteristic curve show a good degree of superposition. But the trend of the model beginning to show an overestimations of the lowering of the groundwater level. Deviation that increases as the flow rates increase.

Table 4.14 - Step drawdown test parameters

STEP	Flow rate	duration
N	kg/s	min
Step 1	0.75	90’
Step 2	1.50	90’
Step 3	3.00	90’
Step 4	6.00	90’
Step 5	12.00	90’

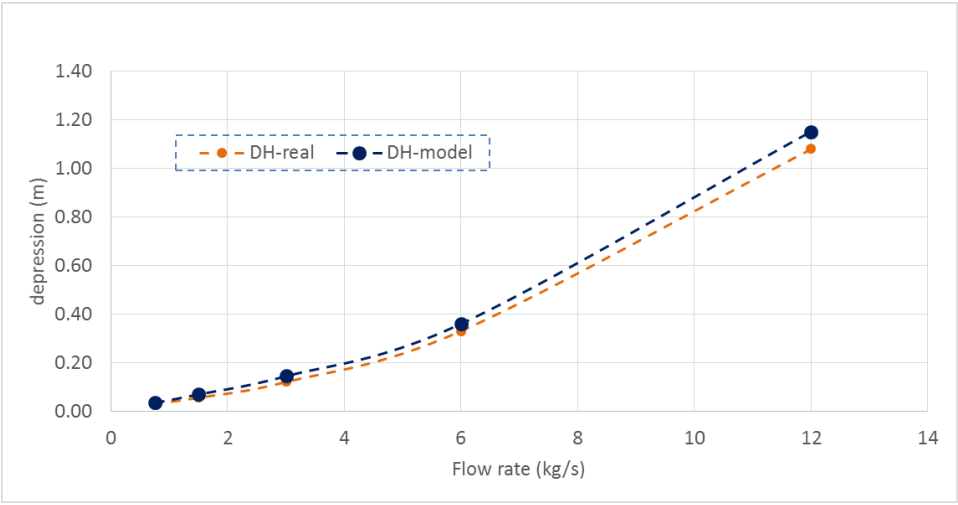

Fig. 4.24 - Step drawdown test results

4.3.3 Ground Heat Exchanger (GHX)

Another possibility to reject the heat produced by the chiller is the use of geothermal probes. The use of geothermal probes for air conditioning dates back many years ago and the study of these solutions is developed [69] especially for heating. The possibility to use the geothermal resources of the Arab peninsula has already been hypothesized by the King Abdullah City for Atomic and Renewable Energy [70] and by the Emirate's universities [71].

In fact, geothermal probes can be used to extract heat from the ground to feed, for example, an heat pump as to release heat by cooling a circuit.

In this research work only the vertical geothermal probe was taken into account. Horizontal ground heat exchanger are strongly affected by the heat absorbed by the irradiation that adversely affecting the performance of a system conceived solely for cooling.

Furthermore, the problem of soil saturation which gradually increases its temperature affect a system that works exclusively in cooling mode.

This problem should be addressed by considering the regeneration capacity of the ground and oversizing the system to work with adequate safety margins. In fact, the average annual influence of geothermal probes on soil temperature can be low but not if referred to short-term [72]. It is therefore necessary to develop models that can take into account the thermal behavior of the ground. The problem concerns the surface layers of the ground, as at a low depth the temperature shows limited variations [73].

The intrinsic difficulty in creating models for transient simulations is mainly related to the knowledge of the soil characteristics [74, 75] and the temperature fluctuations of the soil over time [76, 77, 78].

4.3.3.1 Geothermal Survey

For the development of the ground heat exchanger model, research has been carried out on the soil characteristics in the chosen locations. The geological characteristics of the soil have already been collected with abundant data used for the implementation of the groundwater table model. Particularly important is the knowledge of soil characteristics in the presence of thermal fluxes [79]

4.3.3.2 Model

To simulate the behavior of a vertical geothermal probes a numerical model has been developed in Visual Basic Applications. The choice of this solution is based, as in the previous case, on simulation speeds and direct compatibility with the Trnsys model.

The model includes a finite number of vertical regions (10) of variable thickness and with user defined features. The vertical regions are divided into a number of horizontal concentric regions. Temperature is considered constant inside the regions.

The model uses various user-set parameters and time-varying inputs derived from the Trnsys simulation. Outputs are directly available in the Simulation Studio interface for all other solar cooling system components. Parameters, inputs and outputs are listed in Table 4.15. Ground parameters may vary between vertical layers but not between horizontal regions.

Table 4.15 - Vertical ground heat exchanger inputs, parameters and outputs

INPUT	**Symbol**	**Unit**
Time	t	h
Water temperature	T1	deg. C
Water flowrate	MFR	kg/s
PARAMETER	**Symbol**	**Unit**
Timestep	ts	h
Borehole number		N
Layer thickness	L	m
Thermal Conductivity	λ	W/mK
Layer thermal capacity	Cp	MJ/m^3K
Soil density	ρ	kg/m^3
OUTPUT	**Symbol**	**Unit**
Outlet temperature	T2	deg. C
Heat Rejection Power	HR	kW

The model solves the static equations for the thermal flow adapted to the transient simulation in the concentric grid formed by the horizontal regions. This simplified method allows to solve, with reduced computational cost, the problem of heat transfer in the underground. Using specific heat transfer software requires the solution of complex models that are difficult to integrate with Trnsys and requires computing times incompatible with Trnsys simulation.

The model solves the heat exchange equations between the various regions starting from the cylindrical flow equation (4.21) at each time step. In this equation, T_{in} and T_{ex} represent the temperature at the internal and external interface of the circular crown considered.

$$(4.21)\ \dot{Q} = \frac{\lambda\ 2\pi\ (T_{in} - T_{ex})}{ln\frac{R_2}{R_1}}$$

The equation is appropriately modified to operate in a transient mode by adding a time-related term (4.22).

$$(4.22)\ \dot{Q} = \frac{\lambda\ 2\pi\ (T_{in} - T_{ex})}{ln\frac{R_2}{R_1}} \cdot\ \theta_t$$

Considering the first region, near the borehole, is possible to hypothesize the internal temperature equal to the average of the inlet and outlet water temperatures of the probe (4.23).

$$(4.23)\ T_{in} = \frac{T1 + T2}{2}$$

The eq. (4.24) is obtained by setting the equivalence (4.23) in the Eq. (4.22).

$$(4.24)\ (T1 - T2) = \left(\frac{T1 - 2T_{ex}}{2}\right)\left(\frac{\lambda\ 2\pi\ L}{ln\frac{R_2}{R_1}\ \dot{m}_W \cdot\ cp_W}\right) + \frac{T2}{2}\left(\frac{\lambda\ 2\pi\ L}{ln\frac{R_2}{R_1}\ \dot{m}_W \cdot\ cp_W}\right)$$

Equation (4.25) is obtained by setting A and B to simplify the calculation. (4.24). After this step, it is possible to obtain the unknown T2 (4.26).

$$(4.25)(T1 - T2) = B \cdot\ A + \frac{T2}{2}A$$

$$(4.26)\ T2 = -\left(\frac{BA - T1}{\frac{A}{2} + 1}\right)$$

After the computation of T2, the heat rejected to the ground is evaluated with the eq. (4.28). The power released by the probe at this time step is also equal to the power delivered to the first circular region of the soil (4.29). The ground temperature variation is obtained From the eq. (4.29). Constants with the ridge r represent the parameters of the ground. The mass of the circular soil region is calculated by multiplying the volume for the specific weight (4.30).

The soil temperature of this region at a given time-step is then calculated as the algebraic sum of the input and output powers (4.31).

$$(4.28)\ \dot{Q} = \dot{m}_W \cdot\ cp_W \cdot\ \ (T1 - T2)$$

$$(4.29)\ \dot{Q} = m_r \cdot\ cp_r \cdot\ \ (\Delta_T)$$

$$(4.30)\ V_{R1} = \rho\left({R_1}^2 - {R_0}^2\right) \cdot\ \pi$$

$$(4.31)\ {T^R}_{t+1} =\ {T^R}_t +\ {\Delta T^{R+1}}_t -\ {\Delta T^{R-1}}_t$$

For all other circular regions outside the first, the internal temperature is considered equal to the temperature obtained in (4.31). All equations are solved at each time step for each concentric ground region and for each vertical layer.

4.3.3.3 Model Validation

The model validation of the vertical geothermal probe is based on the comparison between the developed model with the Trnsys one present in the TESS library (Type557) (Fig. 4.25). The Trnsys model was developed at Department of Mathematical Physics at the University of Lund, Sweden [80]

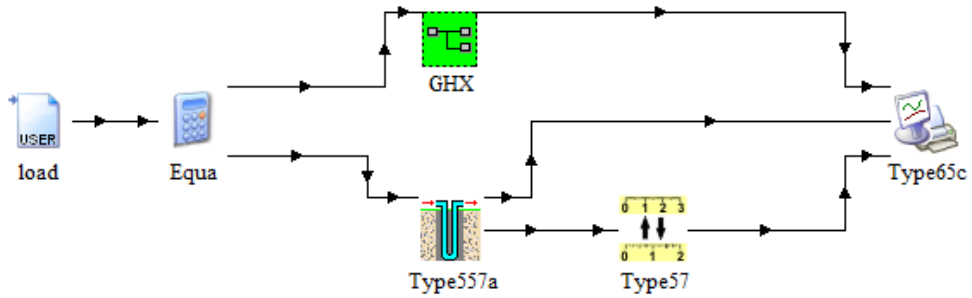

Fig. 4.25 - Ground heat exchanger validation Trnsys deck

The validation simulations use the same soil characteristics and all the other parameters listed in the Tab 4.16.

Table 4.16 - GHX model validation inputs

INPUT	**Symbol**	**Unit**
Water temperature	35	deg. C
Water flowrate	Variable	kg/s
PARAMETER	**Symbol**	**Unit**
Timestep	0.25	h
Borehole number	1	N
Layer thickness	10	m
Thermal Conductivity	3	W/mK
Layer thermal capacity	2.3	MJ/m^3K
Soil density	1500	kg/m^3

The validation simulation uses a flow modulation to highlight transients and the time response of the model (Fig. 4.26). The time-step used for this test is 0.25 hours (15 ').
The maximum water temperature difference obtained between the model developed and the Trnsys one is about 0.32 deg.

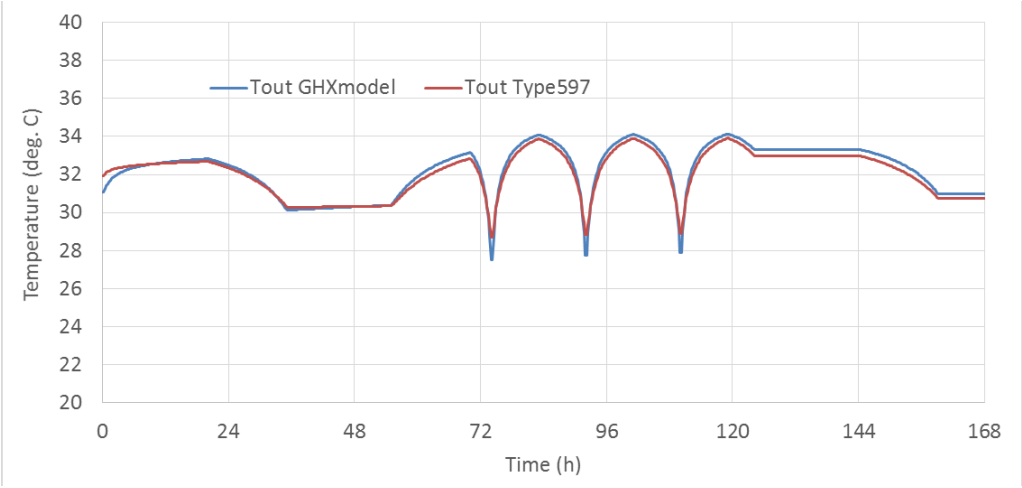

Fig. 4.26 - Ground heat exchanger model validation

4.4 Configurations

The configuration developed covers most of the market available systems. Table 4.17-19 lists all the proposed configurations for solar field, storage options and heat rejection systems.

Table 4.17 shows the different types of solar field coupled with and solar cooling technologies. The collector type has been selected according to the different temperature level required by the chillers avoiding unrealistic simulations.

Table 4.18 shows the types of storage used with different solar cooling systems. Table 4.19 shows the different types of heat rejection systems used in the simulations, in this case all types have been used for all chiller models, with the exception of the Desiccant Evaporative Cooling system that does not need a heat rejection system.

Table 4.17 - Solar field options and configurations

	PV	FPC	ETC	PTC
Compression Chiller	•			
Single Stage Absorption Chiller		•	•	
Double Stage Absorption Chiller			•	•
Triple Stage Absorption Chiller				•
Adsorption Chiller		•	•	
Desiccant Evaporative Cooling		•	•	

Table 4.18 - Storage options and configurations

	Battery	Hot Tank	Cold Tank
Compression Chiller	•		•
Single Stage Absorption Chiller		•	•
Double Stage Absorption Chiller		•	•
Triple Stage Absorption Chiller		•	•
Adsorption Chiller		•	•
Desiccant Evaporative Cooling		•	

Table 4.19 - Heat rejection systems options and configurations

	AIR	CT	GW	GHX
Compression Chiller	•	•	•	•
Single Stage Absorption Chiller	•	•	•	•
Double Stage Absorption Chiller	•	•	•	•
Triple Stage Absorption Chiller	•	•	•	•
Adsorption Chiller	•	•	•	•
Desiccant Evaporative Cooling	•			

5 Optimizations

The proposed models are the result of optimization obtained through the GenOpt software developed by the University of California (Lawrence Berkeley National Laboratory). This process makes it possible to obtain, by using the starting parameters, the optimal configuration by minimizing or maximizing a chosen function [1, 2, 3, 4]
GenOpt software is called by the TrnOpt plug-in for Trnsys software.
The process starts, as shown in Figure 5.1, from the model developed in Trnsys and modified to work with the optimization software. Through a few steps starting from the Trnsys (.dck) file called and edited by the TrnOpt plug-in that launches all the simulations needed to get the problem solved [5].

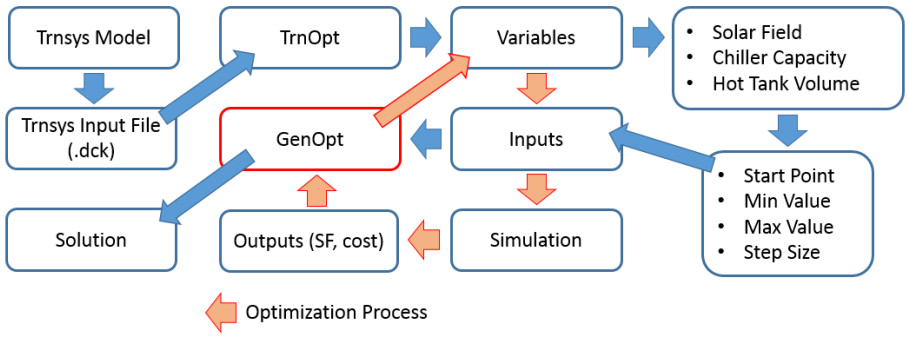

Fig. 5.1 - Optimization process block diagram

The parameters recombined and optimized for the selected cases are: the solar field, the chiller capacity and the tank volume. Each parameters are been setting with a base value, the amplitude of the first variation and the minimum and maximum value that the parameters can assume.
Figure 5.2 details the process inside the optimization process. At the end of the first annual simulation launched with the set baseline values provides the solar fraction of the configuration and the result of the objective function to minimize (5.1), Example equation for configuration ETC+ABS). The objective function is set to provide the cost value of the configuration plus a penalty related to the solar fraction obtained. In the case of solar fraction less than 0.70 (+/- 1%) the penalty forces the system to discard the configuration. For solar fraction above 0.70, the GenOpt is activated to propose a new combination of variables that can reduce the solar fraction. The simulation is launched many time with a new set of parameters until the selected SF value is reached.
Orbiting the correct SF the software starts a new cycle of simulations with the aim of minimizing the objective function (reduce the price of the configuration) keeping the annual solar fraction unchanged.

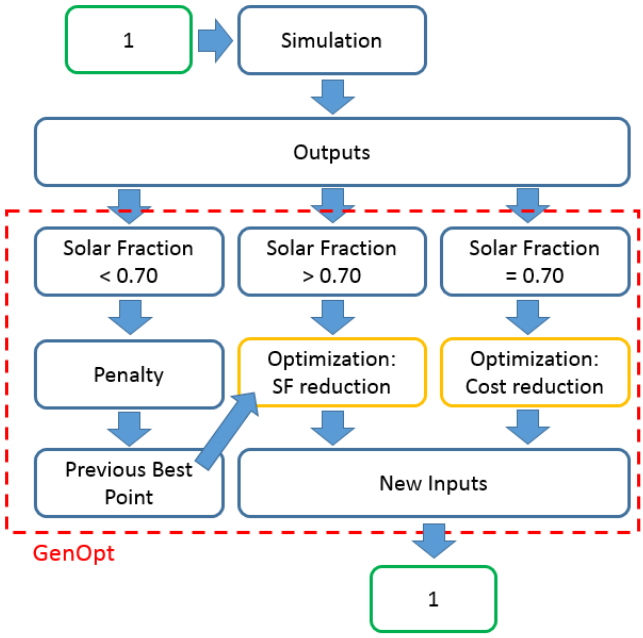

Fig. 5.2 - TrnOpt optimization process (SF = 0.70)

The optimization algorithm called in the GenOpt is the Hooke and Jeeves [6, 7], a direct search algorithm based on a series of preliminary simulations in which it modifies a parameter at a time in both directions (as show in fig. 5.4, 5.5, 5.6 and 5.7). Ended this steps the optimization process starts changing the parameters according to the diagram in Figure 5.3.
The parameters used in the optimization are listed in Table 5.1 and their value varies between two set values for each optimized model. The size of the variation is also predetermined
These values reflect the limits of good functioning and design of the plant.

Table 5.1 - Optimization parameters

Solar Field	Area	m^2
Storage Volume	Volume	m^3
Chiller Capacity	Capacity	kW

The objective functions for the various types of systems based on absorption/adsorption chiller reflect the form reported in eq 5.1, the volume of the tank is considered in the equation as the sum of cold and hot tanks (Eq. 5.2, 5.3). In the PV-based system, the equation adopted is 5.4, the fixed costs of the chiller and the cold storage tank (5.5) are added.

(5.1) $$f_{min} = A_{ETC} \cdot Cost_{ETC} + Cap_{Abs} \cdot Cost_{Abs} + Vol_{tank} \cdot Cost_{tank} + Penalty_{(SF)}$$

(5.2) $$Vol_{tank} = Vol_{hot} + Vol_{cold} = Vol_{hot} \cdot 1.5$$
(5.3) $$Vol_{cold} = Vol_{hot} \cdot 0.5$$

(5.4) $$f_{min} = A_{PV} \cdot Cost_{PV} + Cap_{Battery} \cdot Cost_{Battery} + Vol_{cold} \cdot Cost_{tank} + Penalty_{(SF)}$$
(5.5) $$Cost_{fixed} = Cap_{Chiller} \cdot Cost_{Chiller} + Vol_{tank} \cdot Cost_{tank}$$

The cost value used for simulations is listed in Table 5.2 derived from commercial products for large-size applications with high performance.

Table 5.2 - Unitary cost of component

Collectors	**unit**	**value**
Flate Plate Collectors	$/m^2	380
Evacuated Tube Collectors	$/m^2	500
Parabolic Trough Collectors	$/m^2	480
Photovoltaic	$/m^2	260
Storage	**unit**	**value**
Hot Tank (low temp)	$/m^3	450
Hot Tank (high temp)	$/m^3	850
Cold Tank	$/m^3	450
Battery	$/kWh	510
Chiller	**unit**	**value**
Compression Chiller (air cooled)	$/kW	165
Compression Chiller (water)	$/kW	130
Absorption Chiller	$/kW	400
2s Absorption Chiller	$/kW	530
3s Absorption Chiller	$/kW	610
Adsorption Chiller	$/kW	450
Desiccant Evaporative Cooling	$/kW	320

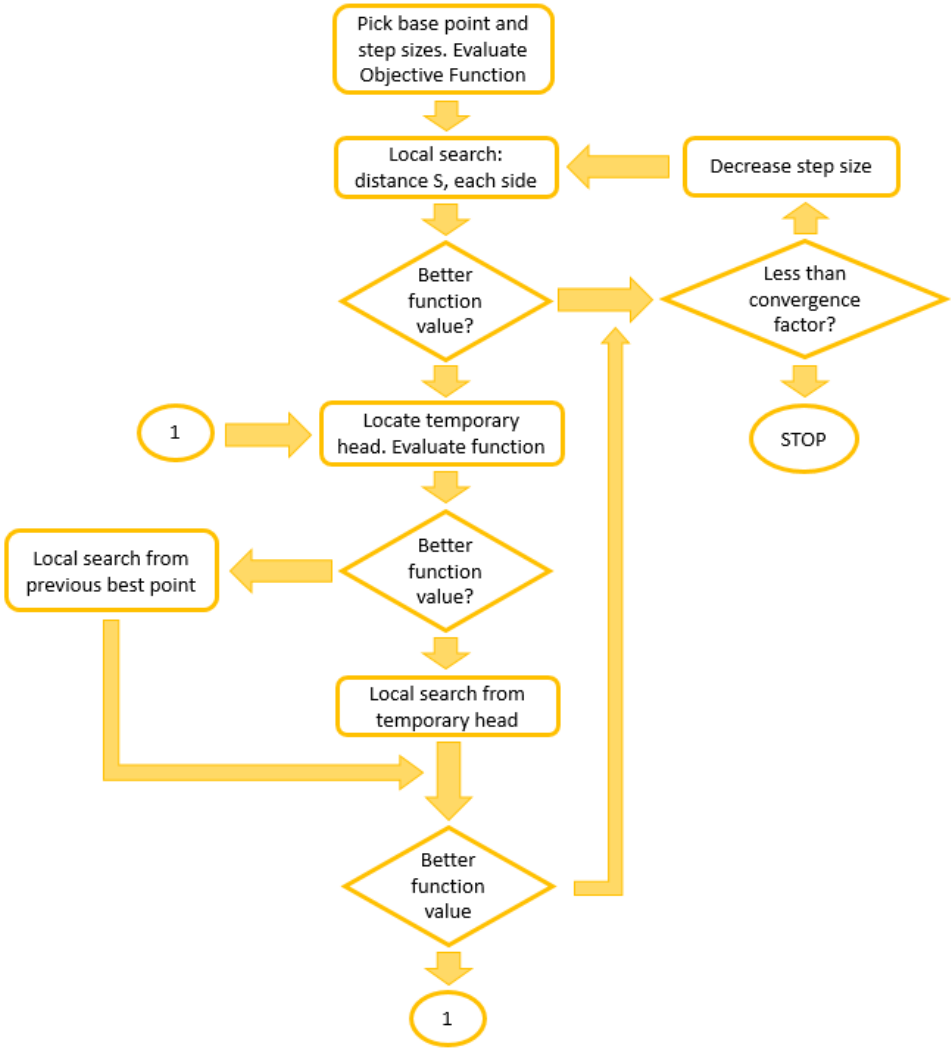

Fig. 5.3 - Hooke and Jeeves optimization process block diagram

Next figures show the optimization path for an ETC + ABS model. This procedure takes about 20 to 50 complete simulations for each model. In order to improve understanding, the penalty value of the overall cost chart (Fig. 5.4) was removed. In all charts, it is possible to notice the operation of the optimizer seeking the best compromise by moving the value of the variables in one direction and the other. The optimization process after achieving the desired solar fraction (0.70) starts a cycle of simulations with the aim of minimizing the cost while maintaining constant annual

energy performance. This passage is visible from the abrupt change of the trend of the components charts after the 25th simulation. In this case, the sizes of the hot tank and chiller are increased despite the size of the solar field (Fig. 5.5, 5.6 and 5.7)

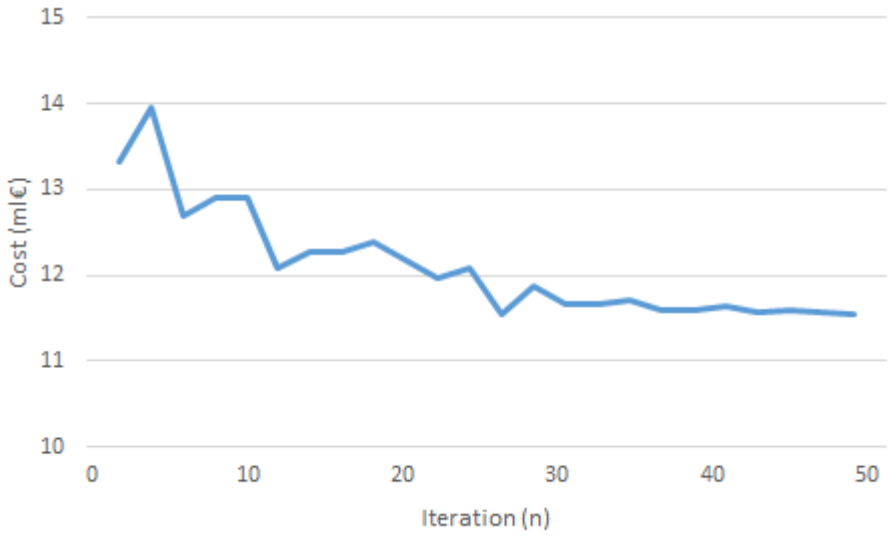

Fig. 5.4 - Global cost optimization path

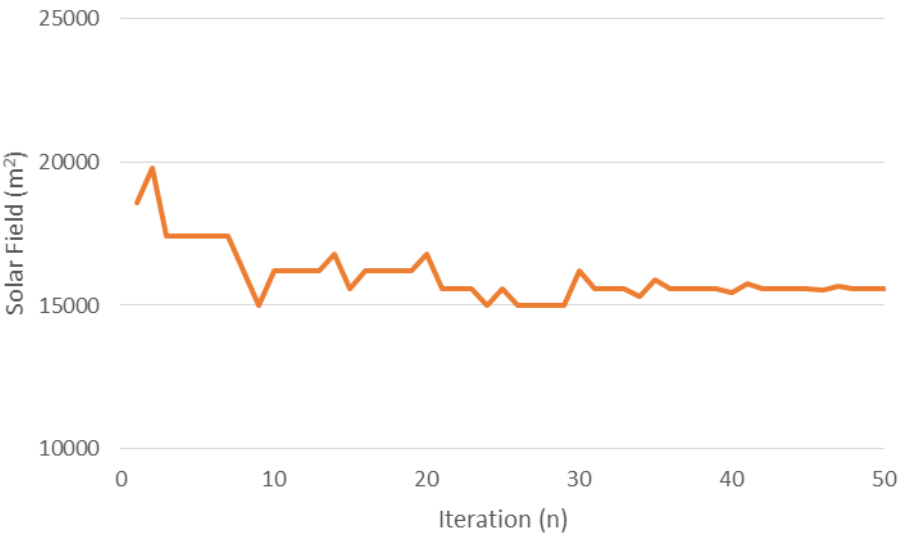

Fig. 5.5 - Solar field area optimization path

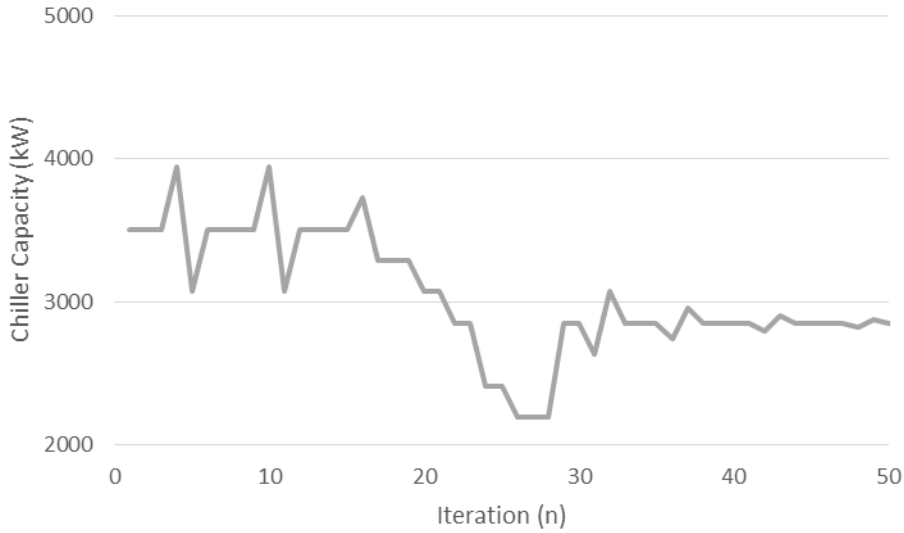

Fig. 5.6 - Chiller capacity optimization path

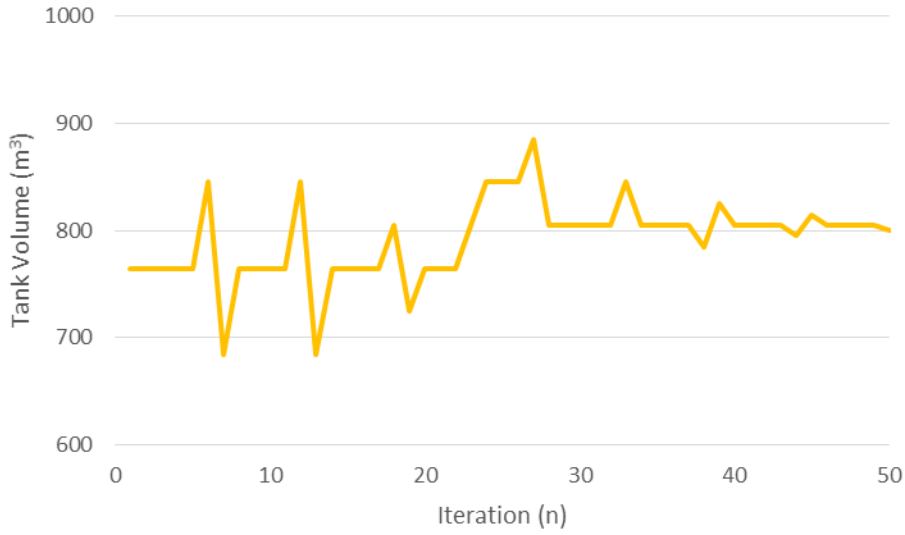

Fig. 5.7 - Hot tank volume optimization path

5.1 Optimizations results

The multivariable optimization process returns the configuration that respects all parameters by minimizing the global cost. The design parameters of the plants obtained from the optimization process can be compared

The following chart of colors (Table 5.3) was adopted in the bar charts.

Table 5.3 - Chart of colors

Heat Rejection	Color
Air Cooler	
Cooling Tower	
Groundwater Well	
Ground Heat Exchanger	

Desiccant Evaporative Cooling	Color
Ventilation	
Ventilation (SL)	
Recirculation	

5.1.1 Compression Chiller

The optimization process of solar cooling based on compression chiller focuses on the size of the photovoltaic field and, where present, the battery capacity.

Battery capacity for selected locations (Dubai Fig. 5.8 and Riyadh Fig 5.9) highlights the importance of the heat recovery system by awarding the most efficient systems. A more efficient heat rejection system allow a small battery. Fig 5.10 shows the optimal size of the photovoltaic field, the picture point out the importance of the heat rejection system.

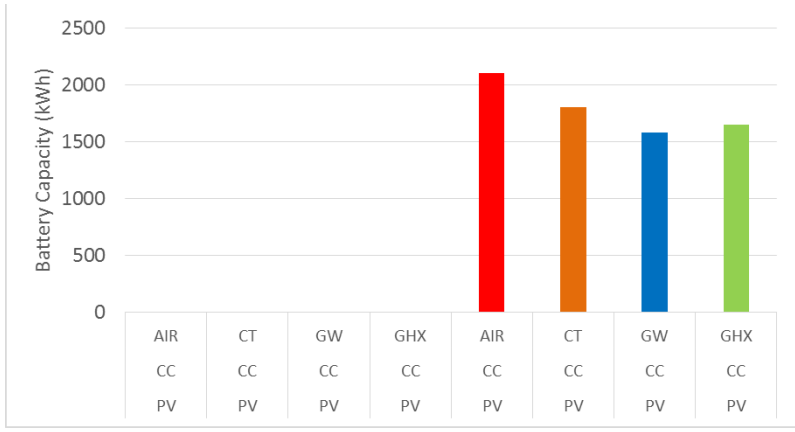

Fig. 5.8 - Battery capacity (CC) Dubai

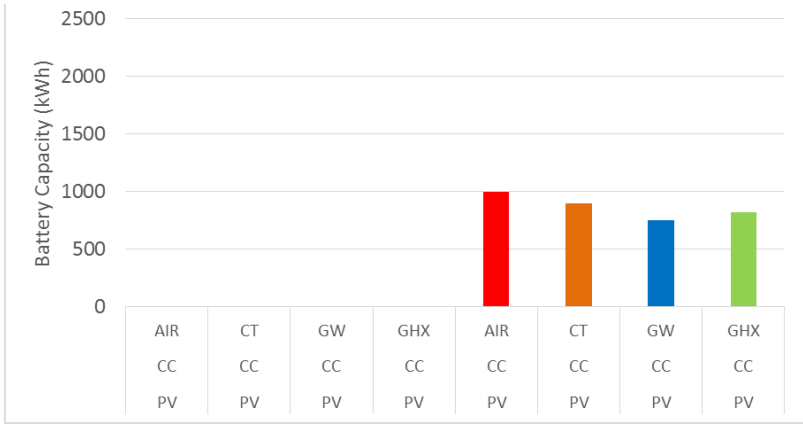

Fig. 5.9 - Battery capacity (CC) Riyadh

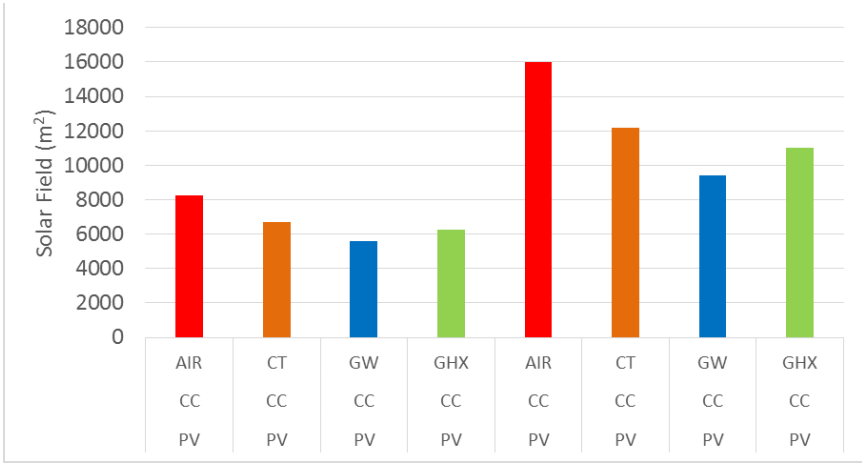

Fig. 5.10 - Solar field area (CC) Dubai

5.1.2 Absorption Chiller

Further considerations can be done analyzing the results of the optimization process for the cooling plant based on the absorption chiller.
Figure 5.11, Figure 5.12 show the size of the solar field and the storage for FPC and single stage ABS configurations. The charts highlight the importance of the collector efficiency and the heat rejection system that allow a reduction in component sizing.
The values of air-cooled systems are not directly comparable with the others because the solar fraction obtained is 50%.

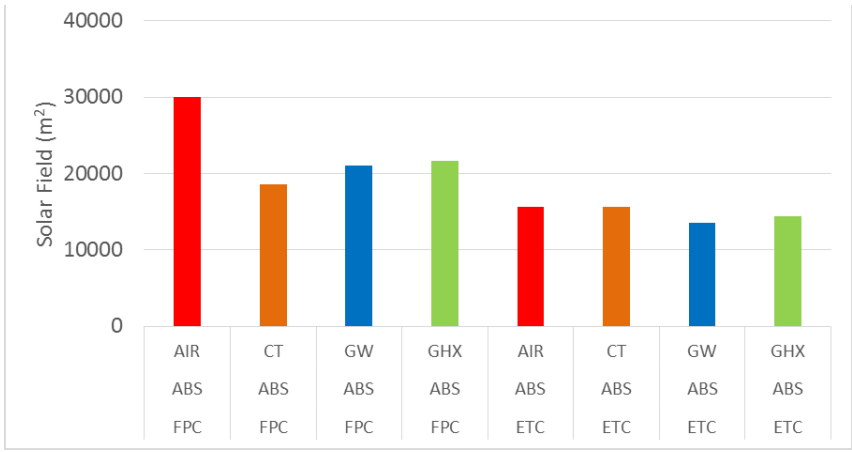

Fig. 5.11 - Solar field area (1sABS) Dubai

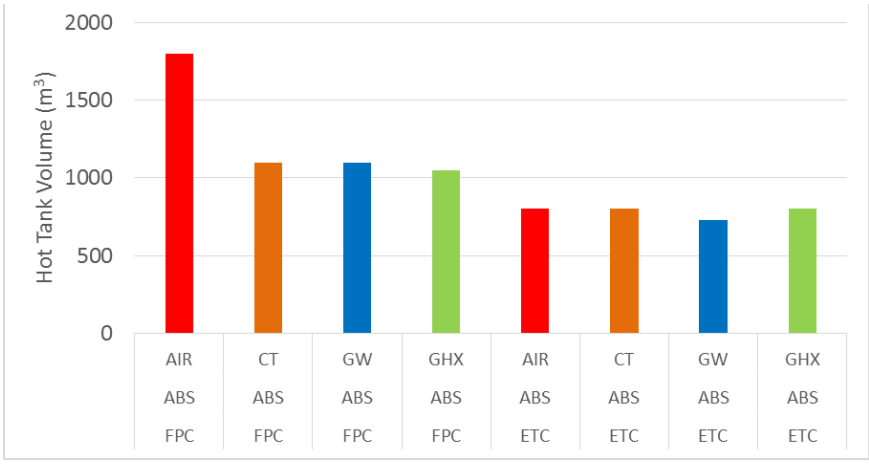

Fig. 5.12 - Hot tank volume (1sABS) Riyadh

To compare the results of the optimization process for all absorption chiller versions adopted, a summarized bar charts were made.
Graphs 5.13 (Dubai) and 5.14 (Riyadh) show the aperture area of the solar field for the three types of chillers powered by different solar collectors.
The solar field area decreases considerably as COP grows and the variation of the solar field area relate to the three different heat rejection systems is quite important.

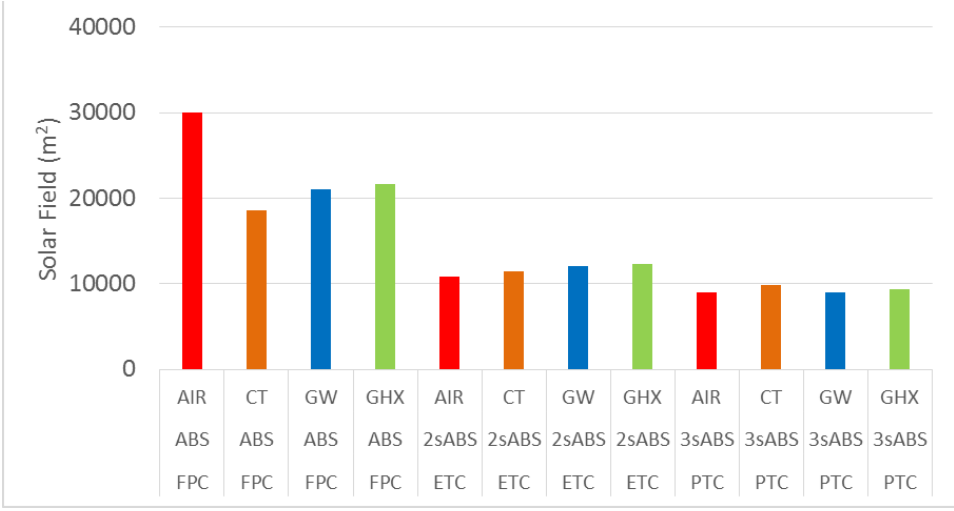

Fig. 5.13 - Solar field area (ABS) Dubai

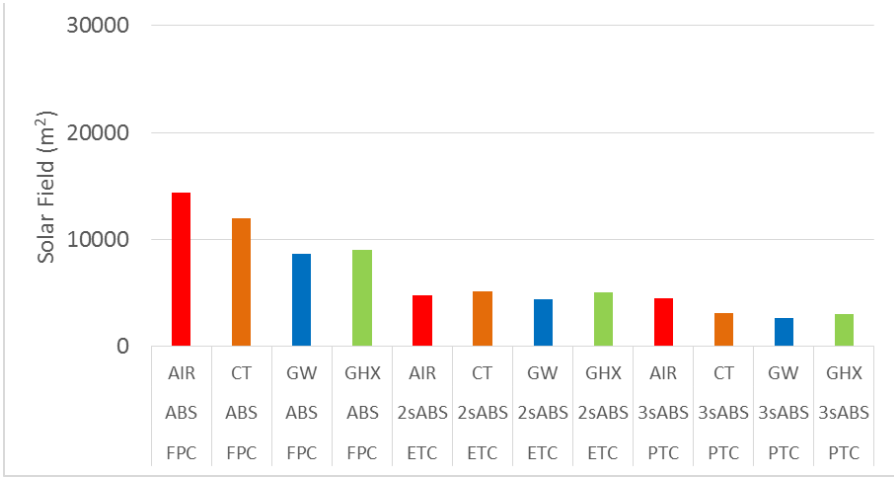

Fig. 5.14 - Solar field area (ABS) Riyadh

Bar charts 5.15 and 5.16 show, for the same solar cooling configurations, the volume of the tank. The trend shown reflects the size of the solar field by accentuating the differences.

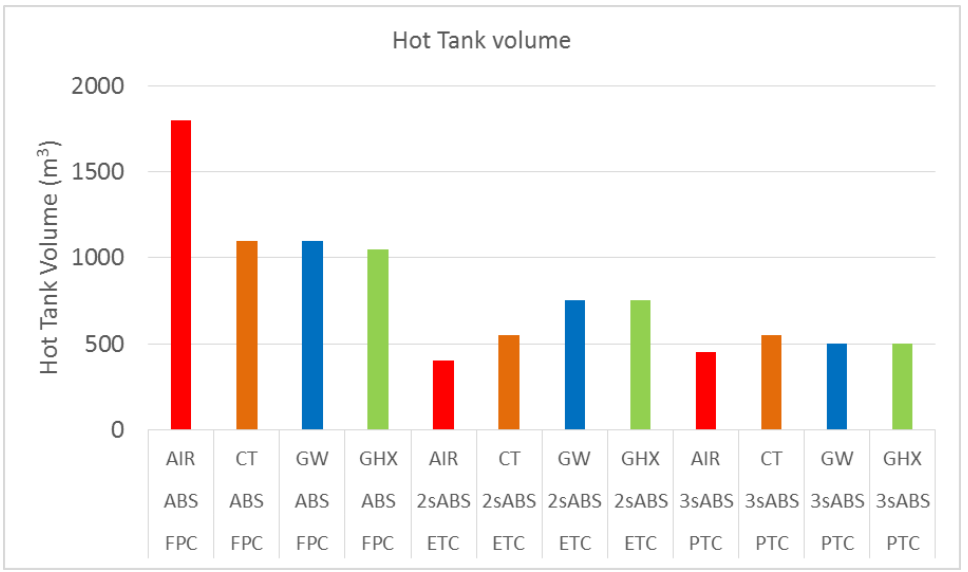

Fig. 5.15 - Hot tank volume (ABS) Dubai

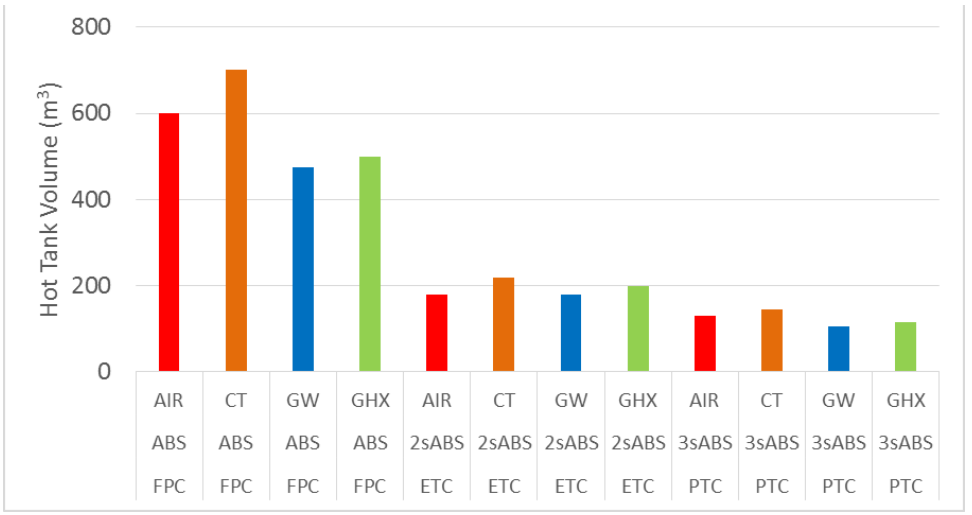

Fig. 5.16 - Hot tank volume (ABS) Riyadh

5.1.3 Adsorption Chiller

The optimization of systems based on adsorption chiller resumes the trend highlighted by previous graphs of absorption chiller. The values of air-cooled systems are not directly comparable with others because the solar fraction obtained is 50%. As shown in Fig .5.17 and 5.18 the adsorption chiller-based systems with respect to the absorption chiller are less affected by the variation in the type of collector and the heat dispersion system

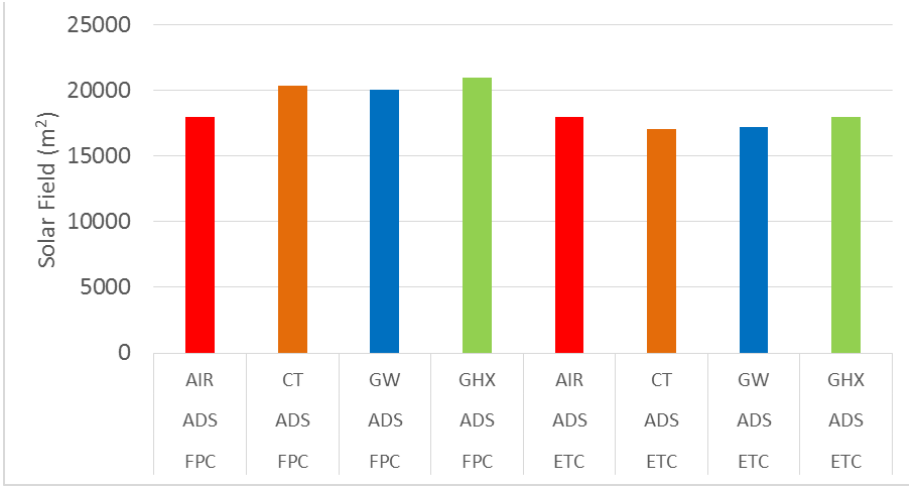

Fig. 5.17 - Solar field area (ADS) Dubai

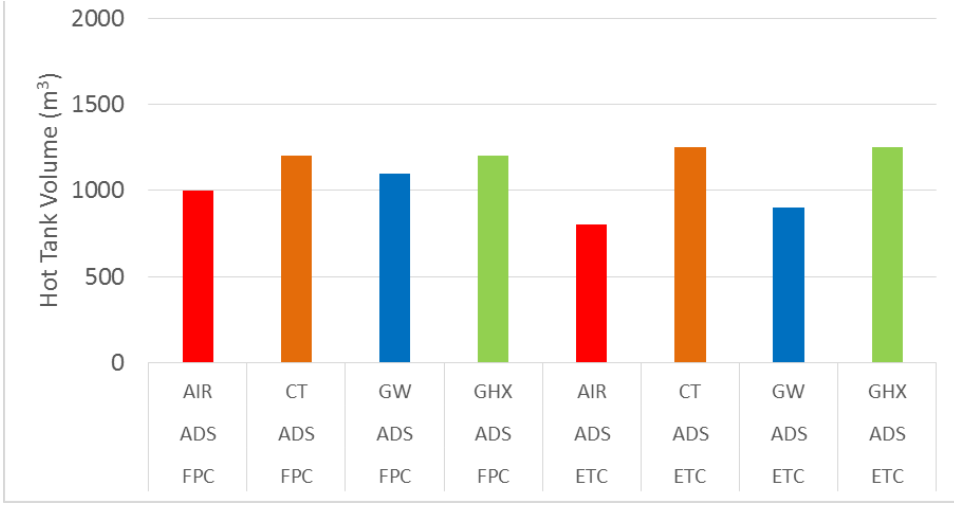

Fig. 5.18 - Hot tank volume (ADS) Dubai

5.1.4 Desiccant Evaporative Cooling

Desiccant Evaporative Cooling models are optimized only for the location of Riyadh, in Dubai the DEC system does not reach, in any configuration, the selected solar fraction of 70%. The results are reported for the single building.

Figure 5.19 shows the size of the solar field for the three configurations analyzed. The trend shows how the recirculating configuration reduces the solar field. Moreover, the difference between the results of the FPC-based configurations and the ETC one is more marked.

Figure 5.20 shows the volume of the tank, the reduction is well underlined both on the basis of the configuration and on the basis of the collector efficiency

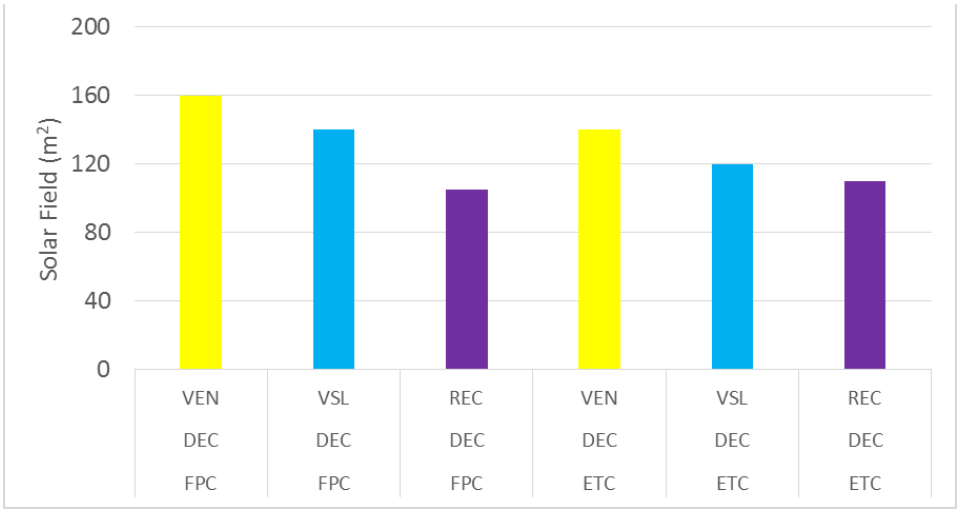

Fig. 5.19 - Solar field area (DEC) Riyadh

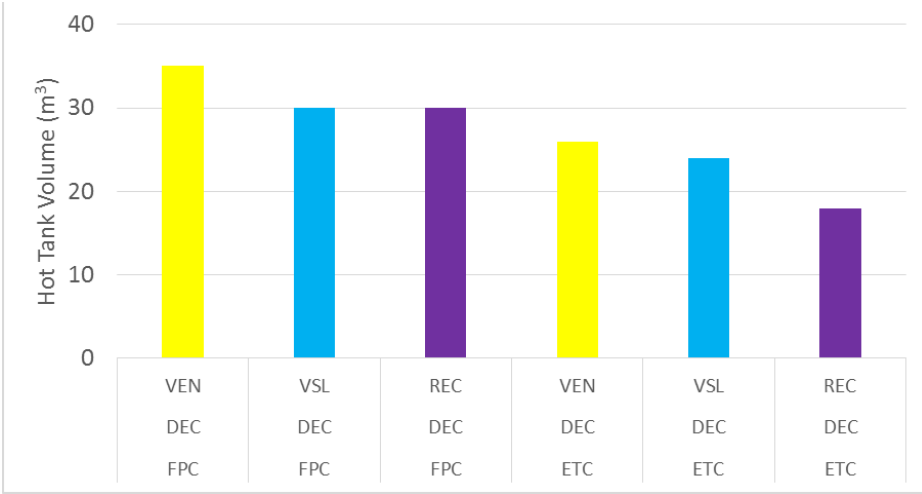

Fig. 5.20 - Hot tank volume (DEC) Riyadh

6 Solar Cooling Simulations and Results

This chapter presents the results of simulations of solar cooling systems.
The first part gives some consideration on field and tanks management whilst the second show the results of the cooling plant.
One result to highlight is the difficulty of air-cooled configurations, temperatures above 33 deg. C forcing the plant to stop to avoid the lithium-bromide crystallization. In these configuration the solar fraction of the project (70%) has been lowered to 50%. Only the configuration based on compression chiller and desiccant evaporative cooling work without risk at higher temperatures. This configuration reach the selected solar fraction also with the dry cooler.
Solar cooling performance analysis is performed by comparing collected energy from solar field and monthly outputs. Cooling production is not considered because is the same for all systems (same Solar Fraction).
The summary graphs were made using the same color legend of the previous chapter.

6.1 Variable speed pump

The use of the variable speed pump allows to obtain a constant temperature out of the solar field by modulating the flow rate (fig 6.1). This operation mode optimize the collecting energy as shown in fig. 6.2. The figures refer to the single solar field of 60 m^2. When the cooling load is low and the tank temperature is close to the collector outlet temperature, the delta T decreases and the flow rate increases until the limit is reached and the pumps are turned off to prevent overheating of the tanks.

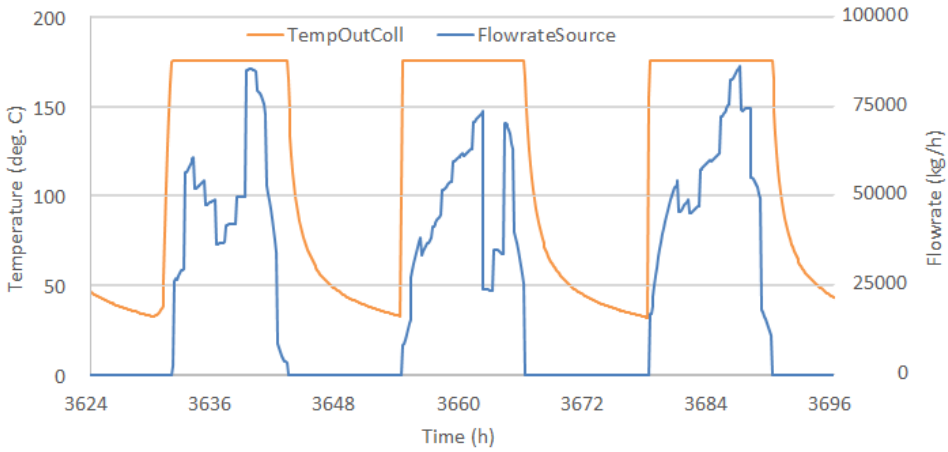

Fig. 6.1 - Solar field with variable speed pump

Fig. 6.2 - Collected heat of the PTC solar field

6.2 Hot tank

The buffer function is well highlighted in fig. 6.3 where are presented the upper and lower temperature of the tank for three types of absorption chiller powered by two different solar fields: ETC and PCT.

The trend of the chart shows the effectiveness of the tanks and the inclination of the curve after sunset indicates that tanks at a higher temperature guarantee an extension of the chiller operation nighttime. In fact, the trend of the yellow line indicates a rapid depletion of the energy level of tank fed by the FPC

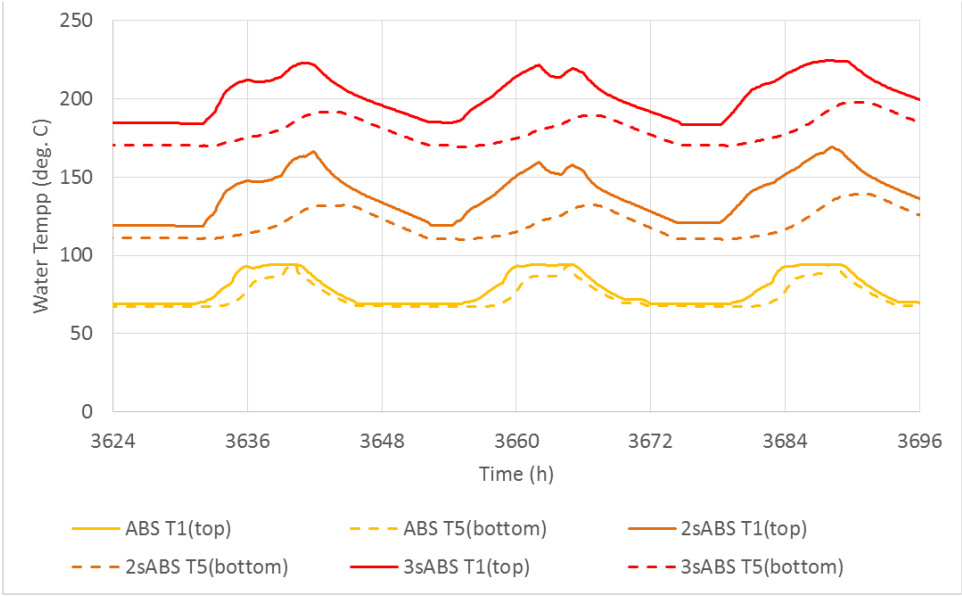

Fig. 6.3 - Comparison between hot tank temperature of different energy source

6.3 Compression Chiller

Solar cooling systems based on photovoltaic field and steam compression chiller offer the advantage of easy integration with all other systems. In fact, they do not need backup machines and the electricity overproduction can be used by other power systems or sold to the electric grid.

The first configuration presented does not utilize storages, electrical or thermal ones. All the electricity overproduction is delivered to the grid with a net metering scheme. This configuration has the same effect of

using an infinite capacity electrical storage. This solution is not feasible; selling GWh of energy creates a system block on the electric grid. If possible, the results are, of course, unquestionably positive.
In the second configuration, part of the energy produced by the PV field is stored in a battery and in a cold tank. The photovoltaic field production, as shown in fig. 6.4, is exported in the winter months where the import is reduced to zero. In the summer months the electric production is used to meet the cooling load with the help of the imported amount.
Figure 6.5 shows the plant management, the chiller are turned on and off to ensure that they work under design conditions to improve performance.

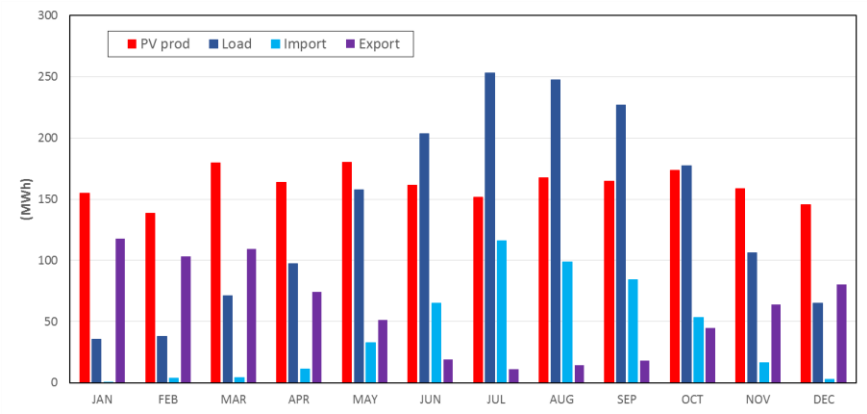

Fig. 6.4 - Dubay montly results of the PV+battery configuration

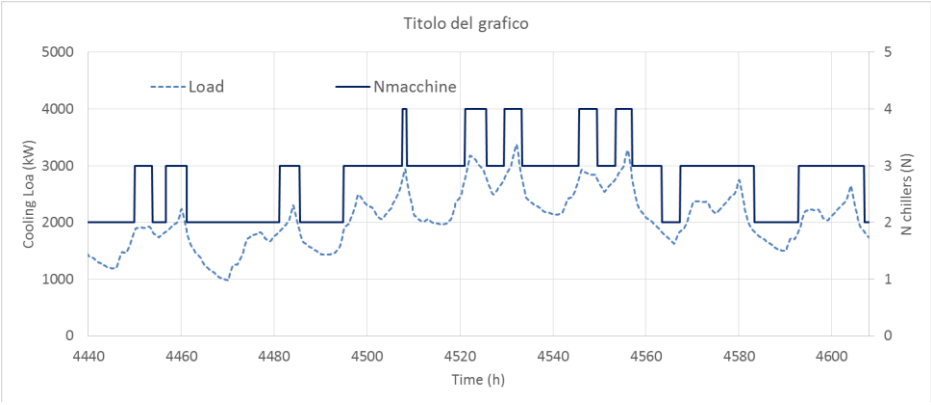

Fig. 6.5 - Chiller control strategy with chillers on-off

Figures 6.6 e 6.7 show the operation of the plant in three days in summer and winter in the location of Dubai. In the summer period, the contribution of the battery is clearly visible through the charge level, which extends the cooling production for a few hours. The energy produced by the photovoltaic field saturates the batteries and then is exported. When the PV production drop in the afternoon, the consumption of the stored energy in the batteries start.

In the winter period (Figure 6.7), electrical production is superfluous and is almost completely exported. Battery charge show a slight decrease only nighttime. A further benefit of the winter period is the improvement of the chiller COP.

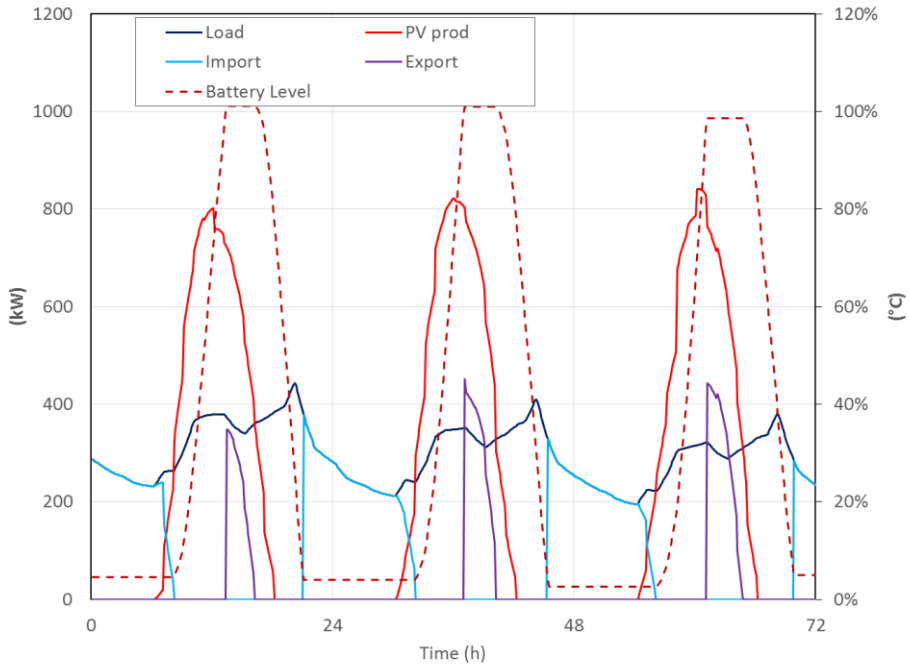

Fig. 6.6 - Dubai summer operation of the PV+CC+battery configuration

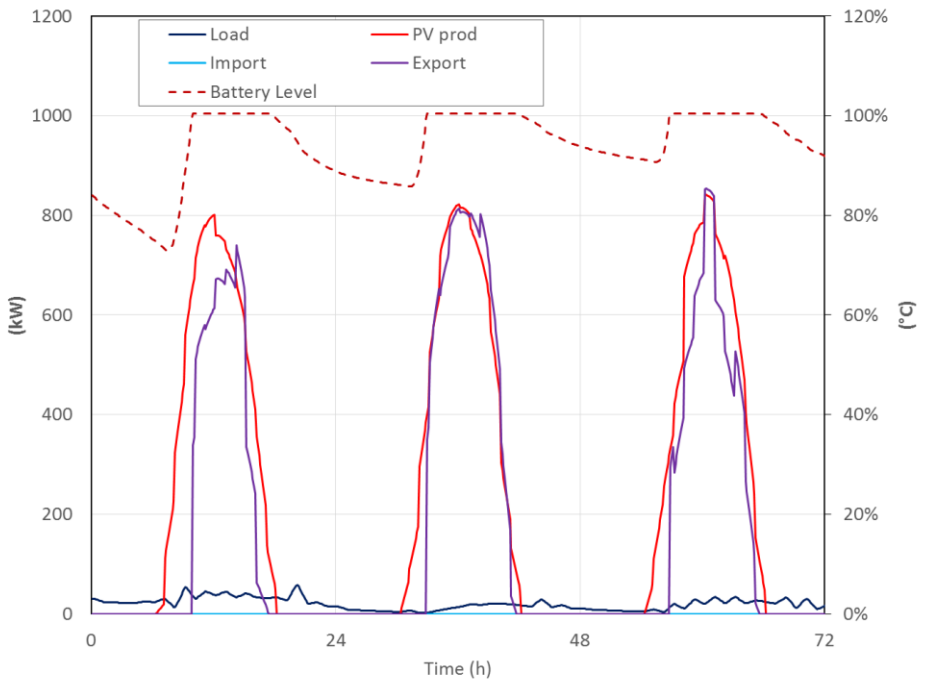

Fig. 6.7 - Dubai winter operation of the PV+CC+battery configuration

In this context, an analysis of heat recovery systems is presented. Photovoltaic production is linked to the consumption of the chiller and COP improves with more efficient heat rejection systems.
The chart in Figure 6.8 (Dubai location) as in the next 6.9 (Riyadh location) shows the electrical consumption of the chiller. The performance of configuration coupled with groundwater heat exchanger shows lower energy consumption, followed by ground heat exchanger configuration and cooling tower configuration.

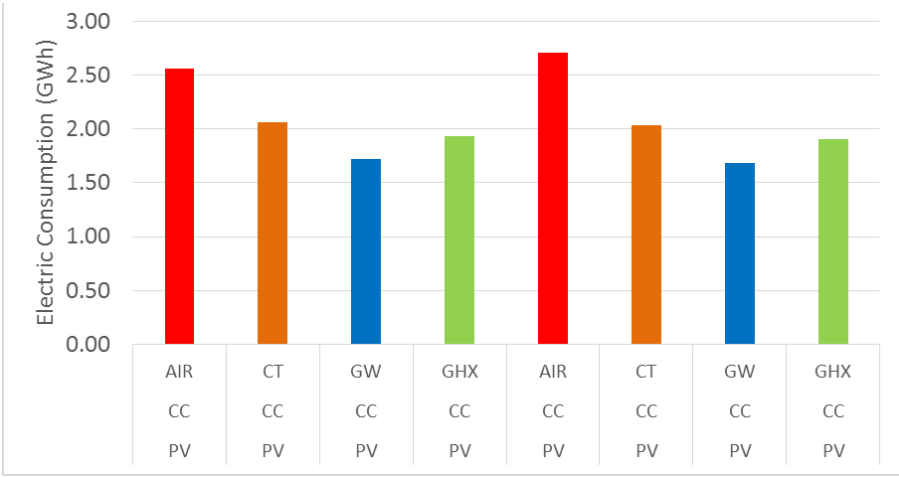

Fig. 6.8 - Electric consumption of PV based solar cooling systems with different heat rejection systems in Dubai

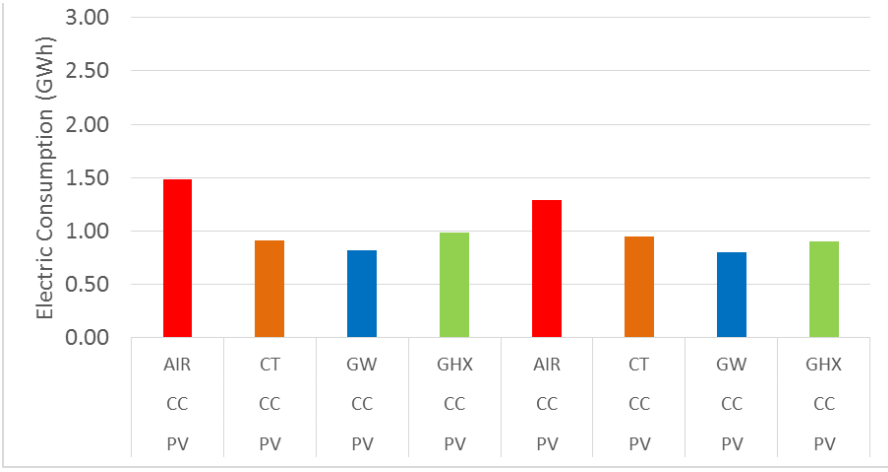

Fig. 6.9 - Electric consumption of PV based solar cooling systems with different heat rejection systems in Riyadh

6.4 Absorption Chiller

The solar cooling systems based on absorption chillers, in the three variants (single, double and triple effect), represent the majority of installed systems. The values of the air-cooled systems are not directly comparable with others since the solar fraction obtained is 50%.

Figure 6.10 shows the monthly results of the plant based on PTC coupled with the two-stage absorption chiller in the Dubai location. The energy collected in some months is inferior to the cold production because the COP of the chiller is above to 1. The configuration perfectly covers the cooling loads during the year leaving the summer peaks at the auxiliary chillers.

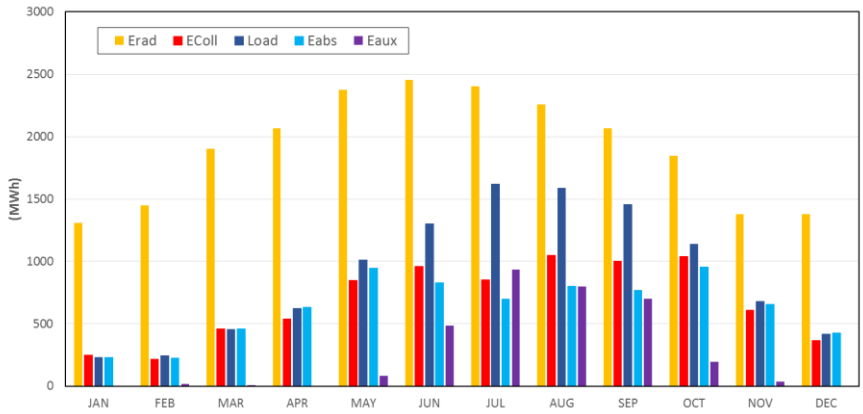

Fig. 6.10 - Dubai monthly results of the PTC+2sABS+GW solar cooling plant

Figures 6.11 and 6.12 show the trend of the main value for three typical summer and winter days. The PTC field, in the summer, collects energy for most of the morning and feeds the absorption chiller to meet the cooling load and recharging the cold tank. In the afternoon the chiller shows intermittent running as it only has to cover the request of the building. Furthermore, the chart shows the importance of the hot tank: the cooling production is ensured also nighttime. The auxiliary chiller only shows some starts during the hot hours to cover cooling loads peaks.
During winter days, the absorption chiller is switched on only intermittently, the two tanks are never discharged and small starts are enough to keep the tanks loaded.

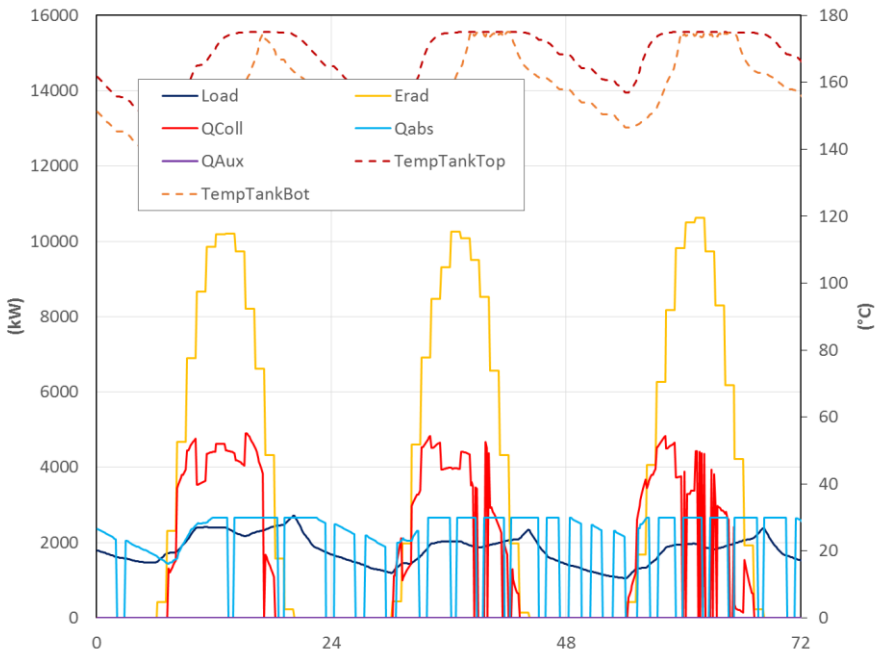

Fig. 6.11 - Summer operation of PTC+2sABS+GW configuration (Dubai)

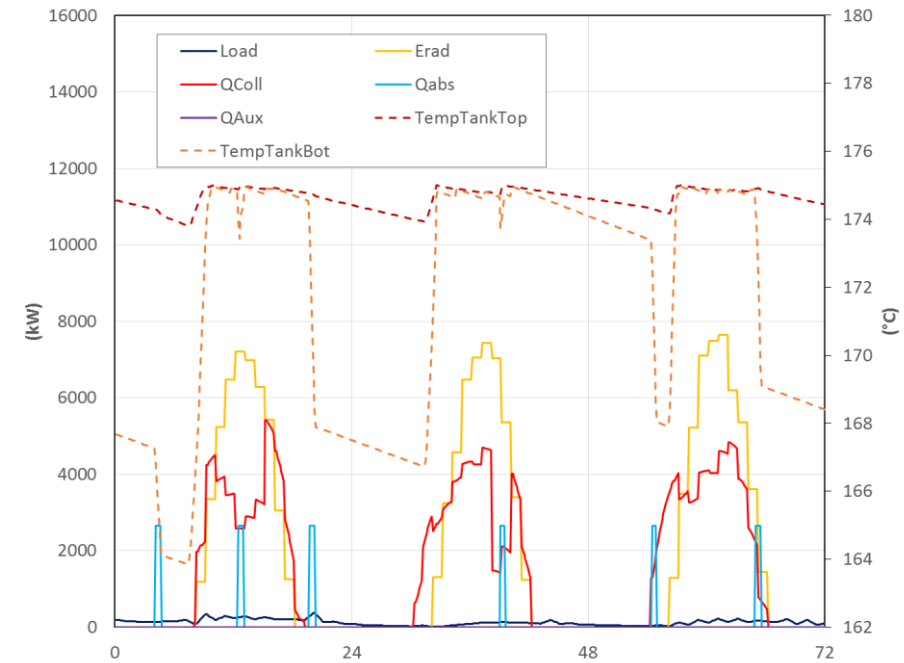

Fig. 6.12 - Winter operation of PTC+2sABS+GW configuration (Dubai)

The figure 6.13 shows the detail of the three typical summer days in Dubai for the air-cooled configuration. The outside temperature forcing the chiller to operate in a discontinuous manner with performance deterioration.

A further comparison, the simulation of the single-stage absorption chiller powered by the ETC field shows less balanced results; the performance of the chiller forces the field to collect more radiation to meet the cooling load. The trend of the principal value for three summer days as reported in figure 6.14. The chiller works without the help of the auxiliary chiller because of its larger size.

However, the tank is discharged rapidly and forces the auxiliary chiller to intervene also daytime.

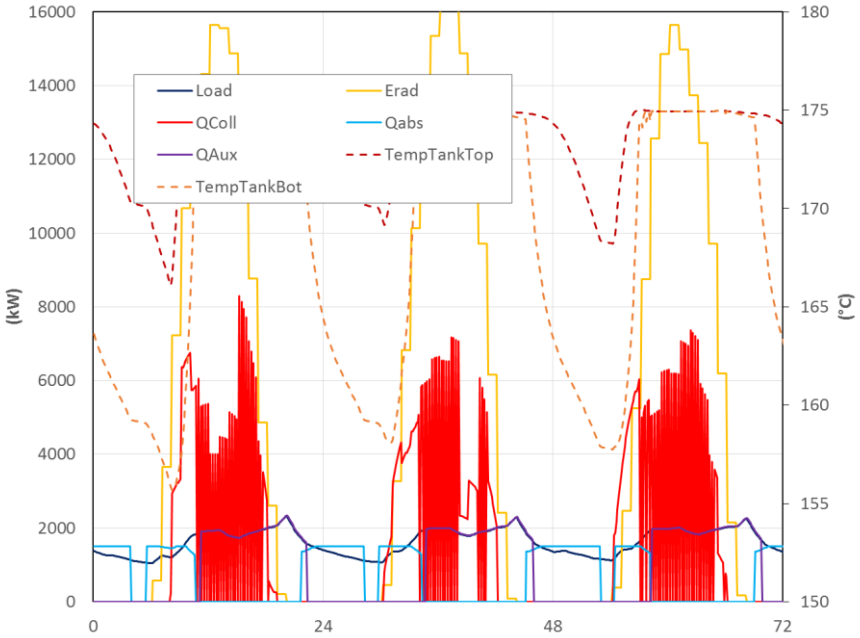

Fig. 6.13 - Summer operation of PTC+2sABS+AIR configuration (Dubai)

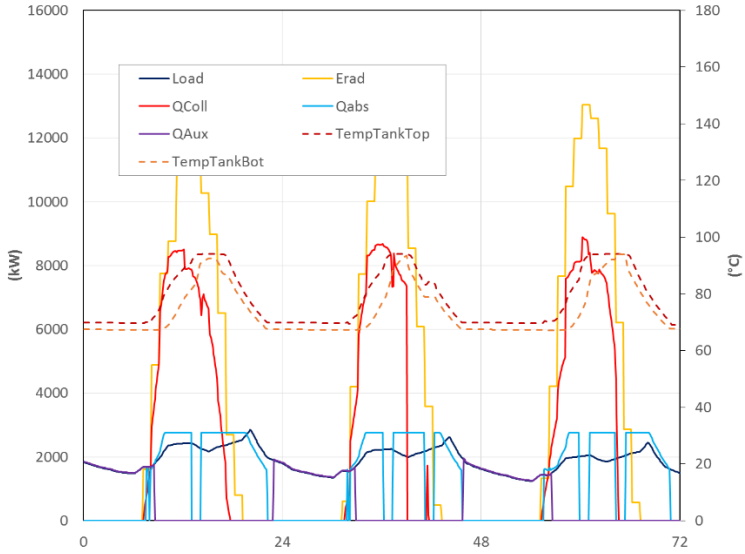

Fig. 6.14 - Summer operation of ETC+ABS+GW configuration (Dubai)

The importance of the heat rejection system for the chiller is shown in the graph below (Fig. 6.15). The difference is well underlined, the two systems guarantee about the same production in the winter months. When air temperatures rising in the summer months the air system loses efficiency and the cooling production is performed only during the night.

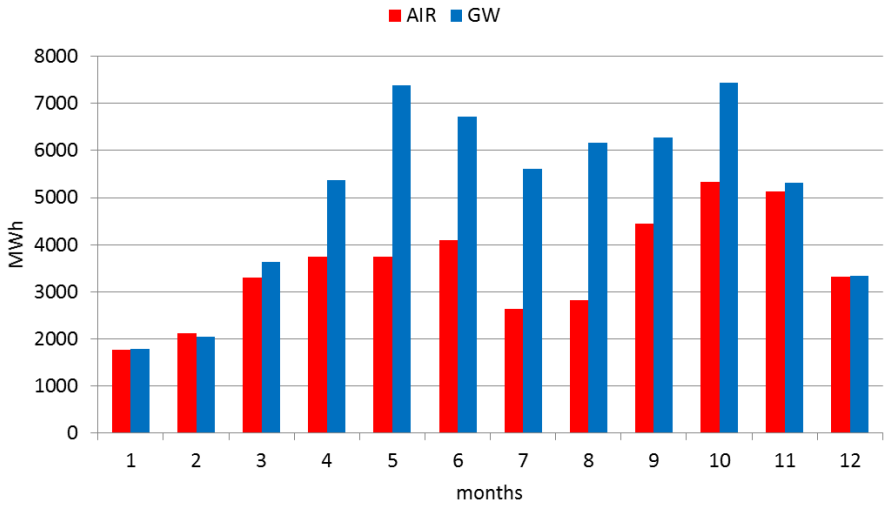

Fig. 6.15 - Cooling production of 2sABS with different heat rejection systems

The analysis continues by presenting the annual results of solar cooling plants in different configurations. Specifically, Fig. 6.16 shows the collected energy for the two stage absorption chiller coupled with two collects systems (ETC and PTC). The four different heat rejection systems are also proposed.

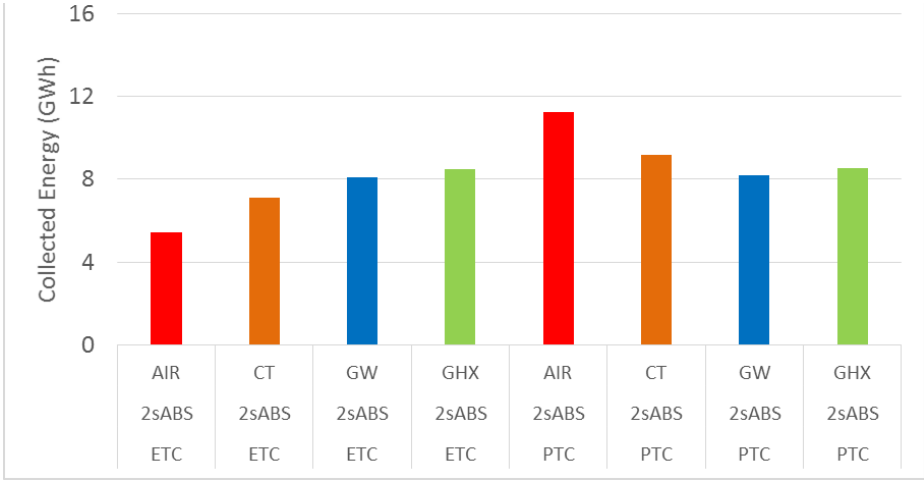

Fig. 6.16 - Collected energy with different solar field (2sABS) Dubai

Figures Fig. 6.17 e 6.18 show graphs of absorption chiller systems results in the two locations. Each type of chiller has been coupled with the collector that respects the thermal input level.
Efficiency improvement is evident in the transition between single effect to double effect chiller. Triple effect does not show interesting performance respect to the double stage one.

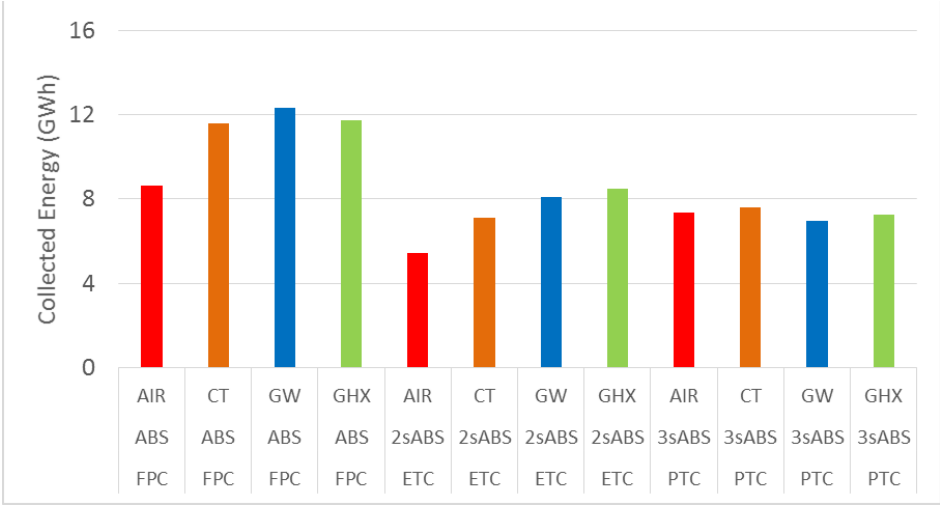

Fig. 6.17 - Collected energy of different absorption chillers - Dubai

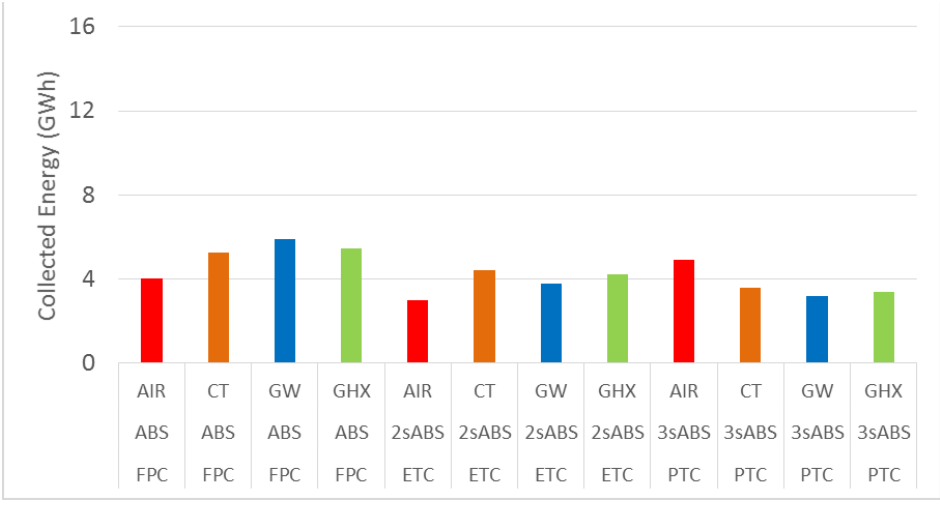

Fig. 6.18 - Collected energy of different absorption chillers - Riyadh

6.5 Adsorption Chiller

Adsorption chillers, over the years, have increased their COP but require thermal input at higher temperatures. This development allows better efficiencies but forces solar collectors to work at higher temperatures by reducing the performance of collector systems.

Figure 6.19 shows the simulation results on monthly basis. The energy produced by the chiller fully cover only a few months a year. The auxiliary chiller production is constant throughout the year.

Figures 6.20 and 6.21 show the operation of the system in three summer and winter days. In the summer the chiller works many hours a day but covers the cooling request only in the central hours of the day. The energy level of the tank drop quickly because the temperature difference is the lowest of all analyzed systems. In winter days the load is very load, just one chiller ignition is sufficient to cover the cooling request throughout the day.

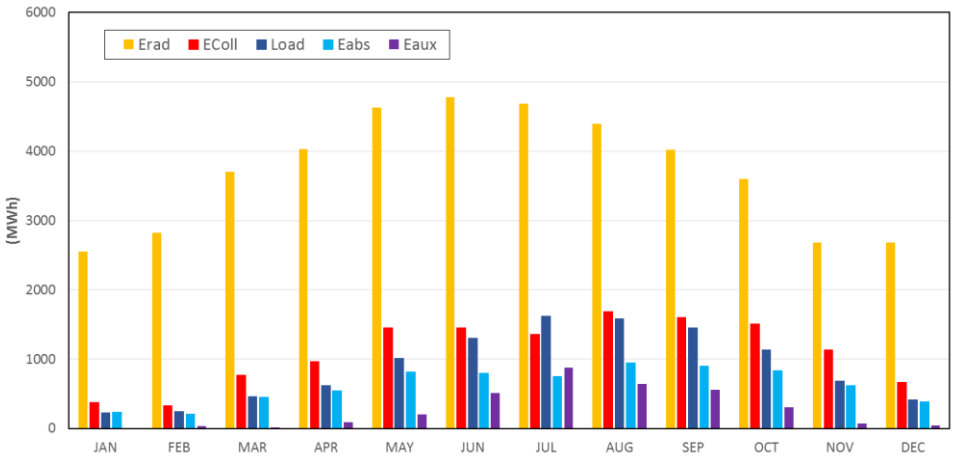

Fig. 6.19 - Monthly results of the FTC+ADS+GW solar cooling plant (Dubai)

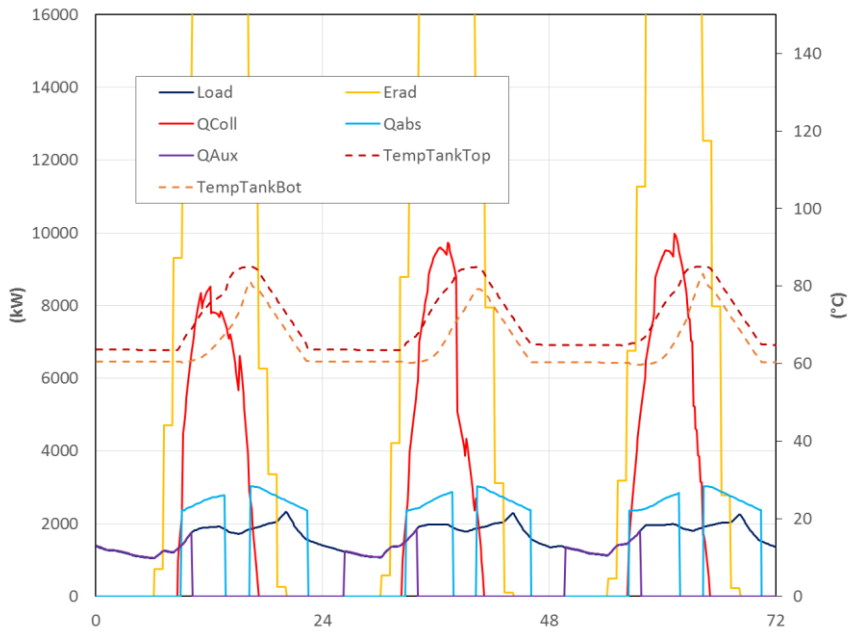

Fig. 6.20 - Summer operation of ETC+ADS+GW configuration (Dubai)

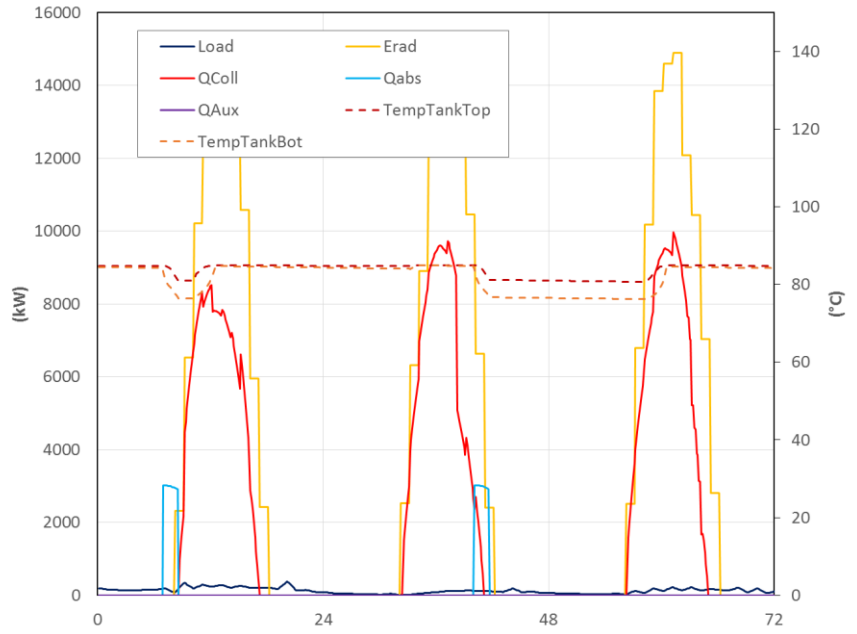

Fig. 6.21 - Winter operation of ETC+ADS+GW configuration (Dubai)

Figures 6.22 and 6.23 show the energy rejected in different configurations for the two selected locations. There are no significant differences between the collectors types and the between the heat recovery systems. The cause is to be found in the lower COP of the chiller that levels the differences of the connected systems.

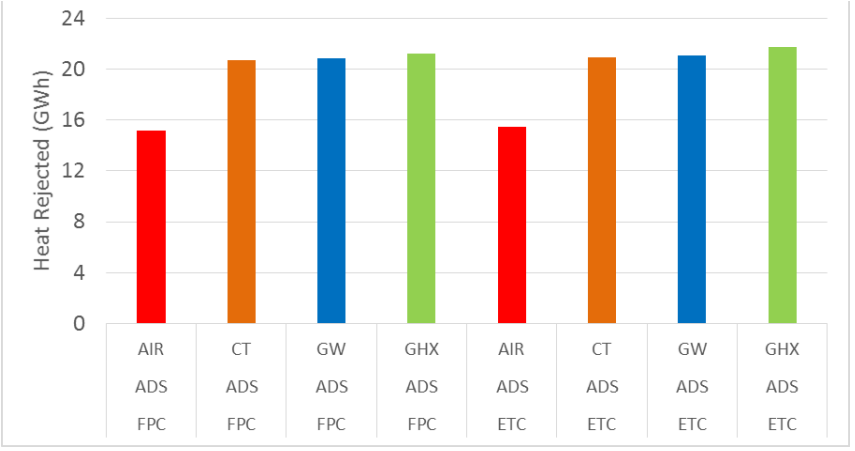

Fig. 6.22 - Heat rejected in different configurations (ADS) Dubai

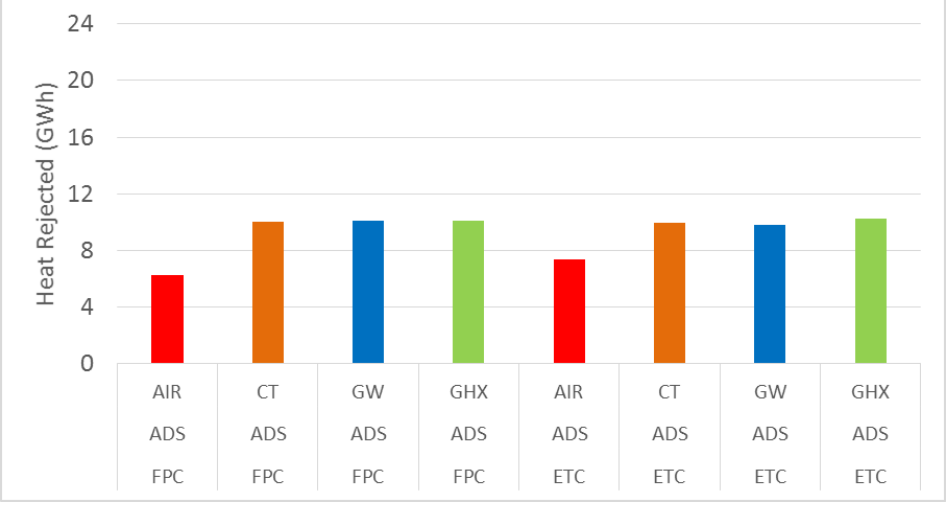

Fig. 6.23 - Heat rejected in different configurations (ADS) Riyadh

6.6 Desiccant Evaporative Cooling

The Desiccant Evaporative Cooling system exhibit very low performance under Dubai's climatic conditions due to the combination of high temperatures and high relative humidity. The ambient condition strongly limits the system's operation, especially by using a 24 deg. C set point. The air enthalpy in many hours of the summer season is too high to get, through the process in ventilation configuration, air at the set-point conditions of temperature and humidity forcing to stop the process in the summer season (Fig. 6.24). In winter months the cooling production (fig. 6.25) cover the cooling load under the limitation of air mass flow rate.

Specifically in Dubai-based simulations the models did not reach the desired solar fraction. The open-circuit system reach only the 20% of solar fraction for all configurations. The sizing values obtained, at the limit of the maximum size imposed, suggest an inability of the system to meet the refrigeration demand in this climatic situation.

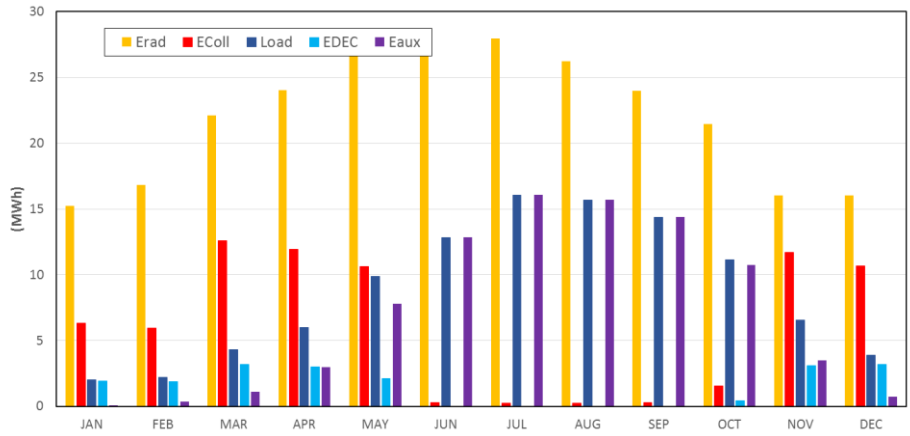

Fig. 6.24 - Months summary of the ETC +DEC (VSL) (Dubai)

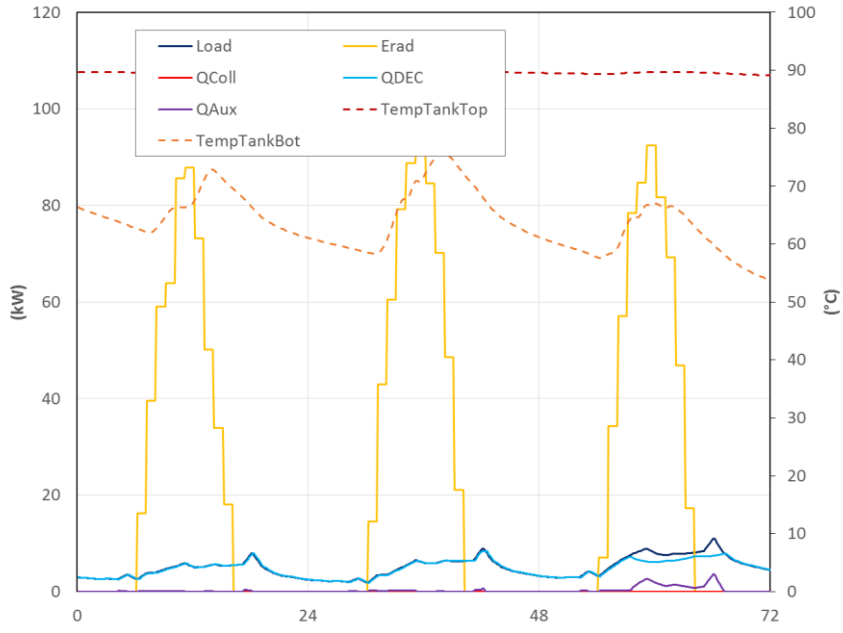

Fig. 6.25 - Winter operation of the FPC+DEC (VSL) (Dubai)

Figure 6.26 shows the main operating values of the DEC system powered by the ETC field in VSL configuration in the Riyadh region. The proportion between the solar energy collected and solar production shows an average COP of about 40%. The air conditioning capacity cover the cooling demand in the winter months, while in the summer the DEC system suffers the limitation of the air flow.

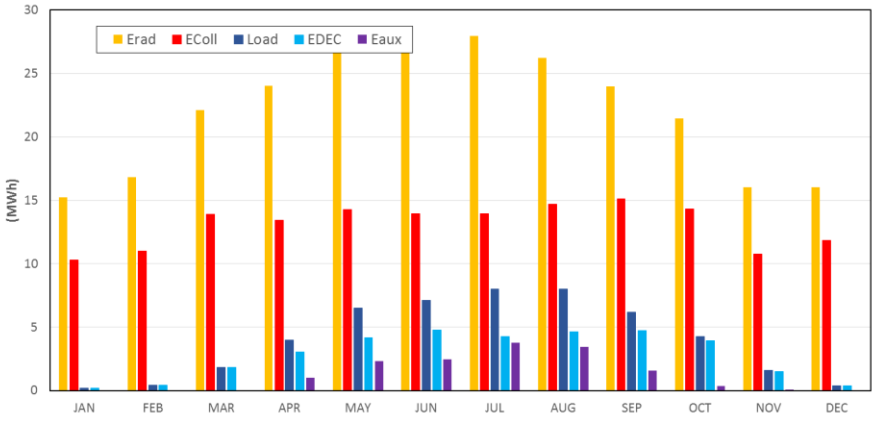

Fig. 6.26 - Months summary of the ETC +DEC (VSL) (Ryiadh)

Figure 6.27 shows the summer DEC operation, the auxiliary chiller cover the peaks of cooling demand. Hot storage temperatures are relatively low according to the operating parameters of the air conditioning system in this region.

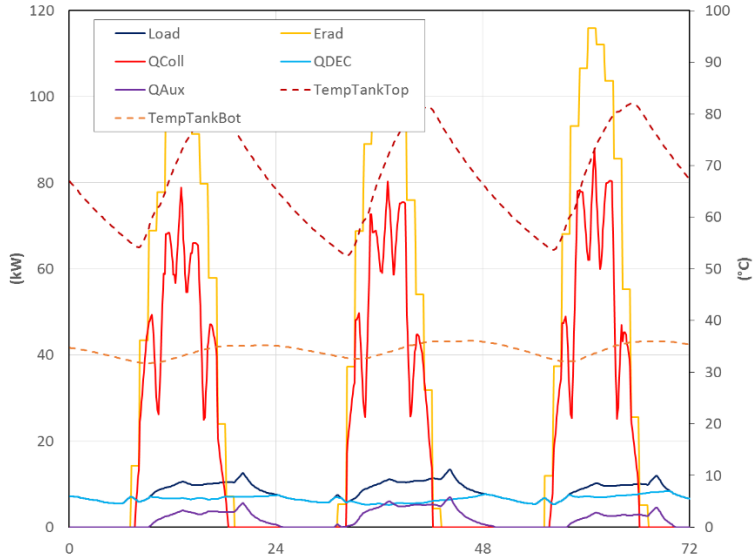

Fig. 6.27 - Summer operation of the ETC +DEC (VSL) (Ryiadh)

A comparison of the different types of DEC configuration is shown in Figure 6.28. The recirculating configuration allows higher COPs (same as Solar Fraction, less energy required).

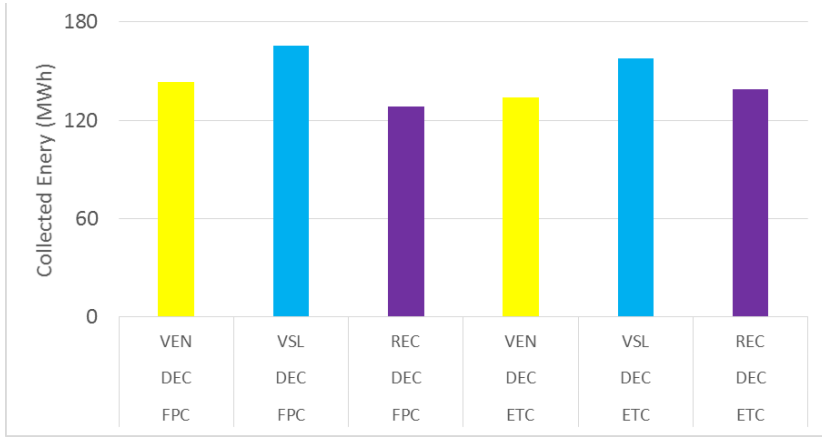

Fig. 6.28 - collected energy (DEC) Riyadh

Another important aspect are presented: the water consumption to feed the system. Evaporative cooling requires continuous water supply. The configurations that ensure better energy performance are also those that consume more process water (Fig. 6.29).

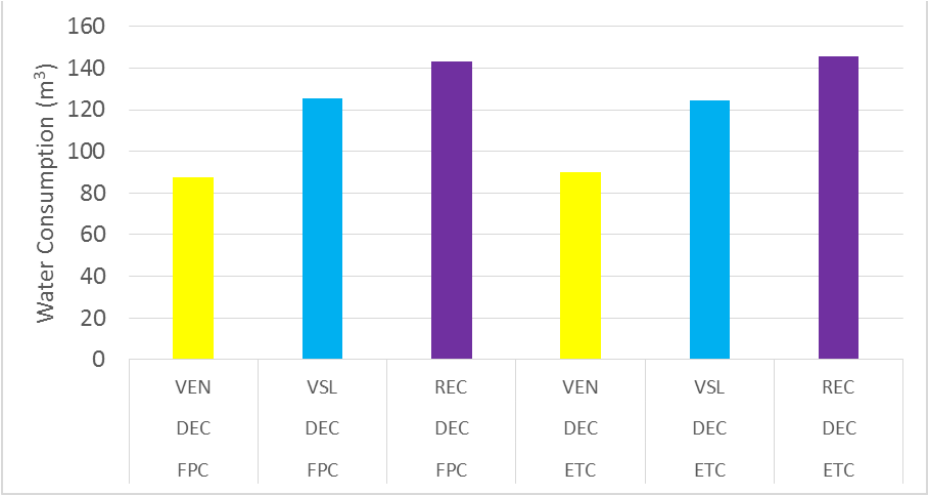

Fig. 6.29 - Water consumption (DEC) Riyadh

6.7 Water Consumption

An important aspect for solar cooling systems in arid or low water resources is the plants water consumption. The typical configuration of this type of solar cooling system involves the installation of evaporator towers for the chiller cooling circuit.

To consider water consumption in subsequent graphs, water consumption is reported for all systems based on evaporative tower. Fig. 6.30 report the results for the Dubai location and Fig. 6.31 for the location of Riyadh.

Fig. 6.30 - Cooling tower water consumption (Dubai)

Water consumption decreases with the improved performance of the solar cooling plant based on absorption/adsorption chiller. Solar cooling systems based on triple effect absorption chillers are characterized by lower water consumption in the location of Dubai.

A different result is obtained for desiccant evaporative cooling systems. In order to compare the results the consumption of a single building was multiplied by the number of compound buildings.

DEC systems are highlighted for less water consumption among all systems analyzed in the inland region while in the coastal regions they fail to reach the target solar fraction.

Compression chiller solar cooling systems are characterized by considerably higher water consumption in coastal regions where climatic conditions force the evaporative tower to work for many more hours.

Fig. 6.31 - Cooling tower water consumption (Riyadh)

6.8 Best Solutions

A further analysis of the energy performance of solar cooling systems is done by comparing them to decide on the best configuration. The data presented is the energy collected.

Figures 6.32 and 6.33 show the difference between the efficiency of cooling plant based on compression chiller and all others. The absorption/adsorption chiller systems show a net decrease in rejected energy proportional to the efficiency of the chiller. In this group, the triple effect absorption chiller fed by PTC is the best configuration, but the performance of the compression chiller systems is more energy efficient. In the location of Riyadh the gap decreases but remains considerable. The desiccant evaporative cooling system shows the lowest efficiency among the systems analyzed.

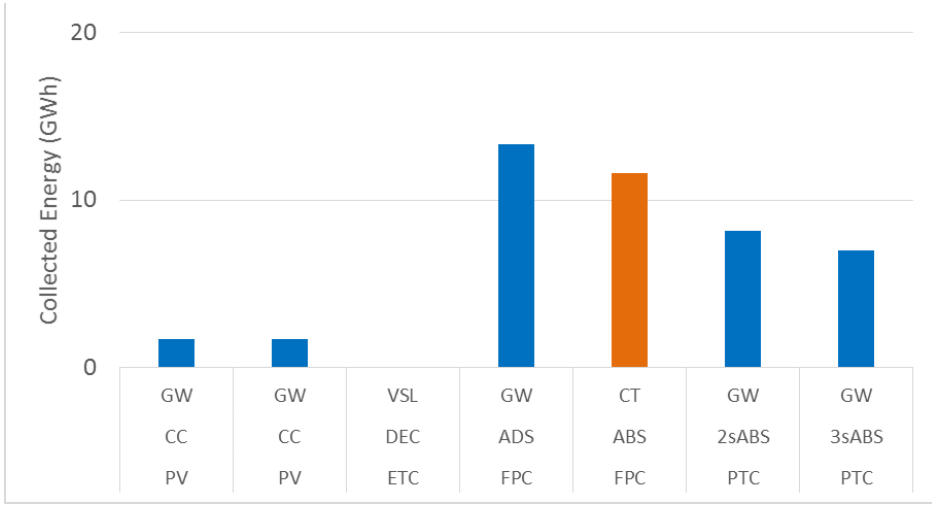

Fig. 6.32 - Collected energy by different solar cooling plant (Dubai)

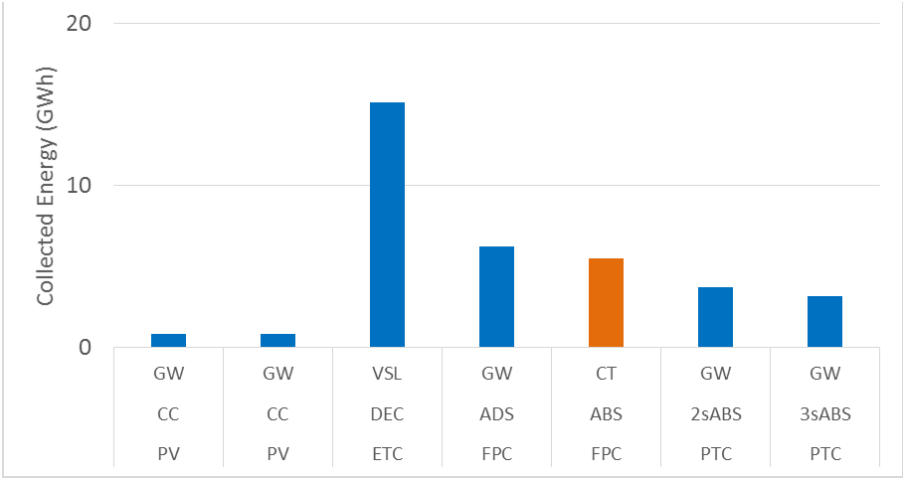

Fig. 6.33 - Collected energy by different solar cooling plant (Riyadh)

To conclude the available comparisons, two other models were developed to simulate the behavior of an Heat Pump capable of meeting the cooling load of a single building.

The comparison, shown in Figs 6.34 e 6.35, is based on the annual electricity consumption. In fact, all solar cooling configurations require electricity for the auxiliary chiller and for drive district cooling pumps.

For both locations, the enormous energy savings are well underlined by applying any of the proposed solar cooling technologies.

Also, in the case of a photovoltaic field, negative values can be obtained as the electric energy exported is greater than the imported one.

The best energy efficient configuration is based on compression chiller coupled with PV field. The second choice results the tripe effect absorption chiller drive by PTC.

Even the DEC system, in the Riyadh region, consumes about half of the electricity compared to a convention system, ensuring the same level of comfort.

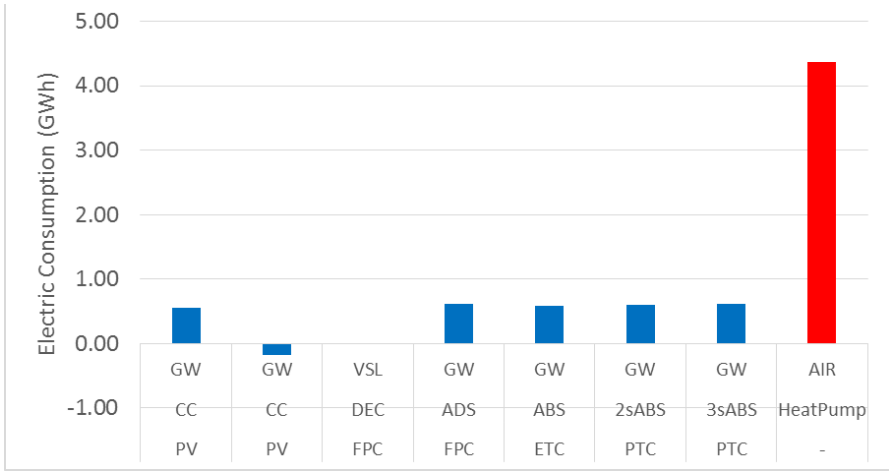

Fig. 6.34 - Annual electric energy balance (Dubai)

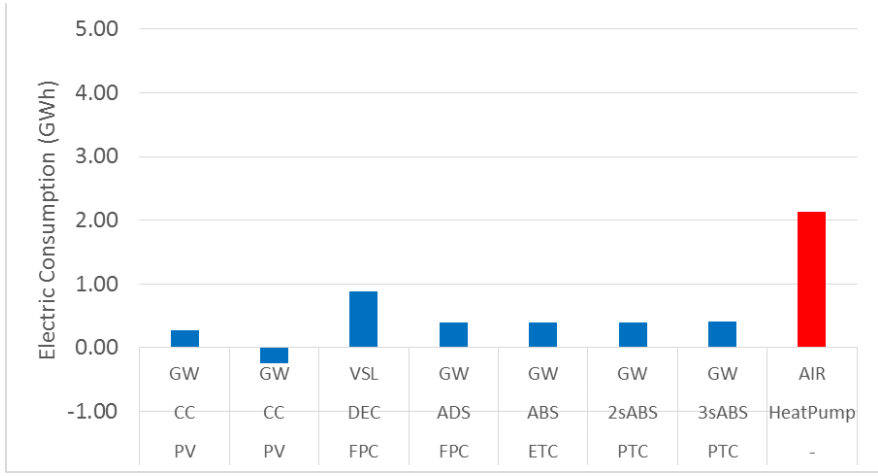

Fig. 6.35 - Annual electric energy balance (Riyadh)

Another important aspect for the greenhouse effect is CO_2 production.
In this paragraph, an estimation of the CO_2 emission is made using solar cooling systems.
The starting data are the annual electricity consumption and the national conversion factor of the electric plants (0.43 UAE, 0.37 KSA) reporte by the World Energy Council [1]. Figures 6.36 and 6.37 show primary energy consumption in tonnes of equivalent oil. Figures 6.38 and 6.39 the CO_2 emitted in the production of the electricity imported from the grid. The results shown in the figure underlined the environmental advantage of applying solar cooling technology.

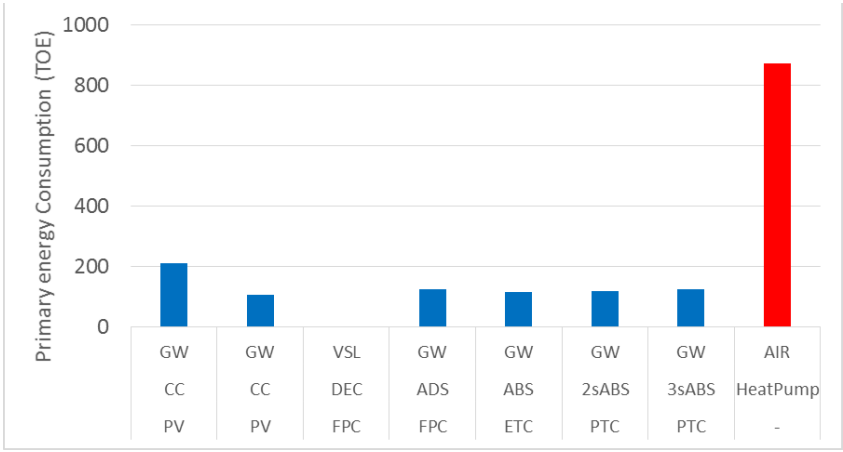

Fig. 6.36 - Primary energy consumption (Dubai)

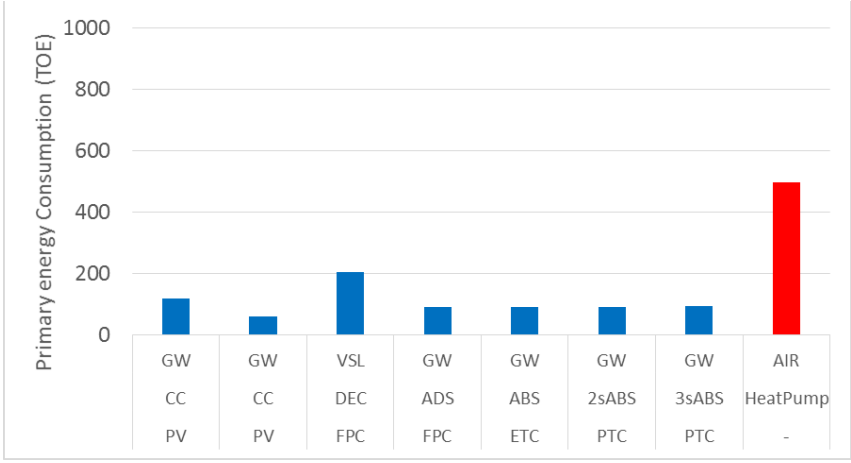

Fig. 6.37 - Primary energy consumption (Riyadh)

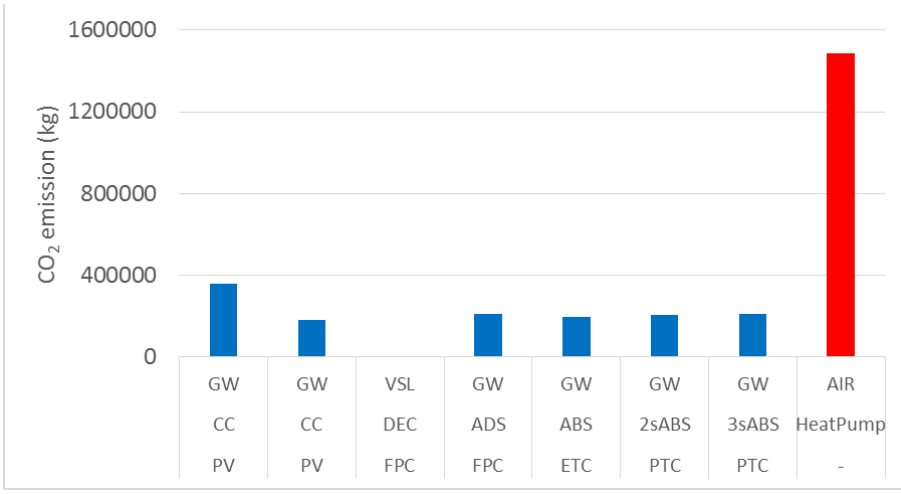

Fig. 6.38 - CO_2 emission (Dubai)

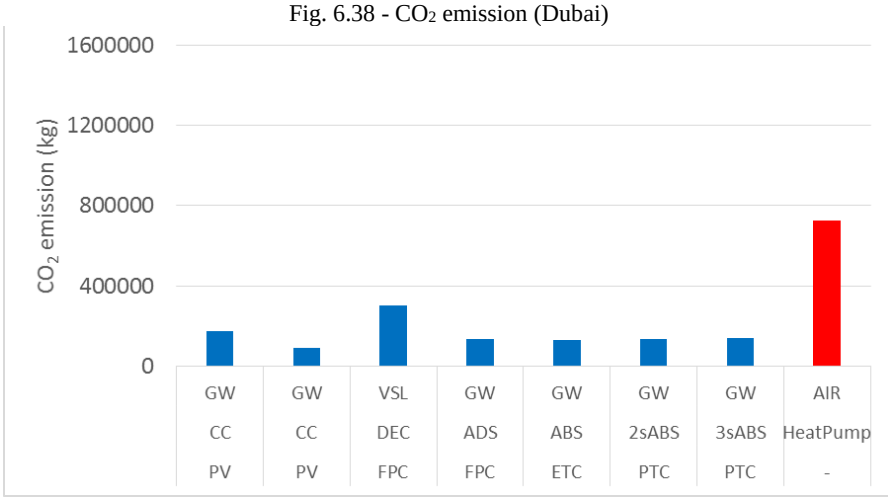

Fig. 6.39 - CO_2 emission (Riyadh)

7 Economic analysis

Economic analysis is an indispensable step in the development of solar cooling systems. The energy validity of a system can be frustrated by a price that puts it out of the market. Table 7.1 shows the costs used for economic analysis divided into four categories: collectors, storage, chiller and heat rejection systems.

Table 7.1 - Unit cost adopted for the economic analysis

Collectors	**unit**	**value**
Flate Plate Collectors	$/m^2	380
Evacuated Tube Collectors	$/m^2	500
Parabolic Trough Collectors	$/m^2	480
Photovoltaic	$/m^2	260
Storage	**unit**	**value**
Hot Tank (low temp)	$/m^3	450
Hot Tank (high temp)	$/m^3	850
Cold Tank	$/m^3	450
Battery	$/kWh	510
Chiller	**unit**	**value**
Compression Chiller (air cooled)	$/kW	165
Compression Chiller (water)	$/kW	130
Absorption Chiller	$/kW	400
2s Absorption Chiller	$/kW	530
3s Absorption Chiller	$/kW	610
Adsorption Chiller	$/kW	450
Desiccant Evaporative Cooling	$/kW	320

Heat Rejection	unit	value
Air Cooler	$/kW	35
Cooling Tower	$/kW	24
Groundwater Well	$/kW	21
Ground Heat Exchanger	$/kW	330

7.1 Compression Chiller

The cost of the solar cooling system based on compression chillers is low for the great availability on the market of this technology.

Figure 7.1 shows the overall cost of the solar cooling plant, referring to the location of Dubai, divided by heat rejection systems. The graph shows the lowest cost of the system coupled with the heat rejection system based on groundwater.

Figure 7.2 shows the same configurations for the location of Riyadh. The trend shown is similar but the absolute value of the cost is significantly lower. Comparing the cost of the plant with respect to the annual cooling load we get the same $/kWh value for the two selected location.

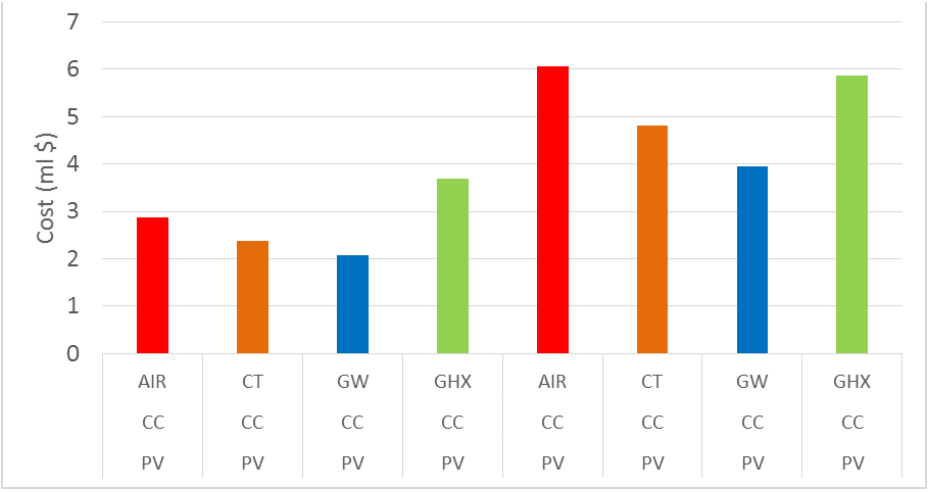

Fig. 7.1 - Cooling plants cost (CC) Dubai

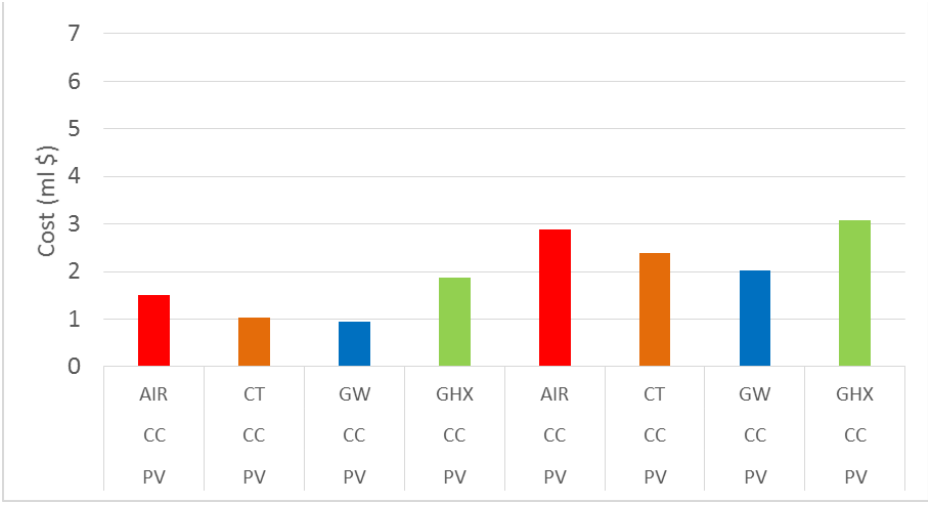

Fig. 7.2 - Cooling plant cost (CC) Riyadh

The first four cases of the Fig. 7.1-2 are characterized by the absence of a battery whose cost is shown in Figure 7.3. The efficiency of the heat rejection systems influence the size of the battery.

The most expensive component of the cooling plant is the solar field, whose cost trend (figure 7.4) reflects the overall cost trend.

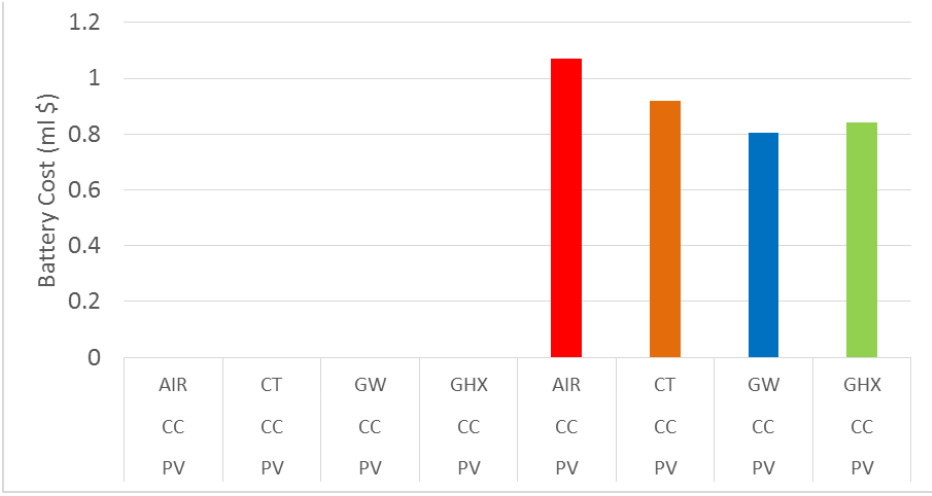

Fig. 7.3 - Battery cost (CC) Dubai

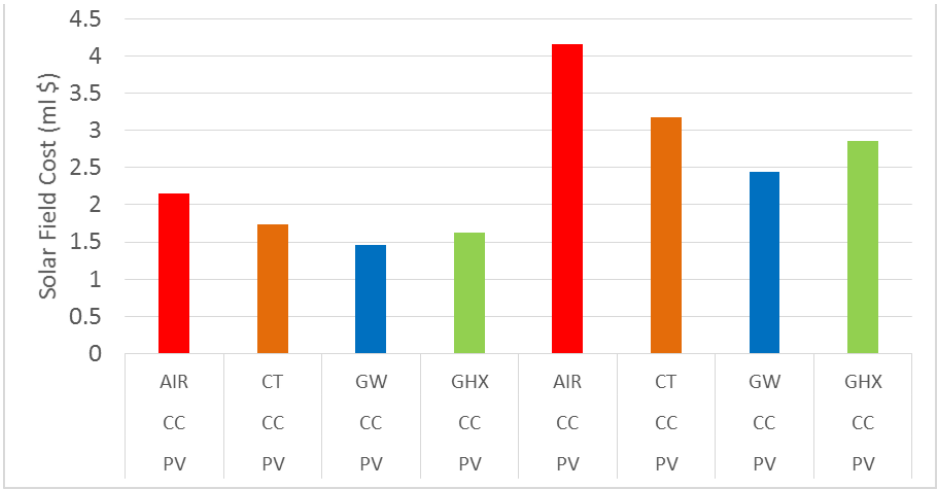

Fig. 7.4 - Solar field cost (CC) Dubai

The cost of the chiller is essentially constant for all configurations. Particularly important is the cost of the heat rejection system in Fig.7.5. The cost of geothermal probes, due to the characteristics of the soil, economically penalize an energetically effective system.

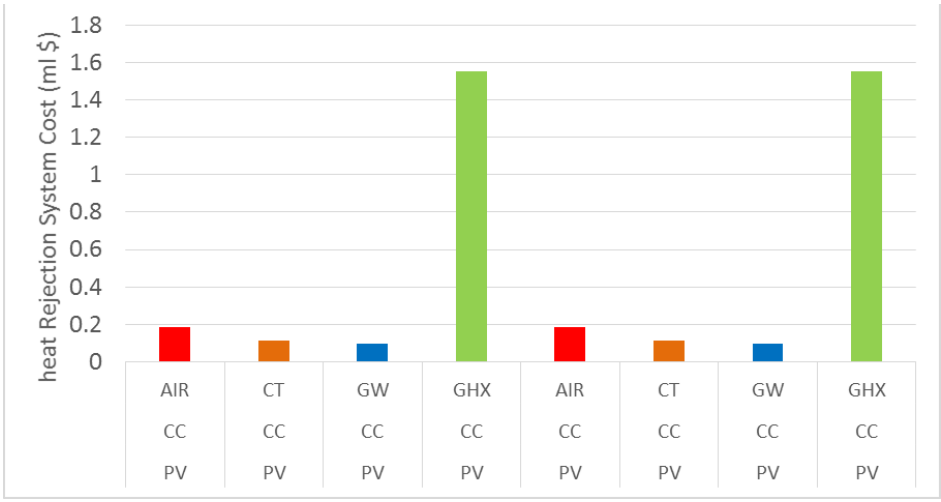

Fig. 7.5 - Heat rejection systems cost (CC) Dubai

7.2 Absorption Chiller

This section presents the economic analysis of solar cooling systems based on the absorption chiller in the three variants: single effect, double effect and triple effect. Figures 7.6 and 7.7 show the single-stage absorption chiller system with different heat rejection systems. In the Dubai location, the system drive by the FPC works better with the evaporative tower, while the ETC configuration is the cheaper when coupled with groundwater heat exchanger.

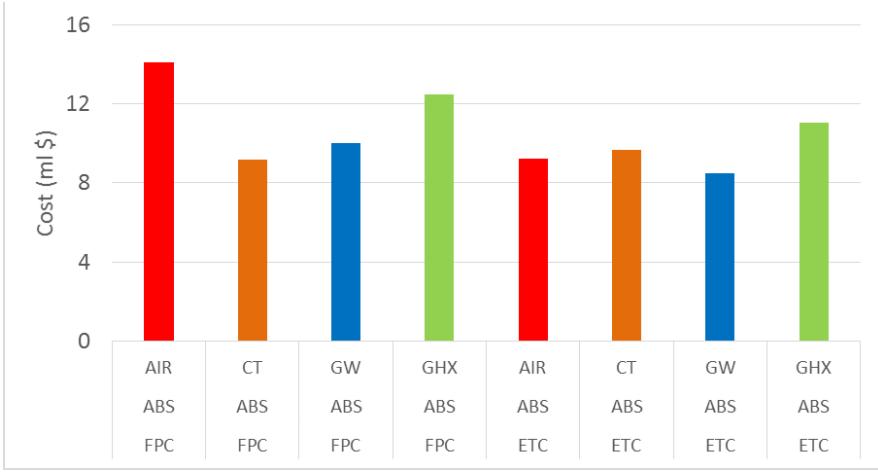

Fig. 7.6 - Cooling plant cost (1sABS) Dubai

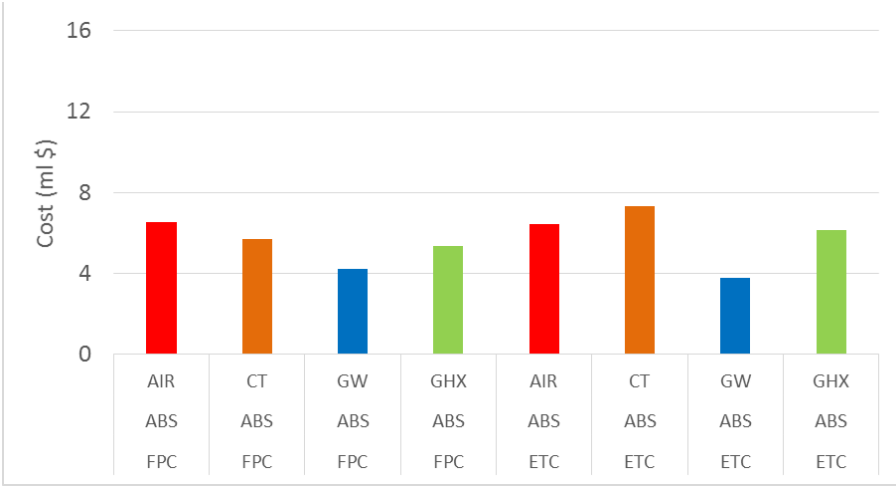

Fig. 7.7 - Cooling plant cost (1sABS) Riyadh

The components cost of the cooling system is shown in Figures 7.8, 7.9 and 7.10 where the cost of the solar field, the storage cost and the heat rejection system cost are represented.

The solar field cost (Fig. 7.8) for the single stage absorption chiller is poorly influenced by the type of collector while it has variations depending on the heat rejection systems.

The cost of the hot tank (Fig. 7.9) is affected by the solar collector system. As the collector efficiency increases, storage cost decreases.

The cost of the heat rejection system (Fig. 7.10) is affected by the difficulty of realization, and the use of geothermal probes is highly unsuitable.

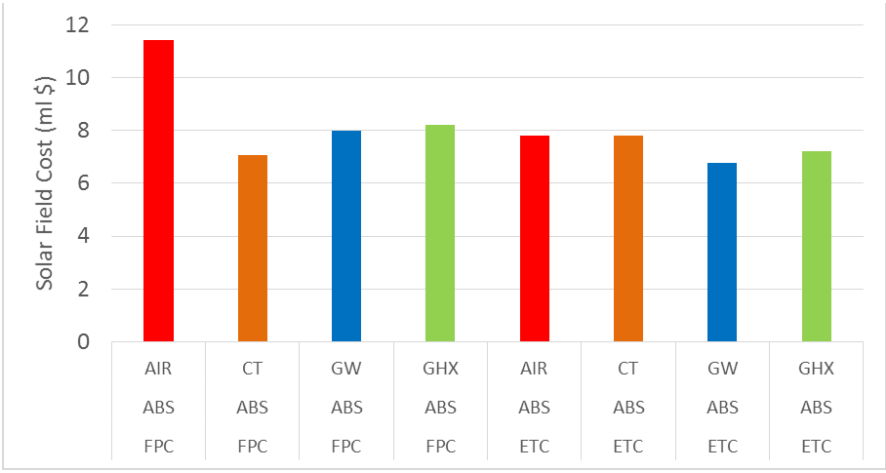

Fig. 7.8 - Solar field cost (1sABS) Dubai

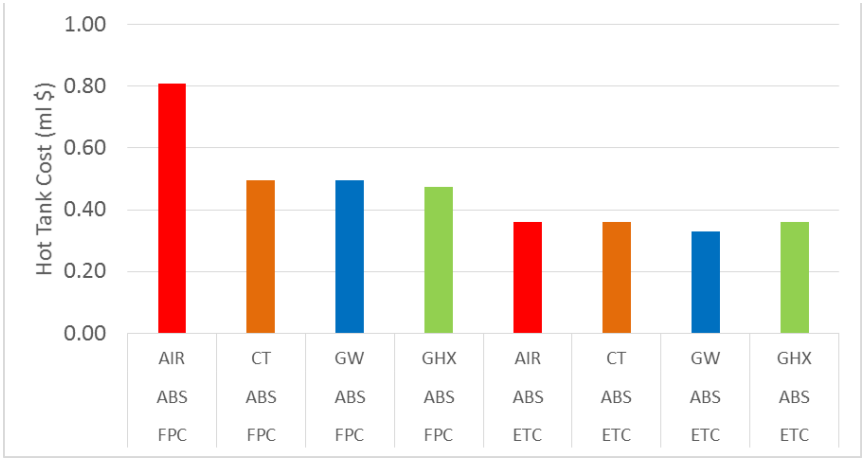

Fig. 7.9 - Hot tank cost (1sABS) Dubai

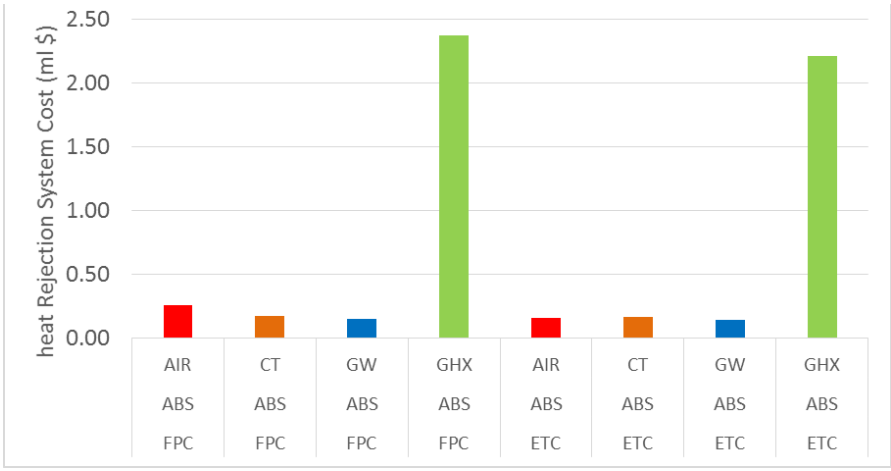

Fig. 7.10 - Heat rejection system cost (1sABS) Dubai

Figures 7.11 and 7.12 show the cost of the absorptions chiller. The cost difference is not so obvious because solar field savings are offset by higher unit cost of chillers and pressurized storage.

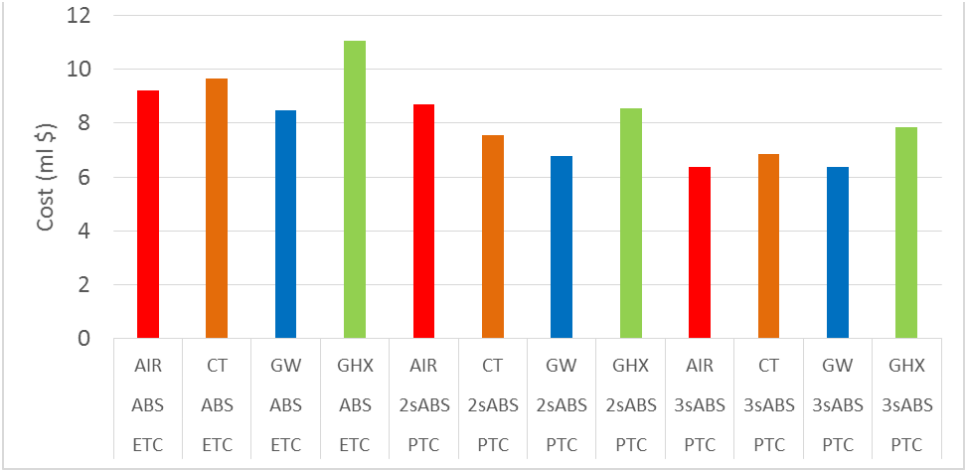

Fig. 7.11 - Solar cooling plant cost (1sABS, 2sABS, 3sABS) Dubai

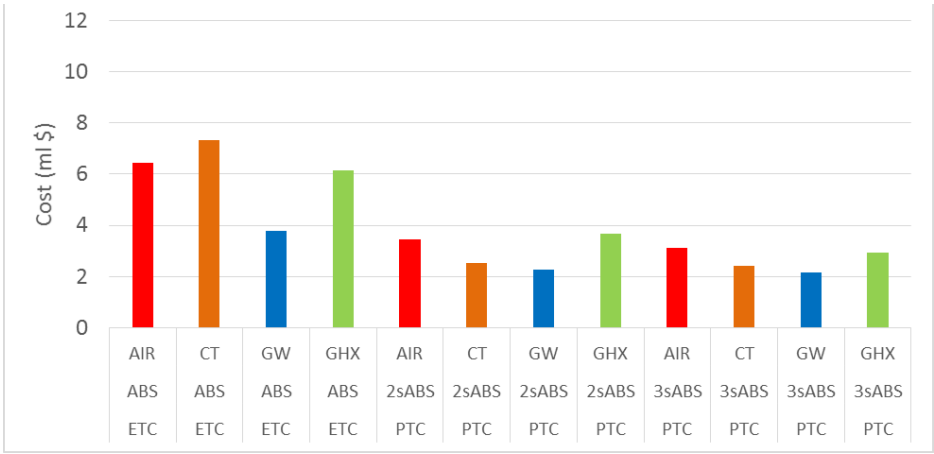

Fig. 7.12 - Solar cooling plant cost (1sABS, 2sABS, 3sABS) Riyadh

7.3 Adsorption Chiller

Figures 7.13 and 7.14 show the costs of the adsorption chiller models.
As for the data presented in the previous chapters, the differences between the various configurations are unclear. Only the cost of the ground heat exchanger is highlighted.

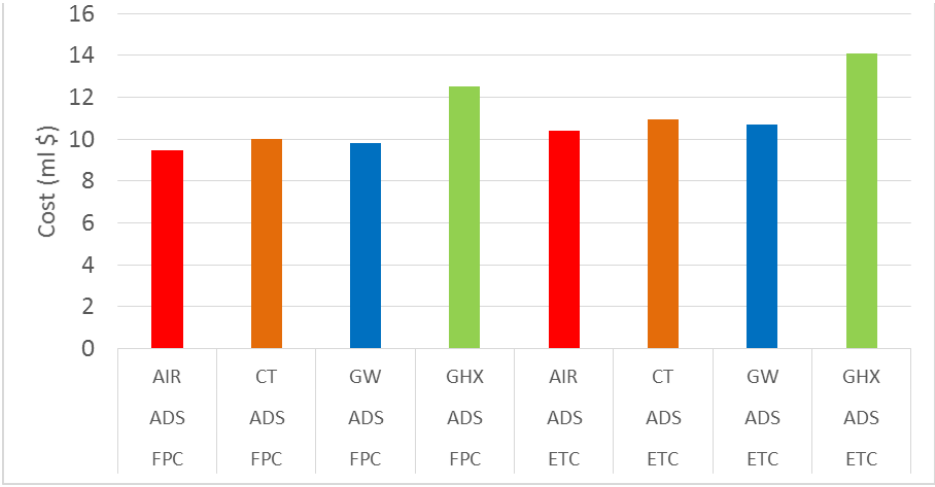

Fig. 7.13 - Cooling plant cost (ADS) Dubai

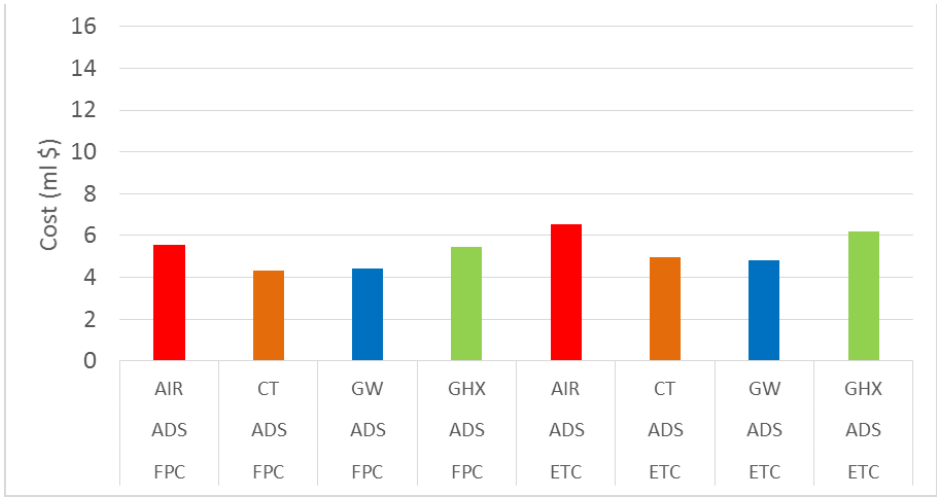

Fig. 7.14 - Cooling plant cost (ADS) Riyadh

7.4 Desiccant Evaporative Cooling

The desiccant evaporative cooling system is a rare application in the solar cooling system. Figure 7.15-16 shows the cost of the DEC systems in the various configurations. The lower cost of the recirculation configuration is due to the smaller storage size and therefore also its cost (Fig. 7.17). the last chart underlined also the importance of the collector efficiency, in the recirculation configuration the cost reduction reach the 35%.

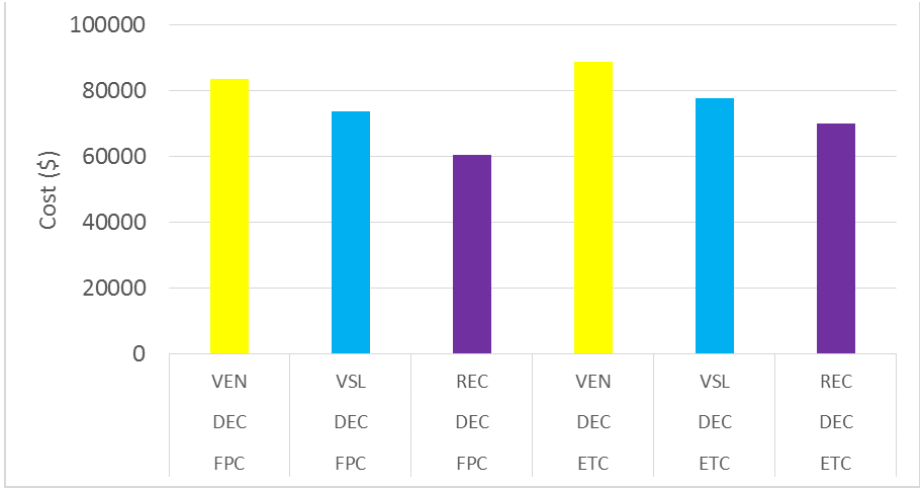

Fig. 7.15 - DEC cost (Riyadh)

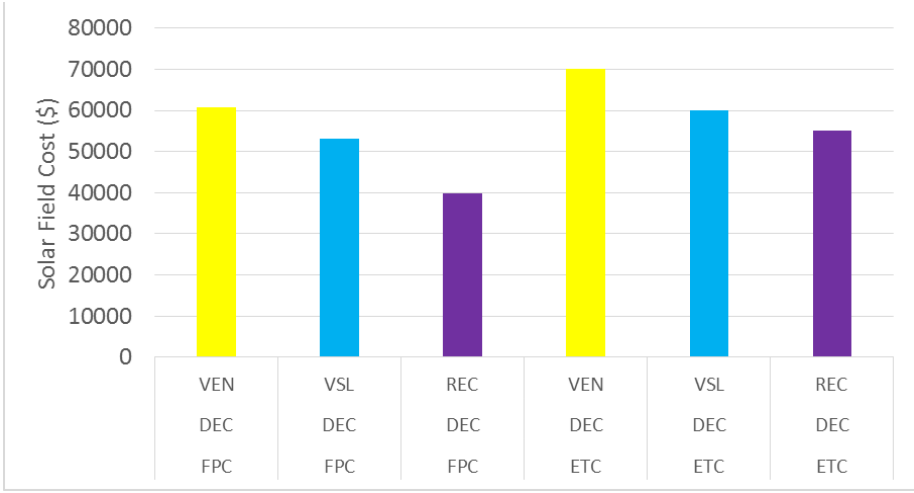

Fig. 7.16 - Solar field cost (DEC) Riyadh

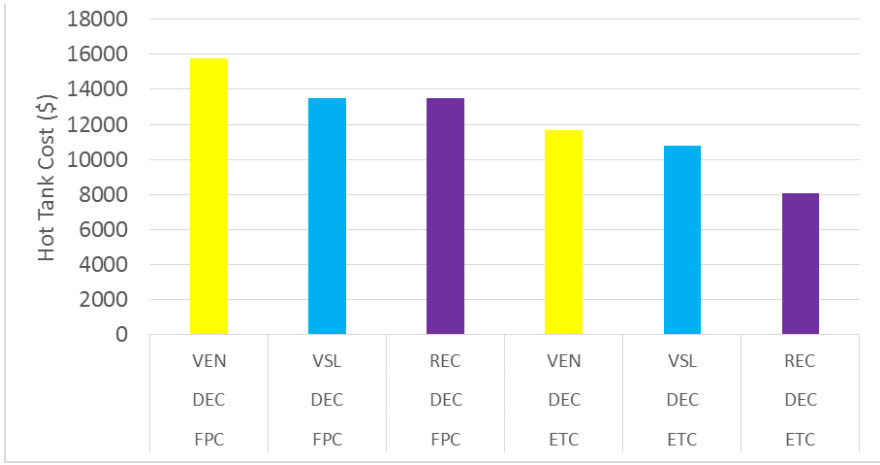

Fig. 7.17 - Hot tank cost (DEC) Riyadh

7.5 Solar Cooling Systems Cost Comparison

This paragraph proposes a comparison of the cost of all configurations.
The graphs in Figures 7.18-19 shows, for all configurations, the cost of the solar cooling system with the best heat rejections systems.
The results reveal the gap between the systems based on photovoltaic field and all others solar cooling systems. This difference is due to the drop in prices of photovoltaic modules and the large availability of compression chillers. The comparison between the two locations shows how in Dubai the PV-based system costs about half of the configuration with PTC and 3sABS. Conversely, in Riyadh the cost of these two technologies is the same.
The benefits of higher COPs of the triple effect chillers are not so important on the economic side. The reduction in the solar field cost (Fig. 7.20, 7.21) is compensated for by the unit cost of the chiller (Fig 7.22, 7.23). Also the cost of high pressures tanks (20 bar) is bigger (Fig. 7.24, 7.25). On the contrary, the cost for the heat rejection systems for the two technologies highlighted is the same (Fig. 7.26 and 7.27).

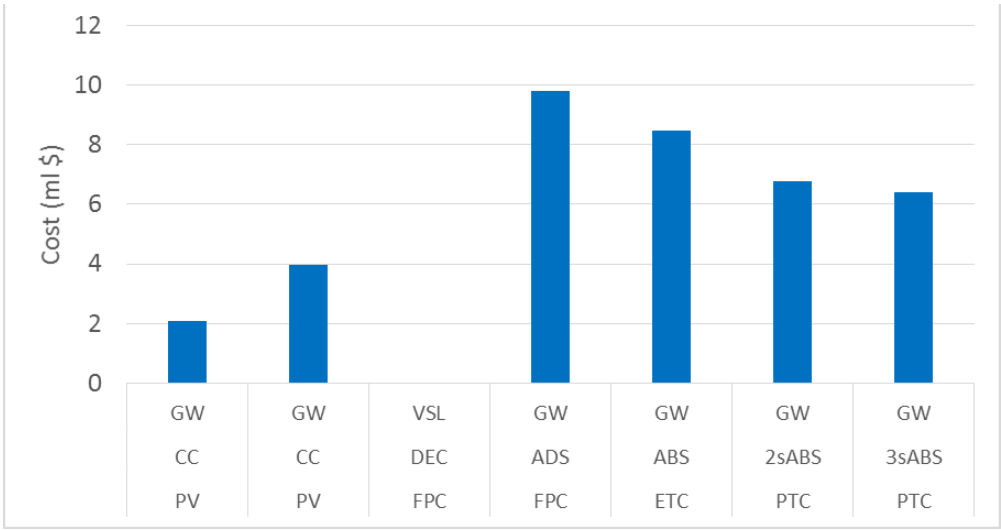

Fig. 7.18 - Cooling plants cost - Dubai

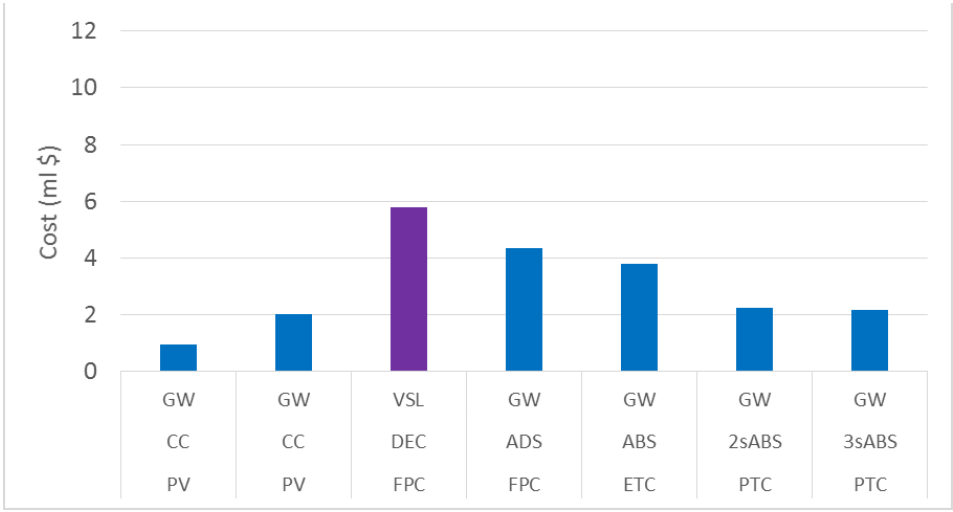

Fig. 7.19 - cooling plants cost - Riyadh

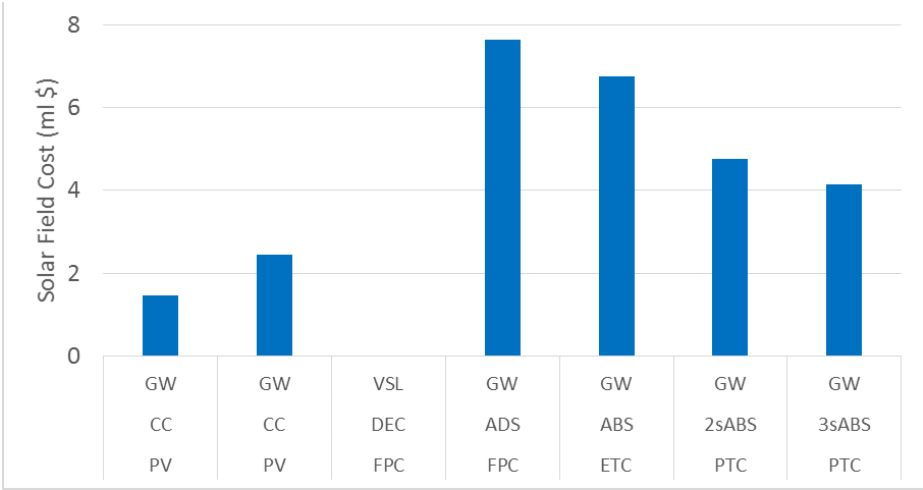

Fig. 7.20 - Solar field cost - Dubai

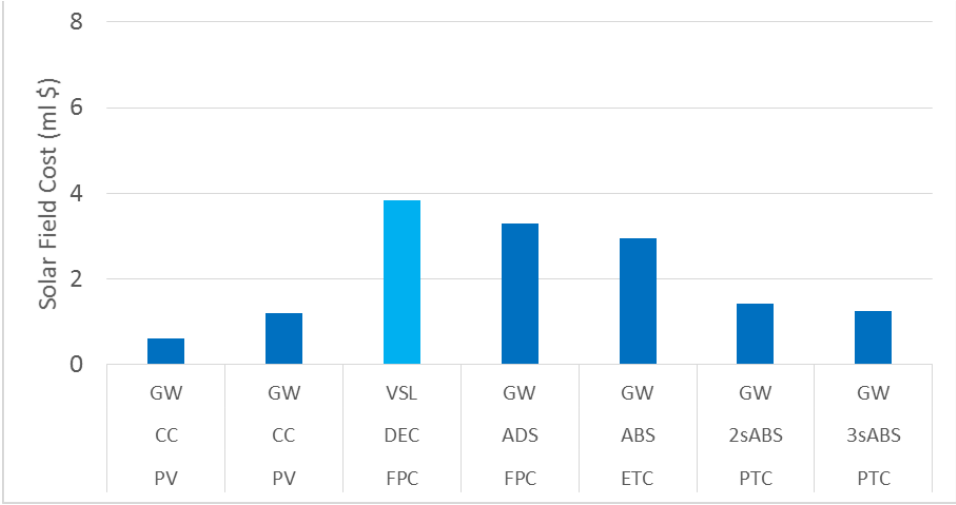

Fig. 7.21 - Solar field cost - Riyadh

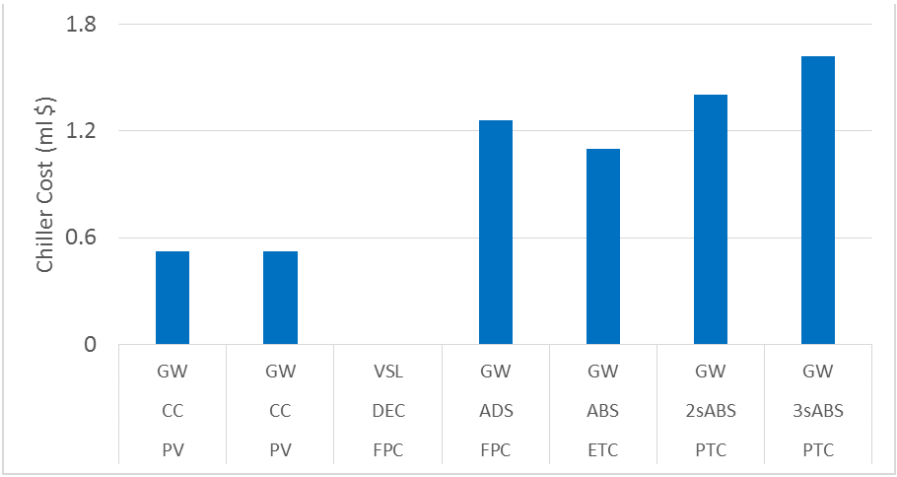

Fig. 7.22 - Chiller cost - Dubai

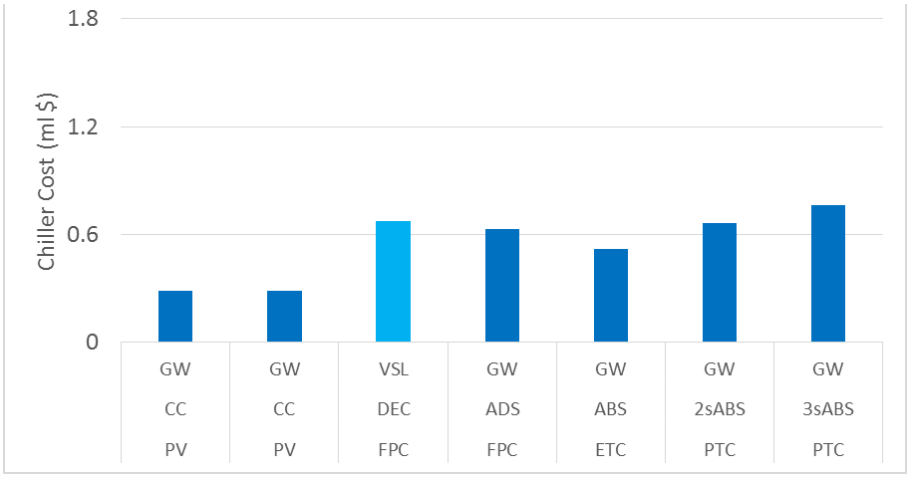

Fig. 7.23 - Chiller cost - Riyadh

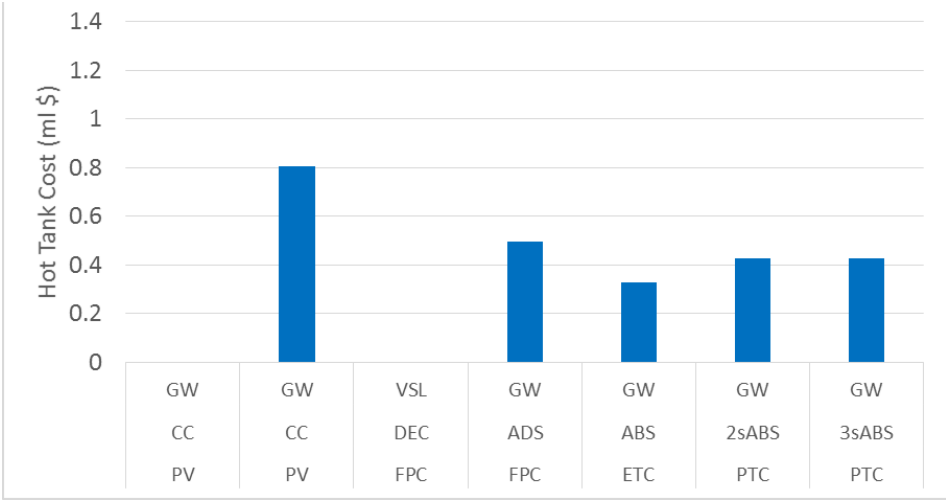

Fig. 7.24 - Storage cost - Dubai

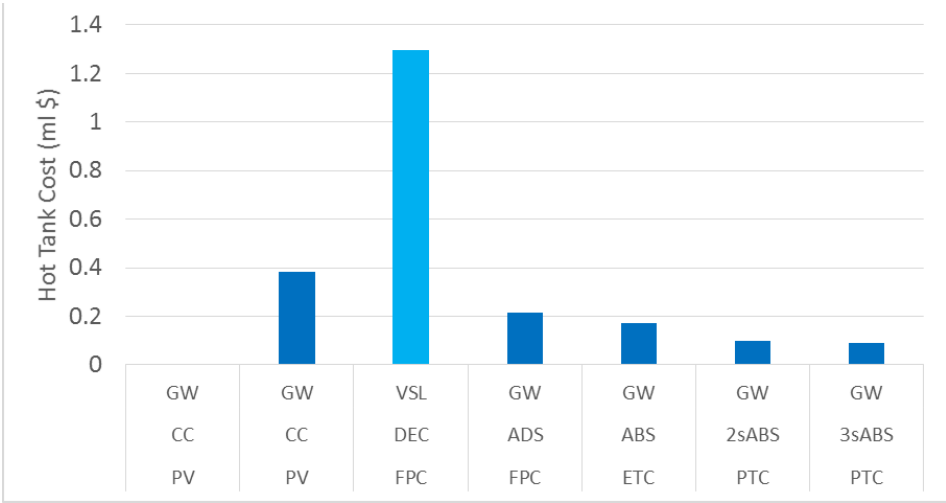

Fig. 7.25 - Storage cost - Riyadh

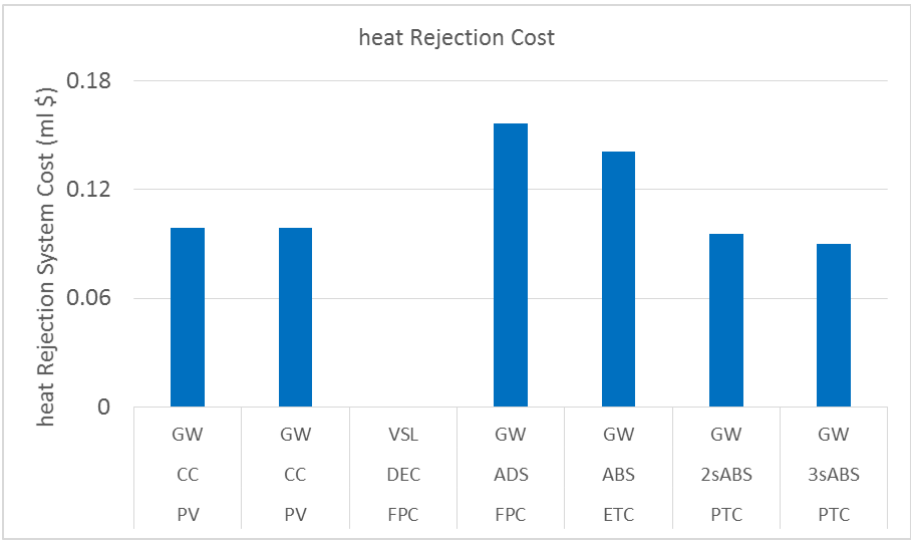

Fig. 7.26 - Heat rejection system cost - Dubai

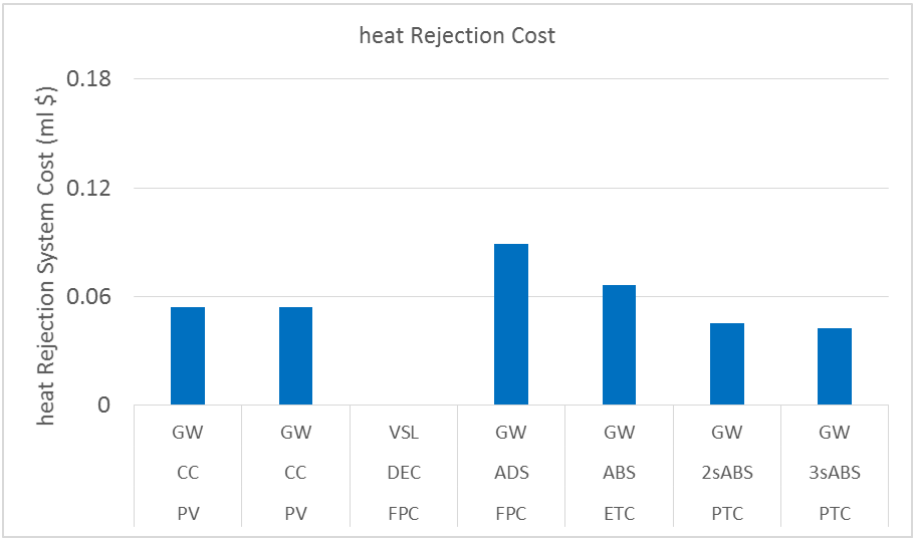

Fig. 7.27 - Heat rejection system cost - Riyadh

7.6 Best Configuration

To properly assess the best solar cooling system, it is not enough to estimate only the cost of the plant. To better analyze the problem, the following graphs (Figs. 7.28 and 7.29) show the overall cost of the plant including the network cost and all the auxiliaries needed to operate the plant. The detailed costs, resumed from the previous chapters, are shown in Table 7.2 (Dubai) and 7.3 (Riyadh). The cost of the residential heat pump (in every single building) is higher than the compression chiller cooling plant configuration also considering the cost of the photovoltaic field and the network. The trend of the charts rewards the solar cooling system with high efficiency and longer operating times. In the coastal area (Dubai) the chart underlined the gap between absorption chiller and compression chiller. In the dry region (Riyadh) the installation cost of both configuration became similar and the choice could be linked to the government directories.

Table 7.2 - Global costs of the best configurations (Dubai)

	Network Cost	Cooling Plant	BackUp Cost	**Global Cost**
PV CC GW	1118571	2074867	0	**3193438**
PV CC GW (battery)	1118571	3958667	0	**5077238**
FPC DEC VSL	0	0	0	**0**
FPC ADS GW	1118571	9796812	130000	**11045383**
ETC ABS GW	1118571	8483355	130000	**9731926**
PTC 2sABS GW	1118571	6784886	130000	**8033456**
PTC 3sABS GW	1118571	6384002	130000	**7632572**
Grid HP AIR	0	3552000	0	**3552000**

Table 7.3 - Global costs of the best configurations (Riyadh)

	Network Cost	Cooling Plant	BackUp Cost	**Global Cost**
PV CC GW	894856.4	950077	0	**1844933**
PV CC GW (battery)	894856.4	2014077	0	**2908933**
FPC DEC VSL	0	5802240	12000	**5814240**
FPC ADS GW	894856.4	4345946	75000	**5315803**
ETC ABS GW	894856.4	3782968	75000	**4752824**
PTC 2sABS GW	894856.4	2266460	75000	**3236316**
PTC 3sABS GW	894856.4	2159829	75000	**3129685**
Grid HP AIR	0	1728000	0	**1728000**

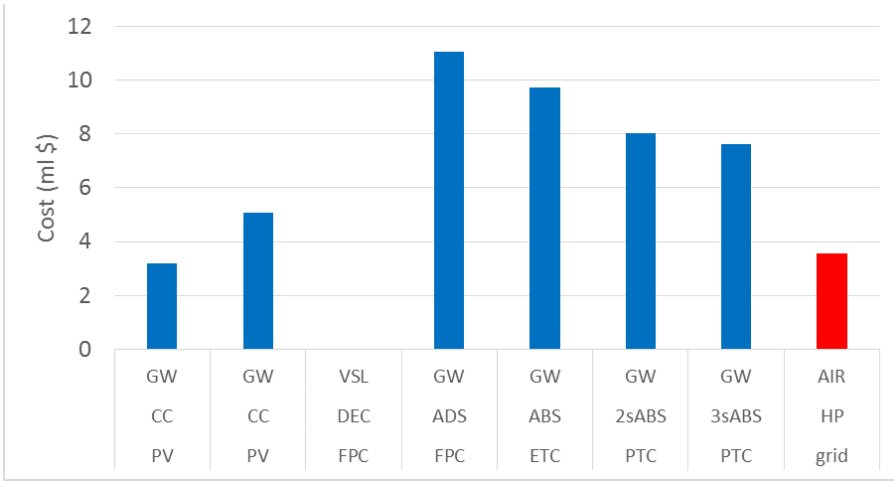

Fig. 7.28 - Cooling plant cost - Dubai

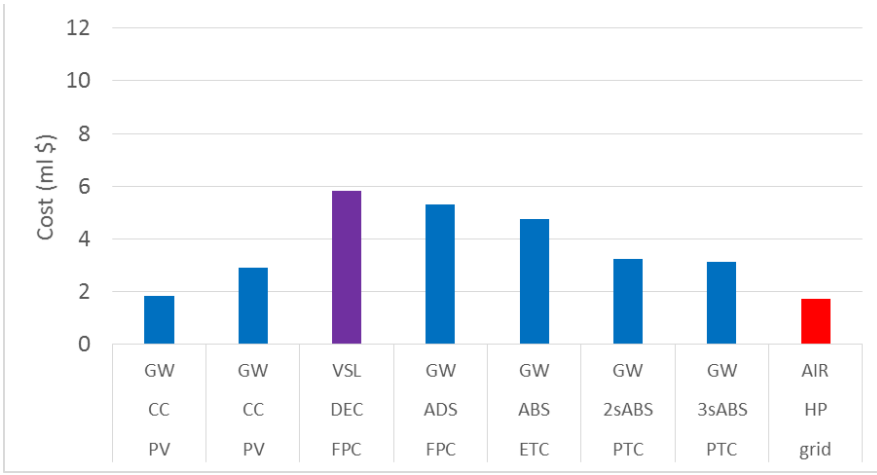

Fig. 7.29 - Cooling plant cost - Riyadh

7.7 Annual Operating Cost

In order to consolidate the economic validity of solar cooling systems, an annual plant management cost analysis is developed and reported in this paragraph.

Figures 7.30 and 7.31 show the annual operating cost for managing solar cooling systems. The difference between the operating cost of the single building heat pump and the others cooling systems allows an estimation of annual savings (Figures 7.32 and 7.33).

Savings may seem high but if compared to the plant cost the results are reported in Figures 7.34 and 7.35 which represent a payback time (in case of interest rate equal to 0; a common situation for this type of application implemented by government entities).

Based on the operating cost we can consider the best solar cooling system based on compression chiller and photovoltaic field with electrical storage. Even the solar cooling system based on PTC and triple stage absorption chiller system shows excellent performances especially in the location of Riyadh.

A further comparison is shown in Figures 7.36 and 7.37, the bar chart represents the ratio between plant cost differences and annual savings. Negative values are possible because some solar cooling systems cost less than the traditional system.

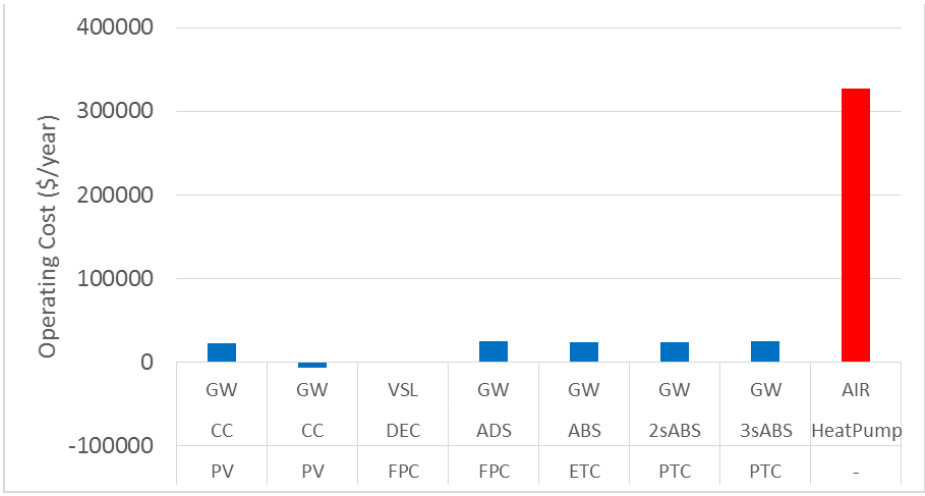

Fig. 7.30 - Operating cost - Dubai

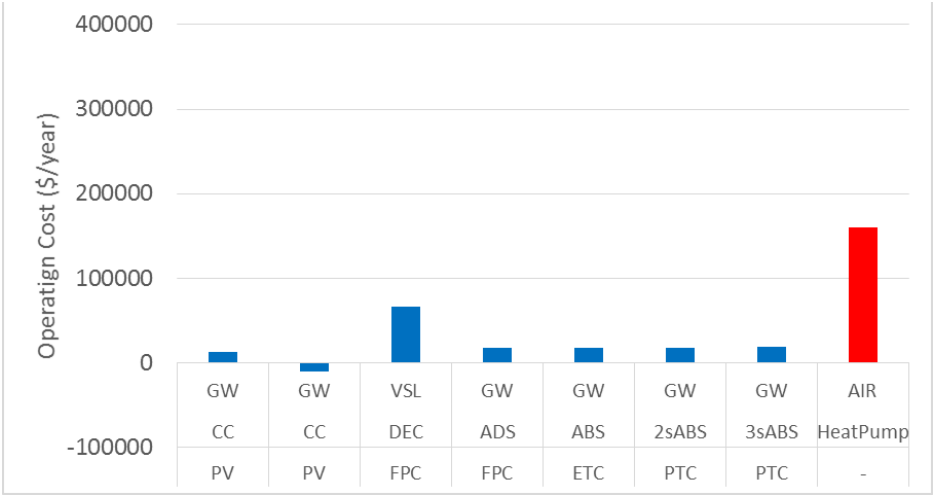

Fig. 7.31 - Operating cost - Riyadh

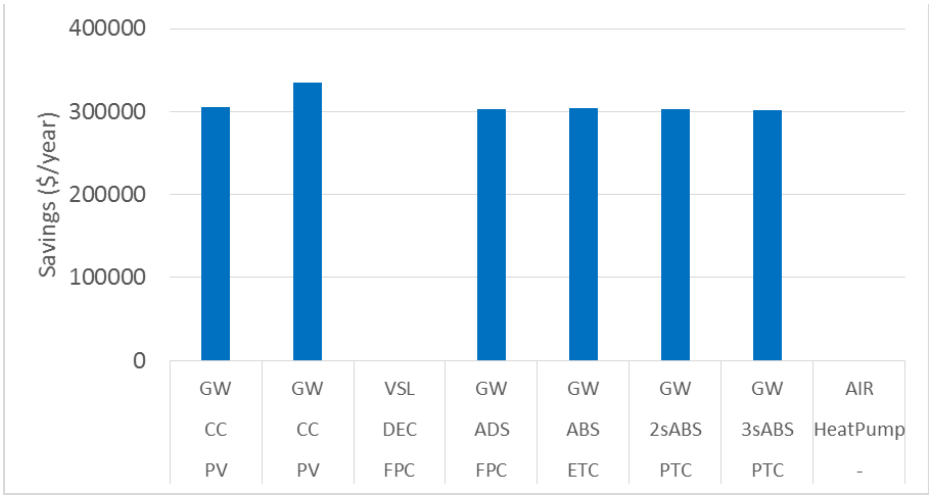

Fig. 7.32 - Annual savings - Dubai

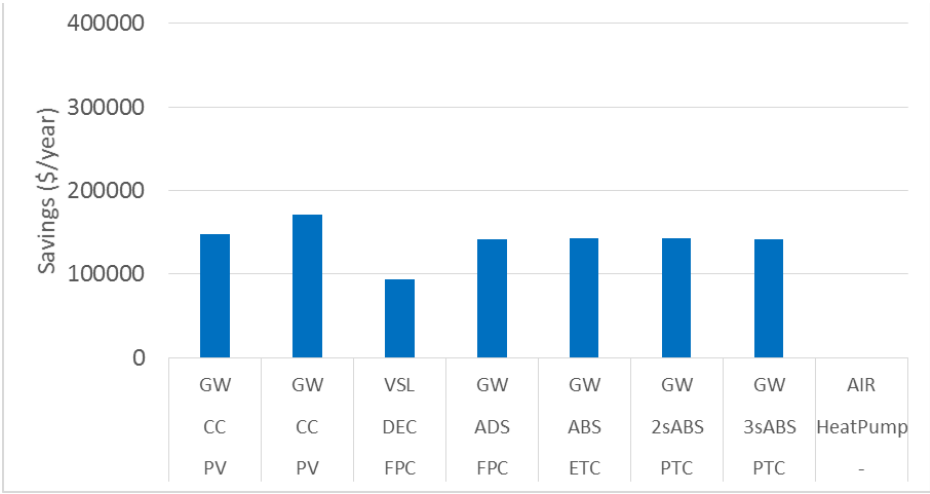

Fig. 7.33 - Annual savings - Riyadh

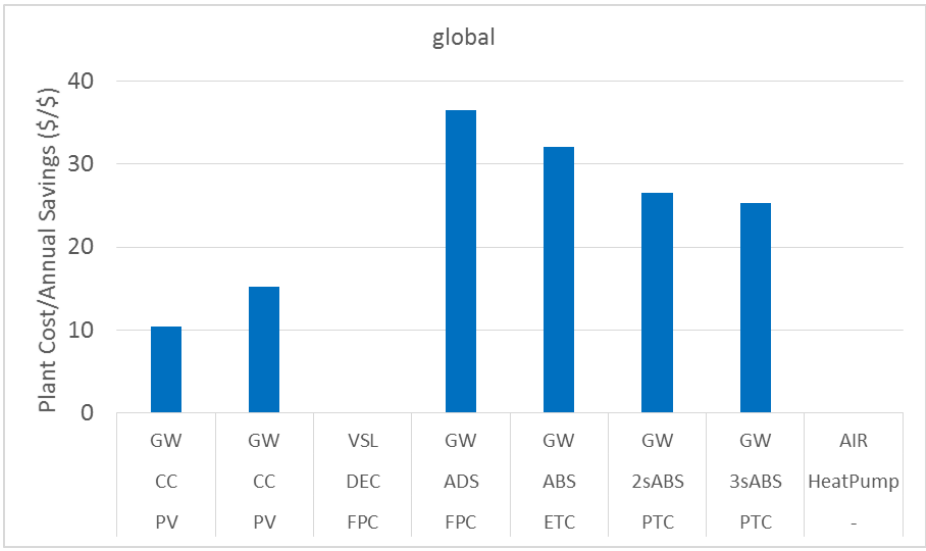

Fig. 7.34 - Pay back time - Dubai

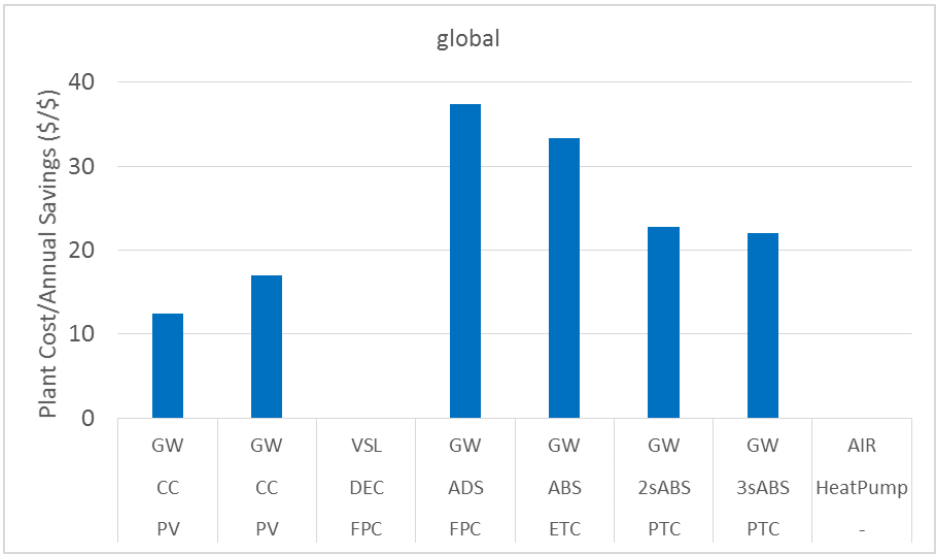

Fig. 7.35 - Pay back time - Riyadh

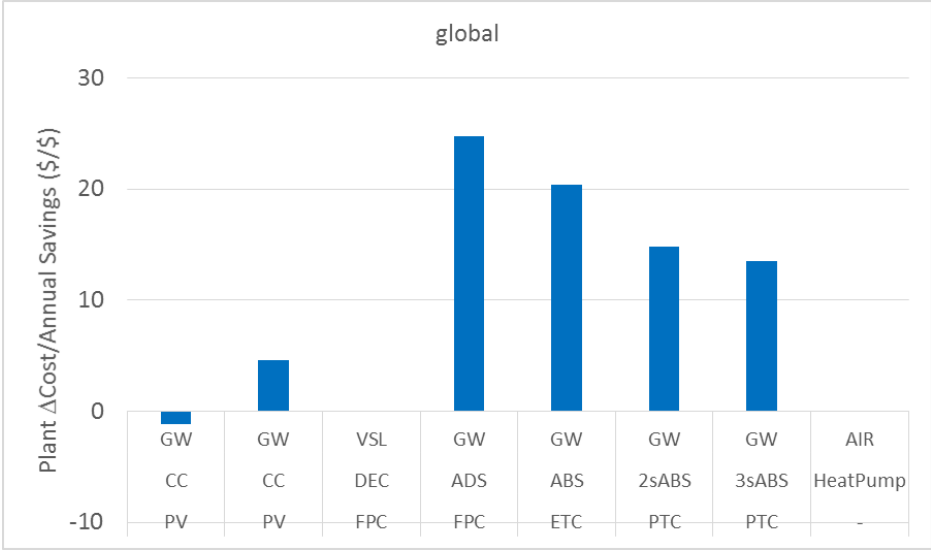

Fig. 7.36 - Pay back time (plant cost difference) - Dubai

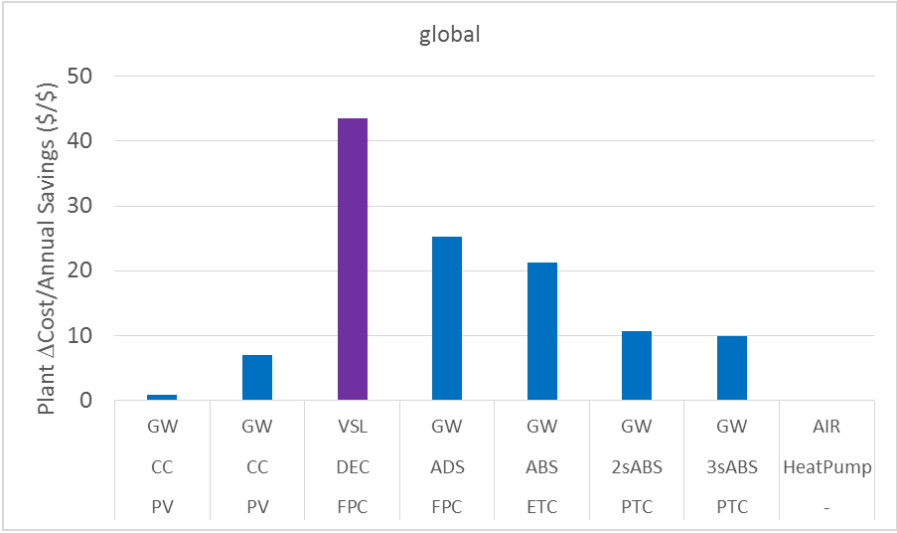

Fig. 7.37 - Pay back time (plant cost difference) - Riyadh

8 Conclusions

The thesis develop a solar cooling idea that includes all aspects of the air conditioning problem.

The first part of the research focuses on the development of low-energy buildings. The modelling of the first PassivHaus Energy+ building in Dubai was developed to predict the energy performance. A preliminary activity of modeling and simulation dictated the design of the building envelop and of the energy systems.

Trnsys is the software used to create the energy model and to predict the building performance. Simulation outcomes have been used to revise the project and size the PV field (40 kWp), the battery pack (25 kWh), the chiller capacity (27.5 kW) and all auxiliary components.

The results show a perfect autonomy of the building even under severe load conditions: the PV field exports electricity to the grid for several hours, whilst importation does not occur all year round, making the house an Energy+ building able to operate also in Off-the-Grid conditions.

The Energy+ building, inaugurated in November 2016, is a pioneering pilot-project and it represents an advance in the field of sustainable construction for all Arabic area.

Starting from its inauguration, the building has been monitored to measure the actual performance under real operating conditions. The first available measurements confirm that the model predictions are very accurate and very close to the monitoring data. Therefore, it can be concluded that the expected targets in terms of energy savings and carbon footprint reduction have been successfully achieved.

The demonstrative building (PassivHouse) was taken into account to develop a comparison between different types of residential building.
The comparison is made between buildings respecting three different regulations: the PassivHouse building, a building designed according to the GreenBuilding Regulation and a third respecting the traditional standars. Gli edifici sono stati modellati e simulati per ottenere lo stesso livello di comfort.
Comparative analysis shows that a building designed according to PassvHouse requires only 20% of cooling compared to the traditional building. The new residential neighborhoods will be built according to GreenBuilding regulation and this version was take into account to simulate the compound load.
To improve the research, the district cooling network was developed. The network allows to efficiently distribute the cooling energy to the users. Central cooling plant permits to use more efficient chillers respect to domestic scale users.
The cooling load of a residential compound of 96 single-family detached homes was evaluated and supposed to be covered by a centralized cooling station with a district cooling system supplying chilled water.
Network design optimization allows annual thermal losses to fall below 10%. The energy required for pumping stations, using optimized water speeds, is minimal.
The next step, achieved the compound cooling load, is modelling and simulate the solar cooling plant. The solar cooling systems considered are analyzed according to the chiller typology: Compression Chiller, Absorption Chiller (single effect, double effect and triple effect), Adsorption Chiller and Solar Desiccant Evaporative Cooling.
Energy sources are different for each plant configuration. Photovoltaic field drives the compression chiller.
The solar field for powering the cooling plants has been selected depending on the thermal input required: Flate Plate Collectors, Evacuated tube Collectors and Parabolic Trough.
Four types of heat rejection systems have been considered: Dry Cooler, Cooling Tower, Groundwater Heat Exchanger and Ground Heat Exchanger.

In order to simulate the operation of a supply well, geological research based on literature and data from existing wells was conducted. The collected data demonstrate the possibility of using groundwater for reject the heat produced by solar cooling systems.
The result of the new Trnsys type is a dynamic groundwater table integrated in the simulations. This approach allows the simulations of the whole cooling plant without the use of specific software.
A similar approach was followed to develop the model of vertical ground heat exchanger. Numerical validation guarantees the correct operation of the models: the errors found are well below the 3%.

An optimization procedure has been developed to determine the size of all main component assuring the cost minimization and an annual solar fraction of 0.7. Transient simulations over 1-year period have been carried out on the proposed configurations to evaluate the energy performance under variable operating conditions.
A transient simulations are carried out, on the proposed configurations, to evaluate the efficiency of all components under variable operating conditions over a one-year period on hourly basis.
The simulation results show that solarized district cooling systems can be efficient if well designed. All the analyzed configurations allow considerable savings of electricity, and CO_2 emitted, compared to the installation of heat pump in each building.
The model based on photovoltaic field is the most efficient cooling plant and allows to export of the surplus of electricity produced by a net-metering scheme. The solution based on adsorption chiller is the most disadvantaged, the low COP requires the installation of a large solar field.
The absorption chillers are the most balanced configurations, ranging from single effects to the Triple Effect powered by PTC, comparable to the Compression Chiller.
The DEC system is the most difficult to design and manage. The configuration has a significant effect on the final efficiency. The water consumption required for operation makes it unusable for use in arid regions.
Furthermore, With regard to heat recovery systems, the results reward the groundwater based system. The Air Cooler works with difficult in hot

climates while the evaporative tower suffers in humid climates and water consumption is high. The ground heat exchanger is an efficient, but expensive, solution.

At an economic level, solar cooling systems reduce the annual operating cost to around 10%, allowing a significant annual savings. Annual savings guarantee the return of the investment in a few years for the systems based on compression chiller. For the triple stage absorption chiller systems, the return time is about 10 years.

In conclusion, the realization of sustainable buildings coupled with solar cooling technologies allows to achieve energy and environmental savings.

The development of high efficiency heat rejection systems allows the use of solar cooling systems even under critical conditions, increasing production and ensuring sustainability.

9 Appendix

9.1 References

9.1.1 Introduction

[1] Nejat, Payam, et al. "A global review of energy consumption, CO 2 emissions and policy in the residential sector (with an overview of the top ten CO 2 emitting countries)." Renewable and sustainable energy reviews 43 (2015): 843-862.

[2] Thalfeldt, Martin, et al. "Facade design principles for nearly zero energy buildings in a cold climate." Energy and Buildings 67 (2013): 309-321.

[3] Alonso, Maria Justo, et al. "Review of heat/energy recovery exchangers for use in ZEBs in cold climate countries." Building and Environment 84 (2015): 228-237

[4] Fokaides, Paris A., et al. "Performance of a Passive House under subtropical climatic conditions." Energy and Buildings 133 (2016): 14-31.

[5] Schnieders, Jürgen, Wolfgang Feist, and Ludwig Rongen. "Passive Houses for different climate zones." Energy and Buildings 105 (2015): 71-87.

[6] Marszal, Anna Joanna, et al. "Zero Energy Building–A review of definitions and calculation methodologies." Energy and buildings 43.4 (2011): 971-979.

[7] Rodriguez-Ubinas, Edwin, et al. "Passive design strategies and performance of Net Energy Plus Houses." Energy and buildings 83 (2014): 10-22.

[8] Trier, Daniel. “Towards Solar District Heating with More than 70% Solar Fraction.” Energy Procedia 70 (2015): 580-586.
[9] Carpaneto, Enrico, Paolo Lazzeroni, and Maurizio Repetto. “Optimal integration of solar energy in a district heating network.” Renewable Energy 75 (2015): 714-721.
[10] Sameti, Mohammad, and Fariborz Haghighat. “Optimization approaches in district heating and cooling thermal network.” Energy and Buildings (2017).
[11] Chorowski, M., Z. Rogala, and P. Pyrka. “System options for cooling of buildings making use of district heating heat.” International Journal of Refrigeration 70 (2016): 183-195.
[12] Lake, Andrew, Behanz Rezaie, and Steven Beyerlein. “Review of district heating and cooling systems for a sustainable future.” Renewable and Sustainable Energy Reviews 67 (2017): 417-425.
[13] Horn, Philip, et al. “Solar Hybrid Heating & Cooling Systems on District Level–The Austrian Project CiQuSo.” Energy Procedia 91 (2016): 980-988.
[14] Gang, Wenjie, et al. “District cooling systems: Technology integration, system optimization, challenges and opportunities for applications.” Renewable and Sustainable Energy Reviews 53 (2016): 253-264.
[15] Marugán-Cruz, Carolina, et al. “District cooling network connected to a solar power tower.” Applied Thermal Engineering 79 (2015): 174-183.
[16] Olsthoorn, Dave, Fariborz Haghighat, and Parham A. Mirzaei. "Integration of storage and renewable energy into district heating systems: A review of modelling and optimization." Solar Energy 136 (2016): 49-64.
[17] Elci, Mehmet, et al. "Grid-interactivity of a solar combined heat and power district heating system." Energy Procedia 70 (2015): 560-567.
[18] Powell, Kody M., et al. "Optimal chiller loading in a district cooling system with thermal energy storage." Energy 50 (2013): 445-453.
[19] Gang, Wenjie, et al. "Performance assessment of district cooling system coupled with different energy technologies in subtropical area." Energy Procedia 75 (2015): 1235-1241.

[20] Nanda, Arun Kumar, and C. K. Panigrahi. "A state-of-the-art review of solar passive building system for heating or cooling purpose." Frontiers in Energy 10.3 (2016): 347-354.
[21] Ghaith, Fadi A., and Rasha Abusitta. "Energy analyses of an integrated solar powered heating and cooling systems in UAE." Energy and Buildings 70 (2014): 117-126.
[22] Zhai, X. Q., et al. "A review for research and new design options of solar absorption cooling systems." Renewable and sustainable energy reviews 15.9 (2011): 4416-4423.
[23] Atmaca, Ibrahim, and Abdulvahap Yigit. "Simulation of solar-powered absorption cooling system." Renewable Energy 28.8 (2003): 1277-1293.
[24] Florides, G. A., et al. "Modelling, simulation and warming impact assessment of a domestic-size absorption solar cooling system." Applied Thermal Engineering 22.12 (2002): 1313-1325.
[25] Assilzadeh, F., et al. "Simulation and optimization of a LiBr solar absorption cooling system with evacuated tube collectors." Renewable Energy 30.8 (2005): 1143-1159.
[26] Figueredo, Gustavo R., Mahmoud Bourouis, and Alberto Coronas. "Thermodynamic modelling of a two-stage absorption chiller driven at two-temperature levels." Applied Thermal Engineering 28.2 (2008): 211-217.
[27] Mazloumi, M., M. Naghashzadegan, and K. Javaherdeh. "Simulation of solar lithium bromide–water absorption cooling system with parabolic trough collector." Energy Conversion and Management 49.10 (2008): 2820-2832.
[28] El Fadar, A., A. Mimet, and M. Pérez-García. "Modelling and performance study of a continuous adsorption refrigeration system driven by parabolic trough solar collector." Solar Energy 83.6 (2009): 850-861.
[29] Lazzarin, Renato M. "Solar cooling: PV or thermal? A thermodynamic and economical analysis." International Journal of Refrigeration 39 (2014): 38-47.
[30] Okoye, Chiemeka Onyeka, and Oğuz Solyalı. "Optimal sizing of stand-alone photovoltaic systems in residential buildings." Energy 126 (2017): 573-584.

[31] Fara, Laurentiu, and Dan Craciunescu. "Output Analysis of Stand-alone PV Systems: Modeling, Simulation and Control." Energy Procedia 112 (2017): 595-605.

9.1.2 Chapter 1

[1] Al-Ugla, A. A., M. A. I. El-Shaarawi, and S. A. M. Said. "Alternative designs for a 24-hours operating solar-powered LiBr–water absorption air-conditioning technology." International Journal of Refrigeration 53 (2015): 90-100.
[2] Li, Dayao, Jiang He, and Lin Li. "A review of renewable energy applications in buildings in the hot-summer and warm-winter region of China." Renewable and Sustainable Energy Reviews 57 (2016): 327-336.
[3] Casals, Xavier Garcia. "Solar absorption cooling in Spain: Perspectives and outcomes from the simulation of recent installations." Renewable energy 31.9 (2006): 1371-1389.
[4] Eicker, Ursula, et al. "Systematic design and analysis of solar thermal cooling systems in different climates." Renewable Energy 80 (2015): 827-836.
[5] Al-Alili, A., et al. "Optimization of a solar powered absorption cycle under Abu Dhabi's weather conditions." Solar Energy 84.12 (2010): 2034-2040.
[6] Zell, Erica, Zell, E., Gasim, S., Wilcox, S., Katamoura, S., Stoffel, T., Shibli, H., Al Subie, M. (2015). "Assessment of solar radiation resources in Saudi Arabia." Solar Energy 119 (2015): 422-438.

9.1.3 Chapter 2

[1] Fokaides, Paris A., Christoforou, E., Ilic, M., & Papadopoulos, A. (2016). "Performance of a Passive House under subtropical climatic conditions." Energy and Buildings 133 (2016): 14-31.
[2] Schnieders, Jürgen, Wolfgang Feist, and Ludwig Rongen. (2015). "Passive Houses for different climate zones." Energy and Buildings 105 (2015): 71-87.
[3] Aelenei, Laura, Petran, H., Tarrés, J., Riva, G., Ferreira, A., Camelo, S., Magyar, Z. (2015). "New challenge of the public buildings: nZEB findings from IEE RePublic_ZEB Project." Energy Procedia 78 (2015): 2016-2021.

[4] Tsoutsos, Theocharis, Tournaki, S., de Santos, C. A., & Vercellotti, R. (2013). "Nearly zero energy buildings application in mediterranean hotels." Energy Procedia 42 (2013): 230-238.
[5] Perlova, Elena, Platonova, M., Gorshkov, A., & Rakova, X. (2015). "Concept Project of Zero Energy Building." Procedia Engineering 100 (2015): 1505-1514.
[6] Daut, I., et al. "Solar powered air conditioning system." Energy Procedia 36 (2013): 444-453.
[7] Kirimtat, Ayca, Koyunbaba, B. K., Chatzikonstantinou, I., & Sariyildiz, S. (2016). "Review of simulation modeling for shading devices in buildings." Renewable and Sustainable Energy Reviews 53 (2016): 23-49.
[8] Lazzarin, Renato M. (2014) "Solar cooling: PV or thermal? A thermodynamic and economical analysis." International Journal of Refrigeration 39 (2014): 38-47.
[9] Vieira, Filomeno M., Pedro S. Moura, and Aníbal T. de Almeida. (2017) "Energy storage system for self-consumption of photovoltaic energy in residential zero energy buildings." Renewable Energy 103 (2017): 308-320.
[10] Okoye, Chiemeka Onyeka, and Oğuz Solyalı. (2017) "Optimal sizing of stand-alone photovoltaic systems in residential buildings." Energy 126 (2017): 573-584.
[11] Fara, Laurentiu, and Dan Craciunescu. "Output Analysis of Stand-alone PV Systems: Modeling, Simulation and Control." Energy Procedia 112 (2017): 595-605.
[12] Chekired, Fathia, F., Smara, Z., Mahrane, A., Chikh, M., & Berkane, S. "An Energy Flow Management Algorithm for a Photovoltaic Solar Home." Energy Procedia 111 (2017): 934-943.
[13] Luthander, Rasmus, R., Widén, J., Nilsson, D., & Palm, J. "Photovoltaic self-consumption in buildings: A review." Applied Energy 142 (2015): 80-94.
[14] Colmenar-Santos, Antonio, A., Campíñez-Romero, S., Pérez-Molina, C., & Castro-Gil, M. (2012). "Profitability analysis of grid-connected photovoltaic facilities for household electricity self-sufficiency." Energy Policy 51 (2012): 749-764.

[15] Widén, Joakim. "Improved photovoltaic self-consumption with appliance scheduling in 200 single-family buildings." Applied Energy 126 (2014): 199-212.
[16] Wang, Yang, Kuckelkorn, J., Zhao, F. Y., Spliethoff, H., & Lang, W. "A state of art of review on interactions between energy performance and indoor environment quality in Passive House buildings." Renewable and Sustainable Energy Reviews 72 (2017): 1303-1319.
[17] Satake, Akihiro, Hiroaki Ikegami, and Yasunori Mitani. "Energy-saving Operation and Optimization of Thermal Comfort in Thermal Radiative Cooling/Heating System." Energy Procedia 100 (2016): 452-458.
[18] Zhao, Kang, Xiao-Hua Liu, and Yi Jiang. "Application of radiant floor cooling in large space buildings–A review." Renewable and Sustainable Energy Reviews 55 (2016): 1083-1096.
[19] Harish, V. S. K. V., and Arun Kumar. "A review on modeling and simulation of building energy systems." Renewable and Sustainable Energy Reviews 56 (2016): 1272-1292.
[20] Mihai, Mirela, Tanasiev, V., Dinca, C., Badea, A., & Vidu, R. "Passive house analysis in terms of energy performance." Energy and Buildings 144 (2017): 74-86.
[21] Rehab, Imane, Andre, P., Silva, C. A., Massy, G., Hannay, J., & Lebrun, J. "Verification of the Energy Balance of a Passive House by Combining Measurements and Dynamic Simulation." Energy Procedia 78 (2015): 2310-2315.
[22] Song, Meng, Alvehag, K., Widén, J., & Parisio, A. "Estimating the impacts of demand response by simulating household behaviours under price and CO 2 signals." Electric power systems research 111 (2014): 103-114.
[23] Hoxha, Endrit, and Thomas Jusselme. “On the necessity of improving the environmental impacts of furniture and appliances in net-zero energy buildings." Science of The Total Environment 596 (2017): 405-416.
[24] Blight, Thomas S., and David A. Coley. "Sensitivity analysis of the effect of occupant behavior on the energy consumption of passive house dwellings." Energy and Buildings 66 (2013): 183-192.

[25] Dubai Municipality, Government of Dubai, Dubai Electricity & Water Authority. “Green building regulation and specification” Greenbuilding@dm.gov.ae
[26] The Executive Council (TEC), Government of Dubai, Ministry of Public Works “Green building guidelines, UAE” MoPWs - 01-290109-01 (2009).

9.1.4 Chapter 3

[1] Morvaj, Boran, Ralph Evins, and Jan Carmeliet. "Optimising urban energy systems: Simultaneous system sizing, operation and district heating network layout." Energy 116 (2016): 619-636.
[2] Oppelt, Thomas, et al. "Dynamic thermo-hydraulic model of district cooling networks." Applied Thermal Engineering 102 (2016): 336-345.
[3] Ameri, Mohammad, and Zahed Besharati. "Optimal design and operation of district heating and cooling networks with CCHP systems in a residential complex." Energy and Buildings 110 (2016): 135-148.
[4] Gang, Wenjie, et al. "Performance assessment of district cooling system coupled with different energy technologies in subtropical area." Energy Procedia 75 (2015): 1235-1241.
[5] Liew, Peng Yen, et al. "Total Site Heat Integration planning and design for industrial, urban and renewable systems." Renewable and Sustainable Energy Reviews 68 (2017): 964-985.
[6] Lund, Rasmus, and Soma Mohammadi. "Choice of insulation standard for pipe networks in 4 th generation district heating systems." Applied Thermal Engineering 98 (2016): 256-264.
[7] Yan, Aibin, et al. "Hydraulic performance of a new district heating systems with distributed variable speed pumps." Applied energy 112 (2013): 876-885.
[8] Pirouti, Marouf, et al. "Energy consumption and economic analyses of a district heating network." Energy 57 (2013): 149-159.
[9] G. Davies, P. Woods “The potential and cost of district heating network.” 2009 Pöyry Energy (Oxford)
[10] Lund, Rasmus, and Soma Mohammadi. "Choice of insulation standard for pipe networks in 4 th generation district heating systems." Applied Thermal Engineering 98 (2016): 256-264.

[11] Jie, Pengfei, et al. "Selecting the optimum pressure drop per unit length of district heating piping network based on operating strategies." Applied Energy 177 (2016): 341-353.
[12] Zeng, Jing, Jie Han, and Guoqiang Zhang. "Diameter optimization of district heating and cooling piping network based on hourly load." Applied Thermal Engineering 107 (2016): 750-757.
[19] Yan, Aibin, et al. "Hydraulic performance of a new district heating systems with distributed variable speed pumps." Applied energy 112 (2013): 876-885.

9.1.5 Chapter 4

[1] Fong, K. F., et al. "Comparative study of different solar cooling systems for buildings in subtropical city." Solar Energy 84.2 (2010): 227-244.
[2] Al-Alili A, Hwang Y, Rademacher R, Review of solar thermal air conditioning technologies, International Journal of Refrigeration, 39 (2014) 4-22.
[3] Lecuona A, Ventas R, Vereda C, Lçpez R, “Absorption solar cooling systems using optimal driving temperatures.” Applied Thermal Engineering, 79 (2015) 140-148
[4] Olsthoorn, Dave, Fariborz Haghighat, and Parham A. Mirzaei. "Integration of storage and renewable energy into district heating systems: A review of modelling and optimization." Solar Energy 136 (2016): 49-64.
[5] Elci, Mehmet, et al. "Grid-interactivity of a solar combined heat and power district heating system." Energy Procedia 70 (2015): 560-567.
[6] Powell, Kody M., et al. "Optimal chiller loading in a district cooling system with thermal energy storage." Energy 50 (2013): 445-453.
[7] Shirazi A, Pintaldi S, White SD, Morrison GL, Rosentgarden G, Taylor RA. “Solar-assisted absorption air-conditioning systems in building: control strategies and operation modes.” Applied Thermal Engineering, 92 (2016) 246-260.
[8] Shirazi, Ali, et al. "A systematic parametric study and feasibility assessment of solar-assisted single-effect, double-effect, and triple-effect absorption chillers for heating and cooling applications." Energy Conversion and Management 114 (2016): 258-277.

[9] Assilzadeh, F., et al. "Simulation and optimization of a LiBr solar absorption cooling system with evacuated tube collectors." Renewable Energy 30.8 (2005): 1143-1159.
[10] Ketfi, Omar, et al. "Performance of a single effect solar Absorption cooling system (Libr-H2O)." Energy procedia 74 (2015): 130-138.
[11] Rouf, Rifat Ara, KC Amanul Alam, and MA Hakim Khan. "Effect of operating conditions on the performance of adsorption solar cooling run by solar collectors." Procedia Engineering 56 (2013): 607-612.
[12] Ali, Muzaffar, et al. "Performance investigation of solid desiccant evaporative cooling system configurations in different climatic zones." Energy Conversion and Management 97 (2015): 323-339.
[13] Ma Y, Guan L, "Performance Analysis of Solar Desiccant-Evaporative Cooling for a Commercial Building under Different Australian Climates" Procedia Engineering 121 (2015) 528-535.
[14] Dayao L, Jiang H, Lin L."A review of renewable energy applications in buildings in the hot-summer and warm-winter region of China." Renewable and Sustainable Energy Review 57 (2016) 327-336.
[15] Bader, Tobias, et al. "Climate Specific Design and Effectiveness of Solar DEC-systems: A Methodological Zoning Approach." Energy Procedia 48 (2014): 778-789.
[16] Ali, Muzaffar, et al. "Performance investigation of solid desiccant evaporative cooling system configurations in different climatic zones." Energy Conversion and Management 97 (2015): 323-339.
[17] Dezfouli, M. M. S., S. O. H. I. F. Mat, and K. Sopian. "Comparison simulation between ventilation and recirculation of solar desiccant cooling system by TRNSYS in hot and humid area." Latest trends in renewable energy and environmental informatics (2013): 89-93.
[18] Fong, K. F., et al. "Advancement of solar desiccant cooling system for building use in subtropical Hong Kong." Energy and Buildings 42.12 (2010): 2386-2399.
[19] Eicker, Ursula, Dirk Pietruschka, and Ruben Pesch. "Heat rejection and primary energy efficiency of solar driven absorption cooling systems." international journal of refrigeration 35.3 (2012): 729-738.
[20] Eicker, Ursula, Dirk Pietruschka, and Ruben Pesch. "Heat rejection and primary energy efficiency of solar driven absorption cooling systems." international journal of refrigeration 35.3 (2012): 729-738.

[21] Kim, D. S., and CA Infante Ferreira. "Air-cooled LiBr–water absorption chillers for solar air conditioning in extremely hot weathers." Energy Conversion and Management 50.4 (2009): 1018-1025.
[22] Muye, James, et al. "Performance study of a solar absorption power-cooling system." Applied Thermal Engineering 97 (2016): 59-67.
[23] Li, Zeyu, Liming Liu, and Jinping Liu. "Variation and design criterion of heat load ratio of generator for air cooled lithium bromide–water double effect absorption chiller." Applied Thermal Engineering 96 (2016): 481-489.
[24] UN-ESCWA and BGR (United Nations Economic and Social Commission for Western Asia; Bundesanstalt fürca Geowissenschaften und Rohstoffe). "Chapter 15 Gulf Umm er Radhuma-Dammam Aquifer System (Centre)" 2013. Inventory of Shared Water Resources in Western Asia. Beirut
[25] Jorgensen, Donald G., and Walid Yasin al-Tikiriti. "A hydrologic and archeologic study of climate change in Al Ain, United Arab Emirates." Global and Planetary Change 35.1 (2003): 37-49.
[26] Schulz, Stephan, et al. "Improving large-scale groundwater models by considering fossil gradients." Advances in Water Resources 103 (2017): 32-43.
[27] Murad, Ahmed A., and R. V. Krishnamurthy. "Factors controlling groundwater quality in Eastern United Arab Emirates: a chemical and isotopic approach." Journal of Hydrology 286.1 (2004): 227-235.
[28] Murad, Ahmed A., et al. "Hydrogeochemical characterization and isotope investigations of a carbonate aquifer of the northern part of the United Arab Emirates." Journal of Asian Earth Sciences 40.1 (2011): 213-225.
[29] Rambo, Khulood A., et al. "Water-Energy Nexus in Saudi Arabia." Energy Procedia 105 (2017): 3837-3843.
[30] Allocca, V., et al. "Groundwater recharge assessment at local and episodic scale in a soil mantled perched karst aquifer in southern Italy." Journal of Hydrology 529 (2015): 843-853.
[31] Ouarda, T. B. M. J., et al. "Evolution of the rainfall regime in the United Arab Emirates." Journal of hydrology 514 (2014): 258-270.

[32] von Freyberg, Jana, Christian Moeck, and Mario Schirmer. "Estimation of groundwater recharge and drought severity with varying model complexity." Journal of Hydrology 527 (2015): 844-857.
[33] DeNicola, Erica, et al. "Climate change and water scarcity: the case of Saudi Arabia." Annals of global health 81.3 (2015): 342-353.
[34] Schulz, Stephan, et al. "Groundwater evaporation from salt pans: examples from the eastern Arabian Peninsula." Journal of Hydrology 531 (2015): 792-801.
[35] Irvine, Dylan J., et al. "Groundwater flow estimation using temperature-depth profiles in a complex environment and a changing climate." Science of The Total Environment 574 (2017): 272-281.
[36] Sherif, M., et al. "Assessment of groundwater quality in the northeastern coastal area of UAE as precursor for desalination." Desalination 273.2 (2011): 436-446.
[37] Zaidi, Faisal K., et al. "Evaluation of groundwater chemistry and its impact on drinking and irrigation water quality in the eastern part of the Central Arabian graben and trough system, Saudi Arabia." Journal of African Earth Sciences 120 (2016): 208-219.
[38] Food and Agriculture Organization of the United Nations "Groundwater Management in Saudi Arabia" 2009 Rome
[39] Alabdula'aly, Abdulrahman I. "Occurrence of radon in groundwater of Saudi Arabia." Journal of environmental radioactivity 138 (2014): 186-191.
[40] Kagabu, Makoto, et al. "Groundwater flow system under a rapidly urbanizing coastal city as determined by hydrogeochemistry." Journal of Asian earth sciences 40.1 (2011): 226-239.
[41] Iwalewa, Tajudeen M., Abdalla S. Elamin, and Sanlinn I. Kaka. "A coupled model simulation assessment of shallow water-table rise in a Saudi Arabian coastal city." Journal of Hydro-environment Research 12 (2016): 46-58.
[42] Cotecchia, Vincenzo. Influenza dell'acqua marina sulle falde acquifere in zone costiere. con particolare riferimento alle ricerche d'acqua sotterranea in Puglia. Edizione Istituto Propaganda Internazionale, 1955.
[43] Nakashita, Shinya, et al. "Temporal variations of groundwater salinity and temperature in a tidal flat in front of a tide pool." Continental Shelf Research 122 (2016): 29-35.

[44] Wang, Chaoyue, et al. "Closed-form analytical solutions incorporating pumping and tidal effects in various coastal aquifer systems." Advances in Water Resources 69 (2014): 1-12.
[45] Malki, Mouna, et al. "Impact of agricultural practices on groundwater quality in intensive irrigated area of Chtouka-Massa, Morocco." Science of The Total Environment 574 (2017): 760-770.
[46] McLing, Travis L., et al. "Wellbore and groundwater temperature distribution eastern Snake River Plain, Idaho: Implications for groundwater flow and geothermal potential." Journal of Volcanology and Geothermal Research 320 (2016): 144-155.
[47] Douglas, G. B., et al. "Potential biogeochemical impacts of heat rejection in the Mullaloo aquifer, Western Australia." Geothermics 53 (2015): 429-445.
[48] Béhaegel, M., P. Sailhac, and G. Marquis. "On the use of surface and ground temperature data to recover soil water content information." Journal of Applied Geophysics 62.3 (2007): 234-243.
[49] Lubenow, Brady L., et al. "Influences on shallow ground temperatures in high flux thermal systems." Journal of Volcanology and Geothermal Research 323 (2016): 53-61.
[50]_ Zhang, Wenke, et al. "Study on heat transfer of pile foundation ground heat exchanger with three-dimensional groundwater seepage." International Journal of Heat and Mass Transfer 105 (2017): 58-66.
[51] McClanahan, Timothy R., et al. "Effects of climate and seawater temperature variation on coral bleaching and mortality." Ecological Monographs 77.4 (2007): 503-525.
[52] Goreau, Thomas J., and Raymond L. Hayes. "Effects of rising seawater temperature on coral reefs." Fisheries and Aquaculture-Volume V (2009): 266.
[53] Alsharhan, A. S. "Petroleum geology of the United Arab Emirates." Journal of Petroleum Geology 12.3 (1989): 253-288.
[54] Macklin, Steve, et al. "Engineering geological characterisation of the Barzaman Formation, with reference to coastal Dubai, UAE." Bulletin of Engineering Geology and the Environment 71.1 (2012): 1-19.
[55] Powers, R. W., et al. "Geology of the Arabian Peninsula—Sedimentary Geology of Saudi Arabia: USG Survey Professional Paper, 560-D." (1966).

[56] Johnson, P. R. "Tectonic map of Saudi Arabia and adjacent areas." Deputy Ministry for Mineral Resources Technical Report USGS-TR-98-3 (IR 948) (1998).
[57] Johnson, Peter R. "Explanatory notes to the map of Proterozoic geology of western Saudi Arabia." Saudi Geological Survey Technical Report SGS-TR-2006-4 62 (2006).
[58] Missimer, Thomas M., et al. "Hydrogeology, water quality, and microbial assessment of a coastal alluvial aquifer in western Saudi Arabia: potential use of coastal wadi aquifers for desalination water supplies." Hydrogeology journal 22.8 (2014): 1921-1934.
[59] Alahmadi, Masoud. "Groundwater quality in some villages northeast of Jeddah city, Saudi Arabia." Ninth International Water Technology Conference, IWTC9 2005,, 2005.
[60] Al-Sefry, Saleh A., and Zekai Şen. "Groundwater rise problem and risk evaluation in major cities of arid lands–Jedddah Case in Kingdom of Saudi Arabia." Water Resources Management 20.1 (2006): 91-108.
[61] Elfeki, Amro, Hatem Ewea, and Nassir Al-Amri. "Linking groundwater flow and transport models, GIS technology, satellite images and uncertainty quantification for decision making: Buraiman Lake Case Study Jeddah, Saudi Arabia." International Journal of Water Resources and Arid Environments 1.4 (2011): 295-303.
[62] Mogren, Saad, et al. "Aquifer boundaries explored by geoelectrical measurements in the Red Sea coastal plain of Jazan area, Southwest Saudi Arabia." International Journal of Physical Sciences 6.15 (2011): 3688-3696.
[63] Sharaf, Mohammed Amin M. "A Study of Subsurface Drainage and Water Quality in Jeddah-Makkah Aquifer Zone, West Central Arabian Shield, Saudi Arabia." Drainage Systems. InTech, 2012.
[64] Sharaf, Mohammed Amin M. "A Study of Subsurface Drainage and Water Quality in Jeddah-Makkah Aquifer Zone, West Central Arabian Shield, Saudi Arabia." Drainage Systems. InTech, 2012.
[65] Al-Taani, A. A., et al. "Groundwater quality of coastal aquifer systems in the eastern coast of the Gulf of Aqaba, Saudi Arabia." Earth Science Research Journal (2013).

[66] Cagatay, M. Namik. "Palygorskite in the Eocene rocks of the dammam dome, Saudi Arabia." Clays and Clay Minerals 38.3 (1990): 299-307.
[67] Alsharhan, A. S., et al., eds. Hydrogeology of an arid region: the Arabian Gulf and adjoining areas. Elsevier, 2001..
[68] Al-Ahmadi, Masoud Eid. "Hydrogeology of the Saq aquifer northwest of Tabuk, northern Saudi Arabia." Earth Sciences 20.1 (2009).
[69] Yang, H., P. Cui, and Z. Fang. "Vertical-borehole ground-coupled heat pumps: A review of models and systems." Applied Energy 87.1 (2010): 16-27.
[70] Hashem, B. "Geothermal development roadmap for the Kingdom of Saudi Arabia." GHC Bulletin August (2012) 28–30.
[71] Asad Salem, Hafiz Elsir Mirghani Hashim "A Feasibility of Geothermal Cooling in Middle East" Latest Trends in Sustainable and Green Development. (2013) 978-1-61804-132-6
[72] Zhou, Shiyu, et al. "Study on ground temperature response of multilayer stratums under operation of ground-source heat pump." Applied Thermal Engineering 101 (2016): 173-182.
[73] Derradji, Mohamed, and Messaoud Aiche. "Modeling the soil surface temperature for natural cooling of buildings in hot climates." Procedia Computer Science 32 (2014): 615-621.
[74] van Manen, Saskia M., and Erin Wallin. "Ground temperature profiles and thermal rock properties at Wairakei, New Zealand." Renewable energy 43 (2012): 313-321.
[75] Pain, Colin F., and Mahmoud Ali Abdelfattah. "Landform evolution in the arid northern United Arab Emirates: Impacts of tectonics, sea level changes and climate." Catena 134 (2015): 14-29.
[76] Christian Hauck , Christin Hilbich, A. Lewkowicz. "Successful field work in Finnmark and Troms, Northern Norway" Norwegian Geological Survey 2008
[77] Popiel, C. O., and J. Wojtkowiak. "Temperature distributions of ground in the urban region of Poznan City." Experimental Thermal and Fluid Science 51 (2013): 135-148.
[78] Tomoyuki Ohtani, Takahito Mizuno, Akihiko Kouda, Satoru Kojima "Seasonall change of underground temperature and the use of geothermal in Gifu city, Japan" Proceedings World Geothermal Congress 2015

[79] Ochsner, Tyson E., Thomas J. Sauer, and Robert Horton. "Soil heat storage measurements in energy balance studies." Agronomy journal 99.1 (2007): 311-319.
[80] Hellstrom, Goran, "Duct Ground Heat Storage Model, Manual for Computer Code", department of Mathematical Physics, University of Lund, Sweden.

9.1.6 Chapter 5

[1] Hang, Yin, et al. "Multi-objective optimization of integrated solar absorption cooling and heating systems for medium-sized office buildings." Renewable energy 52 (2013): 67-78.
[2] Calise, F. "Thermoeconomic analysis and optimization of high efficiency solar heating and cooling systems for different Italian school buildings and climates." Energy and Buildings 42.7 (2010): 992-1003.
[3] Calise, F., M. Dentice d'Accadia, A. Palombo. "Transient analysis and energy optimization of solar heating and cooling systems in various configurations." Solar Energy 84.3 (2010): 432-449.
[4] Calise, F., M. Dentice d'Accadia, L. Vanoli. "Thermoeconomic optimization of solar heating and cooling systems." Energy Conversion and Management 52.2 (2011): 1562-1573.
[5] Calise, F., A. Palombo, and L. Vanoli. "Maximization of primary energy savings of solar heating and cooling systems by transient simulations and computer design of experiments." Applied Energy 87.2 (2010): 524-540.
[6] Al-Sultan, K. S., and M. A. Al-Fawzan. "A tabu search Hooke and Jeeves algorithm for unconstrained optimization." European journal of operational research 103.1 (1997): 198-208.
[7] Kirgat, G. S., and A. N. Surde. "Review of Hooke and Jeeves Direct Search Solution Method Analysis Applicable To Mechanical Design Engineering." International Journal of Innovations in Engineering Research and Technology (IJIERT) 1.2 (2014): 1-14.

9.1.7 Chapter 6

[1] https://www.worldenergy.org/data/efficiency-indicators/

9.2 List of Tables

9.3 List of Figures

9.4 Configurations

ID	SF	SOURCE (m^2)	B (kWh)	CHILLER (kW)	COLD (m^3)	HRS	CITY
P 0 0 1 B 1 E 1	0.70	PV 8250		CC 4000		AIR	Dubai
P 0 0 1 B 1 S 1	0.70	PV 4200		CC 4000		AIR	Riyadh
P 0 0 2 B 1 E 1	0.70	PV 6700		CC 4000		CT	Dubai
P 0 0 2 B 1 S 1	0.70	PV 2640		CC 4000		CT	Riyadh
P 0 0 3 B 1 E 1	0.70	PV 5600		CC 4000		GW	Dubai
P 0 0 3 B 1 S 1	0.70	PV 2345		CC 4000		GW	Riyadh
P 0 0 4 B 1 E 1	0.70	PV 6250		CC 4000		GHX	Dubai
P 0 0 4 B 1 S 1	0.70	PV 2825		CC 4000		GHX	Riyadh

ID	SF	SOURCE (m^2)	B (kWh)	CHILLER (kW)	COLD (m^3)	HRS	CITY
P 0 0 5 B 1 E 1	0.70	PV 16000	2100	CC 4000	200	AIR	Dubai
P 0 0 5 B 1 S 1	0.69	PV 7200	1000	CC 4000	200	AIR	Riyadh
P 0 0 6 B 1 E 1	0.70	PV 12200	1800	CC 4000	200	CT	Dubai
P 0 0 6 B 1 S 1	0.71	PV 5750	900	CC 4000	200	CT	Riyadh
P 0 0 7 B 1 E 1	0.69	PV 9400	1580	CC 4000	200	GW	Dubai
P 0 0 7 B 1 S 1	0.71	PV 4620	750	CC 4000	200	GW	Riyadh
P 0 0 8 B 1 E 1	0.70	PV 11000	1650	CC 4000	200	GHX	Dubai
P 0 0 8 B 1 S 1	0.70	PV 5500	820	CC 4000	200	GHX	Riyadh

ID	SF	SOURCE (m^2)	HOT (m^3)	CHILLER (kW)	COLD (m^3)	HRS	CITY
P 1 1 1 B 1 E 1	0.50	FPC 500	1100	ABS 3000	550	AIR	Dubai
P 1 1 1 B 1 S 1	0.50	FPC 240	600	ABS 1400	300	AIR	Riyadh
P 1 1 2 B 1 E 1	0.70	FPC 310	1100	ABS 3000	550	CT	Dubai
P 1 1 2 B 1 S 1	0.69	FPC 200	700	ABS 1500	350	CT	Riyadh
P 1 1 3 B 1 E 1	0.70	FPC 350	1100	ABS 2900	550	GW	Dubai
P 1 1 3 B 1 S 1	0.70	FPC 145	475	ABS 1350	238	GW	Riyadh
P 1 1 4 B 1 E 1	0.71	FPC 360	1050	ABS 2950	525	GHX	Dubai
P 1 1 4 B 1 S 1	0.71	FPC 150	500	ABS 1350	250	GHX	Riyadh

ID	SF	SOURCE (m^2)	HOT (m^3)	CHILLER (kW)	COLD (m^3)	HRS	CITY
P 1 3 1 B 1 E 1	0.50	FPC 300	1000	ADS 3600	500	AIR	Dubai
P 1 3 1 B 1 S 1	0.49	FPC 200	500	ADS 1250	250	AIR	Riyadh
P 1 3 2 B 1 E 1	0.70	FPC 340	1200	ADS 2800	600	CT	Dubai
P 1 3 2 B 1 S 1	0.70	FPC 145	475	ADS 1400	237.5	CT	Riyadh
P 1 3 3 B 1 E 1	0.69	FPC 335	1100	ADS 2800	550	GW	Dubai
P 1 3 3 B 1 S 1	0.70	FPC 145	525	ADS 1500	262.5	GW	Riyadh
P 1 3 4 B 1 E 1	0.70	FPC 350	1200	ADS 2800	600	GHX	Dubai
P 1 3 4 B 1 S 1	0.70	FPC 145	510	ADS 1350	255	GHX	Riyadh

ID	SF	SOURCE (m^2)	HOT (m^3)	CHILLER (kW)	COLD (m^3)	HRS	CITY
P 1 4 1 B 1 E 1	0.15	FPC 120	30	DEC 45	0	VEN	Dubai
P 1 4 1 B 1 S 1	0.65	FPC 160	35	DEC 25	0	VEN	Riyadh
P 1 4 2 B 1 E 1	0.13	FPC 120	30	DEC 45	0	VSL	Dubai
P 1 4 2 B 1 S 1	0.71	FPC 140	30	DEC 25	0	VSL	Riyadh
P 1 4 3 B 1 E 1	0.15	FPC 140	30	DEC 45	0	REC	Dubai
P 1 4 3 B 1 S 1	0.71	FPC 105	30	DEC 25	0	REC	Riyadh

ID								SF	SOURCE (m^2)		HOT (m^3)	CHILLER (kW)		COLD (m^3)	HRS	CITY
P	2	1	1	B	1	E	1	0.50	ETC	260	800	ABS	1800	400	AIR	Dubai
P	2	1	1	B	1	S	1	0.50	ETC	180	600	ABS	1300	300	AIR	Riyadh
P	2	1	2	B	1	E	1	0.70	ETC	260	800	ABS	2850	400	CT	Dubai
P	2	1	2	B	1	S	1	0.70	ETC	210	525	ABS	1450	263	CT	Riyadh
P	2	1	3	B	1	E	1	0.71	ETC	225	730	ABS	2750	365	GW	Dubai
P	2	1	3	B	1	S	1	0.70	ETC	98	380	ABS	1300	190	GW	Riyadh
P	2	1	4	B	1	E	1	0.71	ETC	240	800	ABS	2750	400	GHX	Dubai
P	2	1	4	B	1	S	1	0.70	ETC	140	450	ABS	1350	225	GHX	Riyadh

ID								SF	SOURCE (m^2)		HOT (m^3)	CHILLER (kW)		COLD (m^3)	HRS	CITY
P	2	2	1	B	1	E	1	0.51	ETC	180	400	2sABS	1500	200	AIR	Dubai
P	2	2	1	B	1	S	1	0.50	ETC	80	180	2sABS	1100	90	AIR	Riyadh
P	2	2	2	B	1	E	1	0.71	ETC	220	580	2sABS	2750	290	CT	Dubai
P	2	2	2	B	1	S	1	0.71	ETC	86	220	2sABS	1250	110	CT	Riyadh
P	2	2	3	B	1	E	1	0.71	ETC	190	550	2sABS	2700	275	GW	Dubai
P	2	2	3	B	1	S	1	0.70	ETC	74	180	2sABS	1200	90	GW	Riyadh
P	2	2	4	B	1	E	1	0.71	ETC	200	560	2sABS	2750	280	GHX	Dubai
P	2	2	4	B	1	S	1	0.71	ETC	84	200	2sABS	1250	100	GHX	Riyadh

ID								SF	SOURCE (m^2)		HOT (m^3)	CHILLER (kW)		COLD (m^3)	HRS	CITY
P	2	3	1	B	1	E	1	0.50	ETC	300	800	ADS	1600	400	AIR	Dubai
P	2	3	1	B	1	S	1	0.50	ETC	185	475	ADS	1250	238	AIR	Riyadh
P	2	3	2	B	1	E	1	0.70	ETC	285	1250	ADS	3000	625	CT	Dubai
P	2	3	2	B	1	S	1	0.70	ETC	132	400	ADS	1400	200	CT	Riyadh
P	2	3	3	B	1	E	1	0.70	ETC	287	900	ADS	2900	450	GW	Dubai
P	2	3	3	B	1	S	1	0.70	ETC	130	380	ADS	1350	190	GW	Riyadh
P	2	3	4	B	1	E	1	0.70	ETC	300	1250	ADS	3200	625	GHX	Dubai
P	2	3	4	B	1	S	1	0.71	ETC	138	420	ADS	1350	210	GHX	Riyadh

ID								SF	SOURCE (m^2)		HOT (m^3)	CHILLER (kW)		COLD (m^3)	HRS	CITY
P	2	4	1	B	1	E	1	0.18	ETC	150	30	DEC	45	0	VEN	Dubai
P	2	4	1	B	1	S	1	0.68	ETC	140	26	DEC	25	0	VEN	Riyadh
P	2	4	2	B	1	E	1	0.15	ETC	120	30	DEC	45	0	VSL	Dubai
P	2	4	2	B	1	S	1	0.70	ETC	126	24	DEC	25	0	VSL	Riyadh
P	2	4	3	B	1	E	1	0.18	ETC	150	15	DEC	45	0	REC	Dubai
P	2	4	3	B	1	S	1	0.70	ETC	110	18	DEC	25	0	REC	Riyadh

ID								SF	SOURCE (m^2)		HOT (m^3)	CHILLER (kW)		COLD (m^3)	HRS	CITY
P	3	2	1	B	1	E	1	0.50	PTC	260	600	2sABS	1500	300	AIR	Dubai
P	3	2	1	B	1	S	1	0.50	PTC	90	200	2sABS	1250	100	AIR	Riyadh
P	3	2	2	B	1	E	1	0.70	PTC	195	600	2sABS	2650	300	CT	Dubai
P	3	2	2	B	1	S	1	0.70	PTC	60	155	2sABS	1250	77.5	CT	Riyadh
P	3	2	3	B	1	E	1	0.70	PTC	172	500	2sABS	2650	250	GW	Dubai
P	3	2	3	B	1	S	1	0.70	PTC	52	115	2sABS	1250	57.5	GW	Riyadh
P	3	2	4	B	1	E	1	0.70	PTC	182	540	2sABS	2700	270	GHX	Dubai
P	3	2	4	B	1	S	1	0.70	PTC	80	100	2sABS	1250	50	GHX	Riyadh

ID								SF	SOURCE (m^2)		HOT (m^3)	CHILLER (kW)		COLD (m^3)	HRS	CITY
P	3	5	1	B	1	E	1	0.50	PTC	150	450	3sABS	2650	225	AIR	Dubai
P	3	5	1	B	1	S	1	0.50	PTC	75	130	3sABS	1350	65	AIR	Riyadh
P	3	5	2	B	1	E	1	0.70	PTC	165	550	3sABS	2650	275	CT	Dubai
P	3	5	2	B	1	S	1	0.70	PTC	52	145	3sABS	1250	73	CT	Riyadh
P	3	5	3	B	1	E	1	0.70	PTC	150	500	3sABS	2650	250	GW	Dubai
P	3	5	3	B	1	S	1	0.70	PTC	47	105	3sABS	1250	53	GW	Riyadh
P	3	5	4	B	1	E	1	0.70	PTC	155	500	3sABS	2650	250	GHX	Dubai
P	3	5	4	B	1	S	1	0.71	PTC	50	115	3sABS	1250	58	GHX	Riyadh